

SEDIMENTARY CYCLICITY IN THE UPPER CRETACEOUS
SUCCESSIONS OF THE HAYMANA BASIN (TURKEY): DEPOSITIONAL
SEQUENCES AS RESPONSE TO RELATIVE
SEA – LEVEL CHANGES

A THESIS SUBMITTED TO
THE GRADUATE SCHOOL OF NATURAL AND APPLIED SCIENCES
OF
MIDDLE EAST TECHNICAL UNIVERSITY

BY

AFGAN HUSEYNOV

IN PARTIAL FULFILLMENT OF THE REQUIREMENTS
FOR
THE DEGREE OF MASTER OF SCIENCE
IN
GEOLOGICAL ENGINEERING

SEPTEMBER 2007

Approval of thesis:

SEDIMENTARY CYCLICITY IN THE UPPER CRETACEOUS
SUCCESSIONS OF THE HAYMANA BASIN (TURKEY): DEPOSITIONAL
SEQUENCES AS RESPONSE TO RELATIVE SEA – LEVEL CHANGES

submitted by AFGAN HUSEYNOV in partial fulfillment of the requirements for
the degree of Master of Science in Geological Engineering Department, Middle
East Technical University by,

Prof. Dr. Canan Özgen
Dean, Graduate School of Natural and Applied Sciences _____

Prof. Dr. Vedat Doyuran
Head of Department, Geological Engineering _____

Prof. Dr. Demir Altıner
Supervisor, Geological Engineering Dept., METU _____

Assis. Prof. Dr. İsmail Ömer Yılmaz
Co-Supervisor, Geological Engineering Dept., METU _____

Examining Committee Members:

Prof. Dr. Asuman Türkmenoğlu
Geological Engineering Dept., METU _____

Prof. Dr. Demir Altıner
Supervisor, Geological Engineering Dept., METU _____

Assis. Prof. Dr. İsmail Ömer Yılmaz
Co-Supervisor, Geological Engineering Dept., METU _____

Assoc. Prof. Dr. Kadir Dirik
Geological Engineering Dept., Hacettepe University _____

Assist. Prof. Dr. Fatma Toksoy Köksal
Geological Engineering Dept., METU _____

Date: 03.09.2007

I hereby declare that all information in this document has been obtained and presented in accordance with academic rules and ethical conduct. I also declare that, as required by these rules and conduct, I have fully cited and referenced all material and results that are not original to this work.

Name, Last name: Afgan HUSEYNOV

Signature:

ABSTRACT

SEDIMENTARY CYCLICITY IN THE UPPER CRETACEOUS SUCCESSIONS OF THE HAYMANA BASIN (TURKEY): DEPOSITIONAL SEQUENCES AS RESPONSE TO RELATIVE SEA – LEVEL CHANGES

Afgan Huseynov

M. Sc., Department of Geological Engineering

Supervisor: Prof. Dr. Demir Altıner

Co-Supervisor: Assist. Prof. Dr. İsmail Ömer Yılmaz

September 2007, 121 pages

The Haymana basin in Central Anatolia (Turkey) formed on a Late Cretaceous to Middle Eocene fore – arc accretionary wedge. The aim of this study is to investigate the sedimentary cyclicity and depositional sequences in the Upper Cretaceous clastic successions of the Haymana basin. To be able to achieve this objective, a 250 m stratigraphic section, which is mainly composed of siliciclastics has been measured in the Haymana Basin.

In this study, detailed lithofacies analyses were performed and five different facies were recognized in the studied interval of the Haymana Formation. Sandstones, shales and conglomerates are the most abundant in the succession. In the measured section, two chronozones were identified based on the biostratigraphic data. These are the lower *Dicarinella asymetrica* chronozone and the upper *Globotruncanita elevata* - *Globotruncana ventricosa* chronozone corresponding to the Upper Santonian and Lower to Middle Campanian, respectively.

Sedimentological analyses, such as provenance, palaeocurrent and grain-size sphericity were also performed and their relation with depositional environment and change in depositional conditions were discussed.

In order to construct the sequence stratigraphic framework, detailed lithofacies analyses and their vertical association were carried out. The studied interval of the Haymana Formation represents a prograding submarine fan subdivided into three depositional sequences, each with several tens of meters thick successions and two sequence boundaries. Each depositional sequence consists of system tracts and turbiditic basic sequences with sandstone and conglomeratic beds overlain by mudstones. Turbiditic basic sequences, the sandstone and mudstone alternation allows distinction of smaller subdivisions, namely, basic cyclic units, which are the building blocks of system tracts and turbiditic basic sequences. Depositional sequences of the studied section of the Haymana Formation may correspond to third order relative sea – level cycles. Accordingly, fourth – and fifth – order (Milankovich) cycles might be proposed as basic sequences and basic cyclic units, respectively.

Keywords: Sedimentary cyclicity, sequence stratigraphy, turbidites, Upper Cretaceous, Haymana basin, Turkey

ÖZ

HAYMANA HAVZASI'NIN (TÜRKİYE) ÜST KRETASE İSTİFLERİNDE SEDİMANTER DEVİRSELLİK: GÖRECELİ DENİZ SEVİYESİ DEĞİŞİMLERİNİ KAYITLAYAN ÇÖKEL SEKANSLAR

Afgan Hüseyinov

Yüksek Lisans, Jeoloji Mühendisliği Bölümü

Tez Yöneticisi: Prof. Dr. Demir Altın

Yardımcı tez Yöneticisi: Assist. Prof. Dr. İsmail Ömer Yılmaz

Eylül 2007, 121 sayfa

Orta Anadolu'daki Haymana yayönü Baseni, Geç Kretase'den – Orta Eosene kadar aktif bir yığışım karmaşığı üzerinde gelişmiştir. Çalışma Haymana Havzasındaki Üst Kretase istiflerinde çökel sekansları ortaya koyarak sedimanter devirselliği yorumlamayı amaçlamaktadır. Bu çalışmayı gerçekleştirebilmek için Haymana Baseninde, çoğunlukla kumtaşı–şeyllerden oluşan bir stratigrafik kesit ölçülmüştür.

Bu çalışmada, detaylı litofasiyes analizi gerçekleştirilmiş ve Haymana Formasyonu'nun çalışılan aralığında beş değişik fasiyes tanımlanmıştır. Kumtaşı, şeyl ve konglomeralar sık karşılaşılan kaya tipleridir. Çalışılan kesitte, biyostratigrafik verilere göre, iki kronozon ayrılmıştır. Bunlar alt *Dicarinella asymetrica* ve üst *Globotruncanita elevata* – *Globotruncana ventricosa* kronozonlarıdır ve yaş olarak Geç Santoniyen ve Erken – Orta Kampaniyene karşılık gelmektedir.

Sedimentar analizler olarak kaynak kaya, eski akıntı, tane boyu ve küresellik analizleri yapılmış ve bu analizlerin sonuçları çökelim ortamı ve çökelim şartlarındaki değişikliklerinin tesbiti için yorumlanmıştır.

Sekans stratigrafisi çatisını oluşturabilmek için, detaylı litofasiyes analizleri yapılmış ve bu litofasiyeslerin dikey dağılımı incelenmiştir. Haymana

Formasyonu'nun alıřılan kısmı ilerleyen denizaltı yelpazesini temsil etmektedir ve bu kısımda her biri bir ka on metre olan, üç sedimanter sekans ve iki sekans sınırı tanımlanmıştır. Her bir sekans, sistem traklere ve turbiditik ana sekanslara ayrılmıştır. Turbiditik ana sekansların içlerinde ise metre ölçekli küçük devirsel birimler tanımlanmıştır. alıřmada sedimentar sekansların 3-cü derece global deniz seviyesi deęişimlerine, turbiditik ana sekanslar ve metre ölçekli devirlerin ise "Milankovich eccentricity" devirlerine karşılık geldięi ortaya koyulmuştur.

Anahtar Kelimeler: Sedimanter devirsellik, sekans stratigrafisi, turbidit, Üst Kretase, Haymana havzası, Türkiye

To the memory of my father....

ACKNOWLEDGEMENTS

I would like to express my deepest gratitude to my supervisor, Prof. Dr. Demir Altiner, whose expertise, understanding, encouragement and patience, added considerably to my graduate experience. I appreciate his vast knowledge and skill in many areas, and his assistance in writing this thesis. I would like to thank to my co-supervisor Assist. Prof. Dr. İ. Ömer Yılmaz for his attention, and I am grateful to him for valuable recommendations, encouragements and helps in field works and labs during my studies.

I am thankful to Assist. Prof. Dr. Fatma Toksoy Köksal for her help during the petrographic studies. Appreciation also goes out to Res. Assist. Kaan Sayit for his help during laboratory studies.

A very special thanks goes out to all my friends for their friendships, motivations and endless encouragements. Especially, I would like to thank Res. Assist. Ayşe Atakul, Elnur Amirov, Farid Babayev, Rufat Aghayev and Elnur Binyatov for their helps in field works and encouragements.

I would like to thank to Mr. Orhan Karaman for the preparation of thin sections.

Finally (at last but does not mean the least), I would like to express my grateful appreciation to my family and my uncle for their support and encouragements during my studies.

I notice that this research would not have been possible without the financial assistance of BP Caspian Sea Exploration, and especially would like to express my grateful appreciation to Greg Riley and David Day for this wonderful opportunity given to me.

TABLE OF CONTENTS

ABSTRACT.....	iv
ÖZ.....	vi
ACKNOWLEDGEMENTS.....	ix
TABLE OF CONTENTS.....	x
LIST OF TABLES.....	xii
LIST OF FIGURES.....	xiii

CHAPTERS

I. INTRODUCTION.....	1
1.1. Purpose and Scope.....	1
1.2. Geographic Setting	2
1.3. Methods of Study.....	3
1.4. Previous Works.....	6
1.5. Geological Setting	10
II. LITHOSTRATIGRAPHY AND BIOSTRATIGRAPHY.....	14
2.1. Lithostratigraphy.....	14
2.2. Biostratigraphy and Chronostratigraphy.....	23
III. SEQUENCE STRATIGRAPHY.....	29
3.1. Historical Background.....	29
3.2. Meter – Scale Fining and Coarsening Upward Units.....	32
3.2.1. Types of fining and coarsening upward units.....	32
3.2.1.1. Basic sequence no. 1.....	33
3.2.1.2. Basic sequence no. 2.....	33
3.2.1.3. Basic sequence no. 3.....	34
3.2.1.4. Basic sequence no. 4.....	34

3.3. Sequence Stratigraphic Interpretation.....	35
3.4. Origin and Duration of Cycles.....	41
IV. SEDIMENTOLOGY.....	46
4.1. Petrography and Classification of Lithofacies.....	46
4.1.1. Limestones.....	47
4.1.1.1. Wackestones.....	47
4.1.1.2. Lime Mudstones.....	47
4.1.2. Mudstones and Shales.....	47
4.1.2.1. Mudstones.....	48
4.1.2.2. Shales.....	48
4.1.3. Sandstones.....	49
4.1.3.1. Litharenites.....	49
4.1.3.2. Lithic greywackes.....	50
4.1.4. Conglomerates.....	50
4.1.4.1. Orthoconglomerates.....	50
4.1.4.2. Paraconglomerates.....	53
4.1.5. Rock fragments.....	54
4.2. Sedimentary Structures.....	59
4.3. Provenance Analysis.....	60
4.4. Palaeocurrent Analysis.....	63
4.5. Grain Size and Sphericity analyses.....	68
4.6. Depositional Environment.....	78
V. CONCLUSION AND RECOMMENDATION.....	81
REFERENCES.....	85
APPENDICES.....	93

LIST OF TABLES

Table 1. Possible correlation of cyclic units observed in the studied interval with other cyclic sequences proposed in literature.....	43
Table 2. Formulae for the calculation of grain – size parameters from a graphic presentation of the data in a cumulative frequency plot. The percentile measure ϕ_n is the grain size in phi units at the n^{th} percentage frequency.....	71
Table 3. Grain size parameters derived graphically, Folk and Ward formulae.....	71
Table 4. Grain size parameters derived graphically, Folk and Ward formulae (thin section samples).....	77

LIST OF FIGURES

Figure 1. Geographic location map of the studied section.....	2
Figure 2. Location of the total measured section (yellow) and detailed studied section (red) (snapshot taken from Google Earth).....	4
Figure 3. General field view of the measured section (from South to North). A -studied interval; B – close –up views of the conglomeratic succession.....	5
Figure 4. Main structural features of Turkey and location map of Haymana Basin (modified after Koçyigit, 1991).....	12
Figure 5. Schematic cross section (not to scale) showing the structural setting of the Haymana Basin during the Campanian to the Lutetian time interval (Koçyigit, 1991).....	12
Figure 6. Simplified geologic map of Haymana Basin from 1:500 000 map of Ankara.....	13
Figure 7. Modified stratigraphic columnar section of the Haymana Basin.....	15
Figure 8. Simplified measured section (for detailed section see appendix A).....	17
Figure 9. Field photographs of the rock units recognized along the measured section. A – Pinkish limestones of the Kocatepe Formation (Upper Santonian), level HAH – 3 – 4 pen for a scale; B – Conglomerates	

of the Haymana Formation, level HAH – 73 (hammer for a scale).	
C – Sandstone - shale alternation in the lower part (HAH - 17) of the Haymana Formation, hammer for a scale.....	20
Figure 10. Field photographs of erosional sedimentary structures observed in the field at the bottom of the sandstone beds. A - Load casts and groove marks, level: HAH – 32; B – Flute marks. Flow from top to bottom, level: HAH – 10.....	21
Figure 11. Field view photograph of the sandstone – shale – conglomerate alternations, levels: HAH 40 to 52.....	22
Figure 12. Chronozones based on biostratigraphy data along the measured section and the <i>calcarata</i> zone identified in the upper layers of the Haymana Formation bu Yüksel (1970).....	26
Figure 13. Plan views of the three main types turbidite depositional systems of Mutti (1985).....	31
Figure 14. Simplified measured section showing cyclic units and sequence boundaries.....	36
Figure 15. Illsutrations of A and B-type basic cyclic units and sub-cycles defined within them.....	38
Figure 16. Illustration of complete Bouma’s sequences observed in the field and interpreted as A3-type sub-cyclic units.....	38
Figure 17. Photographs of shallowing and deepening upward cycles (A – B2 type sub-cycles, B – A2 type sub-cycles).....	39

Figure 18. Comparison of the depositional sequences defined during this study and global sea – level chart (red box showing global - cycles corresponding to our depositional sequences).....	45
Figure 19. Classification of limestones based on depositional texture, Embry A. F. and Klovan J. E., 1971 (after Dunham R. J., 1962).....	48
Figure 20. Photomicrographs of the limestones - wackestones, (M – matrix (limy mud), Ir – iron oxide in the fissure, B – bioclast (planktonic foraminifera)), (A, B : HAH – 1).....	51
Figure 21. Photomicrographs of shales, (Q – quartz, M – matrix (silt-sized quartz and clay minerals)), (A: HAH – 7; B: HAH - 16B).....	52
Figure 22. Classification of sandstones After Pettijohn <i>et al.</i> , (1987).....	53
Figure 23. Photomicrographs of sandstones – lithic greywackes (Q – quartz, L - rock fragments, C - calcite cement), (A: HAH – 15, B: HAH – 23).....	56
Figure 24. Photomicrographs of conglomerates (Q – quartz, L - rock fragments, C - cement), (A, B : HAH-45).....	57
Figure 25. Illustration of rock fragments distribution along the measured section.....	58
Figure 26. Photographs of sedimentary structures observed in the field. A – flute marks at the base of sandstone bed (flow from bottom to the top); B - Load casts structures at the base of conglomerate; C and D – Grazing traces (<i>Nereites</i> ichnofacies?).....	61

Figure 27. Photographs of sedimentary structures observed in the field. A – laminated sandstone bed, HAH – 11; B – ball structures, HAH – 74; C – normal graded bed, HAH – 54; D – reversed graded bed, above HAH – 76; E – multiple graded bed, HAH – 69.....	62
Figure 28. Triangular diagram showing average compositions of sand derived from different provenance terranes. After Dickinson (1985).....	64
Figure 29. Photographs of pebbles and cobbles in conglomeratic successions, used for palaeocurrent direction (A – layer one, palaeocurrent direction is SE; B – layer two, palaeocurrent direction is W; red arrows show imbrication).....	66
Figure 30. Rose diagram illustrating palaeocurrent direction for the first bed (HAH - 55).....	67
Figure 31. Rose diagram illustrating palaeocurrent direction for the second bed (last conglomeratic bed in the studied interval).....	67
Figure 32. Graphic presentation of grain size data for bed one (HAH-55) (A-histogram, B –cumulative frequency curves plotted with an arithmetic scale).....	69
Figure 33. Graphic presentation of grain size data for bed two (last conglomeratic unit in the studied interval) (A-histogram, B –cumulative frequency curves plotted with an arithmetic scale).....	70
Figure 34. OP index diagram for bed one.....	72
Figure 35. OP index diagram for bed two.....	73

Figure 36. Graphic presentation of grain size data for a sample HAH - 39 (A -histogram, B –cumulative frequency curves plotted with an arithmetic scale).....	74
Figure 37. Graphic presentation of grain size data for sample a HAH - XI (A -histogram, B –cumulative frequency curves plotted with an arithmetic scale).....	74
Figure 38. Graphic presentation of grain size data for sample a HAH – 42 (A -histogram, B –cumulative frequency curves plotted with an arithmetic scale).....	75
Figure 39. Graphic presentation of grain size data for sample a HAH - 43 (A -histogram, B –cumulative frequency curves plotted with an arithmetic scale).....	75
Figure 40. Graphic presentation of grain size data for sample a HAH – 48 (A -histogram, B –cumulative frequency curves plotted with an arithmetic scale).....	76
Figure 41. Graphic presentation of grain size data for sample a HAH – 45 (A -histogram, B –cumulative frequency curves plotted with an arithmetic scale).....	76
Figure 42. Transport modes in relation to size distributions (Friedman & Sanders, 1978).....	77
Figure 43. Submarine-fan facies model. (a) Classic model of fan with suprafan lobes, some active, some abandoned. (b) Succession produced through fan growth and lobe progradation.....	80

CHAPTER I

INTRODUCTION

1.1. Purpose and Scope

The main objective of this study is to investigate the sedimentary cyclicality by analyzing various depositional sequences in the Upper Cretaceous successions of the Haymana basin. In order to carry out this objective, several studies were performed based on different disciplines of geology including lithostratigraphy, biostratigraphy, sequence stratigraphy and the sedimentology.

The Haymana basin, like many other central Anatolian basins, is characterized by Upper Cretaceous – Middle Eocene clastic turbidite sediments at its center, passing into platform carbonates and continental red beds towards the margins (Yüksel 1970; Görür 1981; Çiner 1992). Since the central parts of the basin is characterized by more than 5000 m thick of deep marine deposits (Koçyigit et al., 1988) including reworked conglomerates enclosed in bioclastic and epiclastic sandy turbidites, a 250 m thick stratigraphic section was measured in the central part of the basin, where turbidite successions and mass flow deposits are widely exposed. The measured section comprise reddish to pinkish pelagic limestones at its base, and composed of fine-grained muddy to silty deposits at in the middle, sandy-conglomeratic low and high density turbidite successions at the top. In general, this measured stratigraphic succession shows an overall transgressive-to-regressive cycle. Within the defined system tracts, meter-scale cycles were identified on the basis of lithological facies description in the field, petrographic and detailed microfacies analysis in the laboratory. According to paleontological and biostratigraphic analysis, the measured section was divided into planktonic foraminiferal biozones, and the sequence stratigraphic framework was discussed and compared sequence stratigraphic global curve.

Sedimentological studies, based on grain and matrix composition and the texture, yielded several data on the anatomy and provenance of the sedimentary material which make up the bulk of the siliciclastic successions, and their relation with depositional environment and change in depositional conditions.

1.2. Geographic setting

The Haymana town is located about 70 km SW of Ankara in Central Anatolia (Figure 1). The study area is located at approximately 5 km northeast

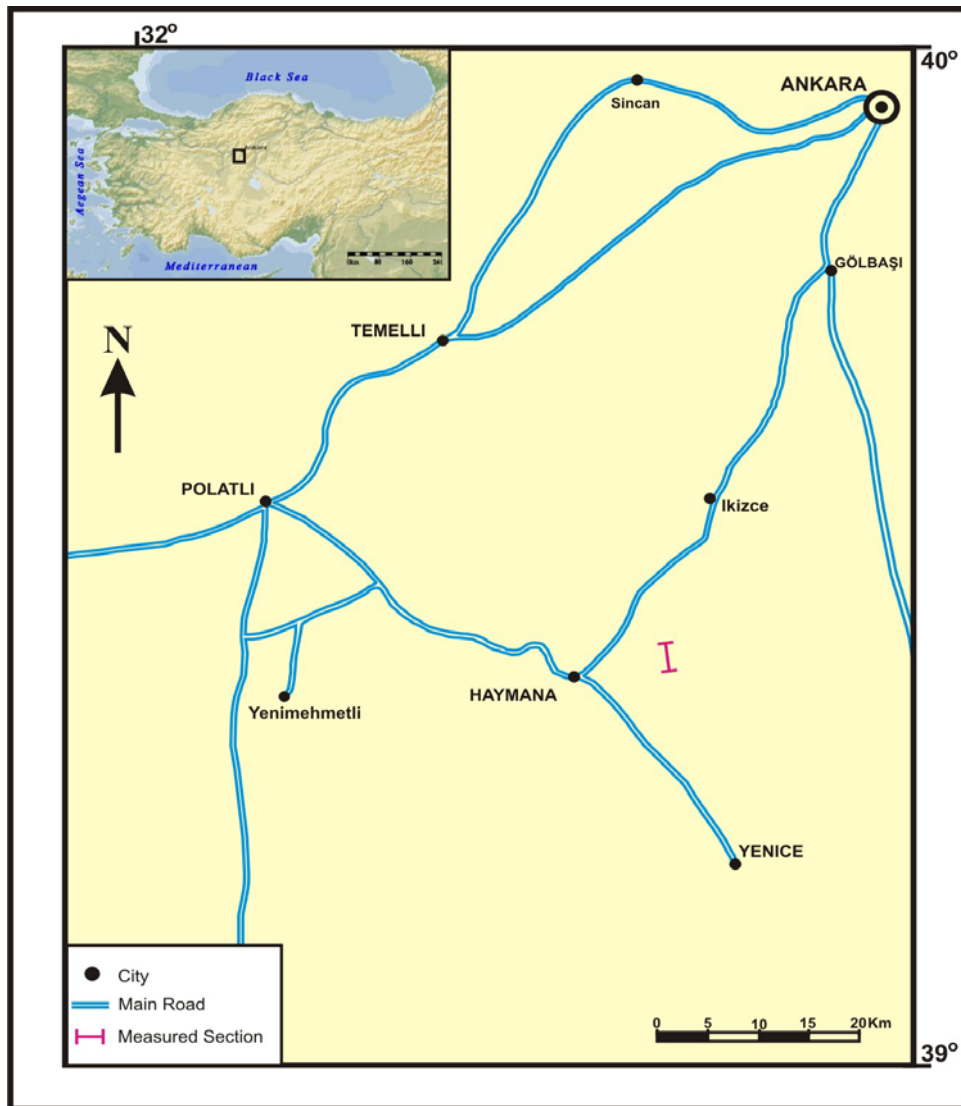


Figure 1. Geographic location map of the studied section.

of the town of Haymana. The measured section starts at coordinates 36461162⁰ E – 4366574⁰ N and finishes at 36461141⁰ E – 4366851⁰ N. The base of the section is easily accessible from the town.

1.3. Methods of Study

This study mainly consisted of field and laboratory work. In the field, a stratigraphic section 250 m in thickness was measured. At the bottom, the succession is mainly composed of reddish to pinkish colored limestones, changing upward into sandstone - shale rhythmic alternations whereas the upper part of the section mainly consists of conglomerates, and sandstones intercalated with mudstones and shales (Figures 2, 3). 150 m from bottom the measured section were studied in details due to time saving and sandstone – shale rhythmic depositon in the lower parts. During the field work, lithologic descriptions and sedimentary structures were carried out in the field. 80 samples were collected nearly from each sandstone and shale bed, and from thick conglomeratic successions, samples were collected from the bottom, middle part and from top.

Detailed petrographical, sedimentological, palaeocurrent, grain size analysis of conglomeratic beds has been carried out in the field and paleontological analyses were carried out in the laboratory. For this purpose, thin sections were prepared from all samples.

In the laboratory, point counting analyses were carried out in order to classify the sandstone, limestone and shale beds, and to understand the response of mineral and rock fragment concentrations in the beds to change in depositional environments. Approximately 500 - 1500 points were counted in most of the thin sections by using J. Swift Co., apparatus. Predictions about sandstone provenance were carried out from thin section analyses. In two conglomeratic successions in the field, approximately 200 pebbles were collected and measured in 3 dimensions by using Vernier Caliper and detailed grain size and sphericity analyses were performed in order to give some information about depositional environment and paleocurrent direction.



Figure 2. Location of the total measured section (yellow) and detailed studied section (red) (snapshot taken from Google Earth, www.earth.google.com).

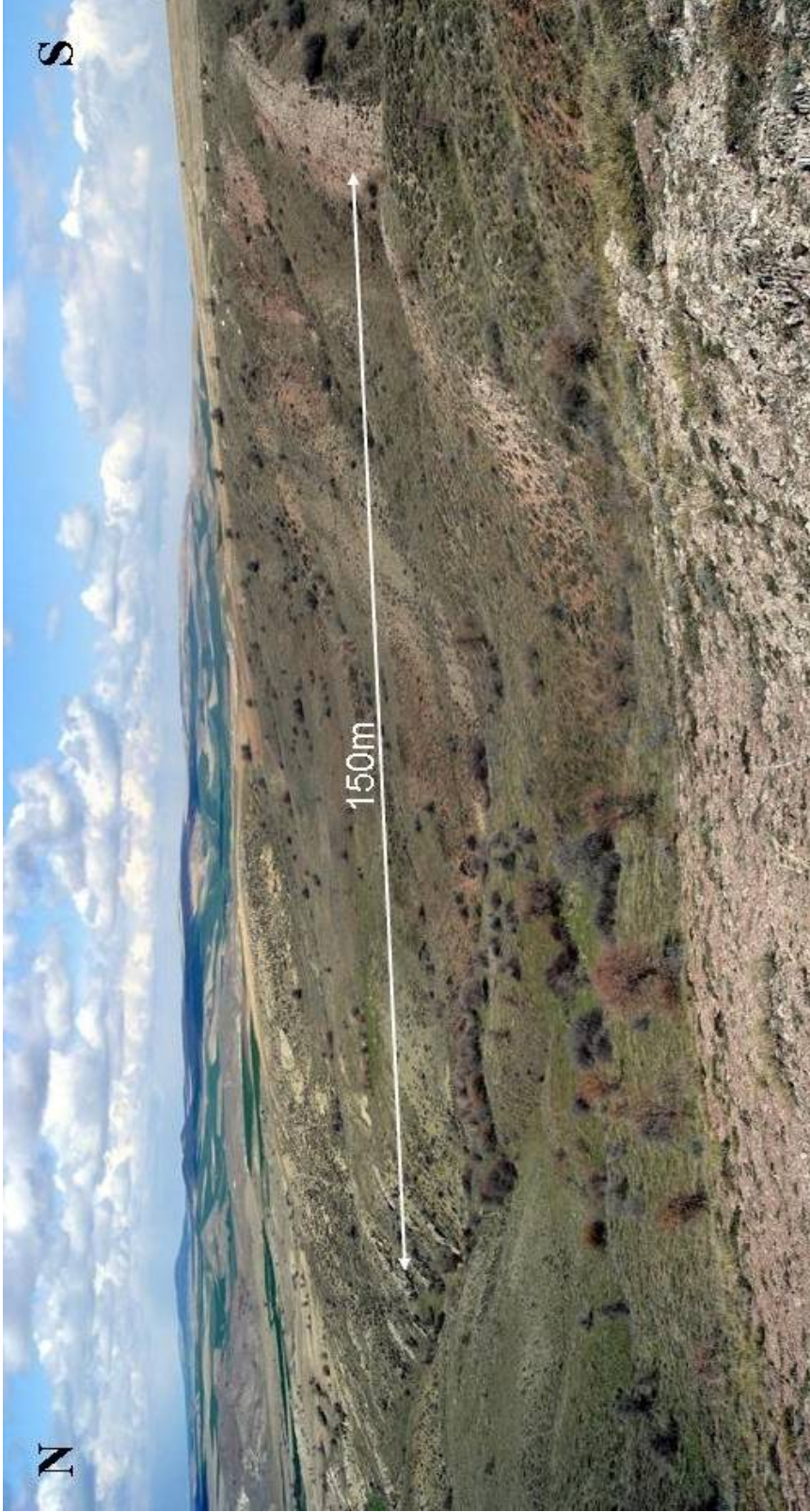


Figure 3. General field view of the measured section (from South to North).

1.4. Previous Work

In the Haymana region, various geological studies were performed for different purposes by many researches over the last century. One of the earliest geological studies in the Haymana region was carried out by Chaput (1936). In his work, Cretaceous and Eocene successions in the Haymana region were recognized and from different outcrop studies he predicted the distribution of flysch sequences in the region. Following study of Chaput, many studies were carried out for scientific and economic purposes (Rigo de Righi and Cortesini, 1959; Reckamp and Özbey, 1960; Schimidt, 1960; Yüksel, 1970; Akarsu, 1971; Sirel, 1975). Ünal et al. (1976) studied the stratigraphy and paleogeographical evolution of the Upper Cretaceous – Lower Tertiary sediments in the Haymana - Polatlı region. A geological map in the scale of 1:25000 for an approximately 2800 km² area was prepared and several stratigraphic sections were measured comprising Mollaresul, Dereköy, Haymana, Beyobaşı and Yeşilyurt Formations spanning in age from Late Cretaceous to Eocene. Among these formations, Cretaceous successions were divided into Dereköy, Haymana and Beyobaşı Formations.

In the Haymana region, the biostratigraphic frame of the Cretaceous to Eocene successions was studied by various investigators. Upper Cretaceous units, of the basin were studied based on planktonic and benthonic foraminifers, calcareous nannoplanktons by Toker (1979), Özcan and Özkan–Altıner, (1999, 1997), Özkan–Altıner and Özcan (1999).

Lithostratigraphic successions of Paleocene-Eocene age are usually characterized by rapid facies changes and the biostratigraphy of these units was based on the systematic description of *Nummulites*, *Assilina* and *Alveolina* species by Sirel and Gündüz (1976). Other paleontologic stratigraphic investigations were carried out by Meriç and Görür (1981), Sirel (1999), Özcan et al. (2001).

Some intervals of the turbidity facies of Haymana region had been thought to be oil saturated for a long time and for this purpose sedimentological study of the oil-saturated sandstones of the Haymana region were performed by Şenalp and Gökçen (1978). They interpreted these oil – saturated turbidite facies as channel

fill sediments deposited in the lower part of the submarine fans which gradually merge into abyssal plain. Along with petrographic work, they also studied the bottom sedimentary structures like flute casts and groove marks, and interpreted the depositional environment as a deep marine basin fill deposit. These sedimentary erosional structures (flute casts and groove marks) were observed also in the field at the bottom of the turbiditic sandstone beds. One of the recent work related with oil exploration in the Haymana basin was carried out by Grove et al. (2000). Their work included that the Haymana Formation constitutes one of the three primary exploration targets in the Haymana-Polatlı Basin. It consists of flysch sediments that contain potentially important turbidite sand units deposited in submarine fans. Oil-impregnated turbidite sands of the Haymana Formation crop out in the eastern portion of the basin on the Çaldağ Anticline and point to a potential play for submarine fan traps in the subsurface. As a conclusion, they all suggested a good understanding of the evolution of the Haymana Basin and careful sedimentological studies of turbidite formations which are essential in finding more proximal parts of the basin where the oil is likely to be accumulated.

The tectonic evolution of accretionary forearc basins in Central Anatolia which have been carried out by many researches (Şengör and Yılmaz, 1981; Görür et al., 1984; Koçyigit et al., 1988; Koçyigit 1991. According to these studies, the Haymana Basin developed within a continental and oceanic collision regime along the northern branch of the Neo-Tethys. Because of the existence of Tertiary calcalkaline volcanism (Galata volcanism), and the presence of ophiolitic basement in the basin, the Haymana Basin was thought to be developed in an accretionary wedge which was active from the Late Cretaceous to the Late Eocene. Arc activity in the Sakarya continent during the Paleocene suggests that subduction was towards the north (Fourquin 1975; Şengör and Yılmaz, 1981). One of the characteristics of the Haymana Basin is its highly deformed sedimentary fill, which is more than 5000 m thick in the center of the basin (Koçyigit, 1991).

The most recent cyclostratigraphic studies, have been performed by Çiner et al. (1993, 1994, 1996) in the Haymana basin. Çiner et al. studied the Middle

Eocene Beldede Braid-Delta Complex (Çiner et al., 1993). They carried out lithofacial analysis and applied sequence stratigraphic concepts in order to interpret the depositional environments and controlling factors exerting on the development of sequences and divided Beldede Braid-Delta complex into elementary units and elementary sequences. The cyclicity in the Middle Eocene Yamak turbidite complex of the Haymana basin has been performed by the same researches (Çiner et al., 1996). This complex represents a prograding submarine fan. It was subdivided into three depositional sequences, each consisting of a turbidite system with sandstone and conglomeratic sandstone beds alternating with mudstones. Each turbidite system has been subdivided into basic sequences which were composed of several basic units. Depositional sequences in this complex have been interpreted to correspond to third – order sea-level cycles of tectonic origin. Çiner et al. (1996) also studied the cyclicity in the Middle Eocene Çayraz Formation mainly made up of carbonates, which represents the youngest lithostratigraphic unit of the Haymana basin. The aim of their study was to describe coarsening-upward and shallowing-upward nummulite-bearing carbonate cycles of different magnitudes and the sequence stratigraphic frame of their study area.

Çiner (1996) studied the distribution of small scale sedimentary cycles throughout some selected basins (Haymana and Sivas basins) in Central Anatolia including the Haymana Basin. The aim of his work was to present the characteristics of small-scale cyclicities observed in different parts of basins and also to carry out their autocyclic or allocyclic origin. Hardgrounds developed on the tops of elementary units of the Çayraz carbonate platform of the Haymana Basin suggests a decrease in carbonate sedimentation created by the rapid rise in sea-level indicating an allocyclic governing mechanism in the formation of the carbonate cycles. However, the mechanism governing the cyclicity in the elementary sequences of Yamak submarine fan of the Haymana Basin is less clear and thought to be controlled by autocyclic processes such as channel shift or lateral accretion. High order cyclicities in the Haymana probably might have been controlled by tectonic processes (Çiner et al., 1993b). Another studies in sequence

stratigraphy and turbidites in Turkey were carried out by Gürbüz (1999), Turgut and Eseller (2000), Varol et al., (2000).

Outside of Turkey, investigations of deep-sea sediments began with the voyage of Challenger (1872-76), which established the general morphology of the ocean basins and type of sediments they contained. Bouma (1962) reported on his analysis of hundreds of graded beds in the flysch of the Pira Cava of southeast France. He demonstrated that there was a preferred sequence of sedimentary structures in each graded bed although many had the top or bottom of the sequence missing. He proposed the ideal turbidite model with 5 subdivisions in a general fining upward trend.

However, researches through the 1970s showed that the Bouma sequence was only strictly applicable to medium – grained sand-mud turbidites. Consequently, parallel sequence models were developed for both coarse-grained (conglomeratic) turbidites (Lowe, 1982) and fine – grained (mud-rich) turbidites (Stow & Shanmugam, 1980). Stow (1984-1986), proposed three fan types (elongate or mud-rich, radial or sand-rich, and fan delta or gravel-rich fans), but also emphasized on the importance of different types of slope-apron and basin plain systems. Combined approaches based on sequence stratigraphy and sedimentary processes in deep-marine clastic systems were studied by many researches from the late 1970s to 1990s (Mitchum et al., 1977; Vail et al., 1977; Mutti, 1985; Posamentier and Vail, 1988; Van Wagoner et al., 1990; Walker, 1992; Posamentier et al., 1993). Sediment transport, facies classification and depositional processes in deep marine environments were investigated by Stow (1994), Stow et al. (1996).

Submarine fan sequence in the forearc basin fill has been recently studied by Ito (1997) in the Boso Peninsula of Japan. He defined chronostratigraphic surfaces in stratigraphic successions of deep marine facies by correlating volcanic ash beds of submarine fan deposits with shallow marine deposits which, in general, are more sensitive to relative sea-level change.

Einsele (1991, 2000) proposed forearc basin types, their general characteristics and sedimentary successions. He divided forearc basins into:

accretionary, residual, constructed and composite basin types as and purposed idealized sedimentary successions for residual basins. He also studied the cyclicity and factors controlling cycles in the deep-sea sediments.

Under the light of all these previous studies, this study has been undertaken in order to investigate the sedimentary cyclicity by analyzing various depositional sequences in the Upper Cretaceous clastic successions of the Haymana Basin. Sequence stratigraphic concepts have also been applied in order to understand the response of these deep-marine facies to sea-level fluctuations.

1.5. Geological Setting

The Haymana basin (presently 60 x 60 km in size Çiner (1996)) is located about 70 SW of Ankara in Central Anatolia (Figure 4). It is a forearc basin that formed on an accretionary wedge (cf. Dickinson and Selly, 1979). This wedge formed during the Late Cretaceous to Late Eocene on the oceanic crust of the northern branch of Neo-Tethys (Izmir – Ankara Suture Zone) by the convergence and collision of the Eurasian continent to the north, and the intervening Sakarya continent (Fourquin, 1975; Şengör and Yilmaz, 1981; Görür et al., 1984, 1989; Koçyigit et al., 1988; Koçyigit 1991) (Figures 4, 5). After the closure of the north Neo – Tethys Ocean, deformation continued until the Late Pliocene. In the studied area, represented successions are spanning in age from Late Cretaceous to Eocene (Figure 6).

The basement of the Haymana Basin, in which the cumulative thickness of the Upper Cretaceous - Tertiary deposits reaches thousands of meters, is composed of the Jurassic – Lower Cretaceous carbonate cover of the Sakarya Continent (Şengör & Yilmaz 1981), the Karakaya Complex forming a part of the pre - Jurassic basement of the Sakarya Continent (Şengör et al., 1980), and the Ankara Melange (Bailey & McCallien 1953, Norman 1975, Ünalán et al., Görür and Derman 1978, Norman et al., 1980). Above this composite basement, mostly above an unconformity and according to the references given above, are turbidites which consist dominantly of sandstone – shale intercalations with frequent conglomerates, olistostromes and debris-flow deposits forming the Haymana

Formation of Late Cretaceous age. This thesis work is mainly related with the investigation of these deposits in the Haymana Formation. These clastics are mainly composed of texturally and mineralogically immature mafic and ultramafic rocks of ophiolitic origin, derived most probably from the Karakaya Complex and the Ankara Melange and metamorphic rock fragments, including composite quartz, and potassic and sodic feldspars derived from the basement of the Sakarya Continent (Ünalán et al., 1976; Görür and Derman 1978). Around the basin margins, deep-sea deposits pass laterally and vertically into richly fossiliferous shallow marine sandstones, shales and limestones with *Hippurites* sp., *Orbitoides* sp., *Cyclolites* sp. with various gastropods and lamellibranches. Because of extensive tectonic deformation, it is not possible to trace the passage from turbiditic strata into shelf and continental outcrops (Çiner, 1992). During Paleocene, deposition of terrestrial redbeds of the Kartal Formation and reefal limestones of the Çaldağ Formation characterized the Basin edges.

The Early and Middle Eocene witnessed the deposition of thick turbidite successions in the central part of the basin, which occupied larger area than its Paleocene predecessor. Eocene turbidites of the Haymana Basin constitute the Eski Polatlı Formation and contain clasts of serpentinite, dunite, peridotite, diabase, basalt, radiolarian chert and glaucophane schist, derived from the ophiolitic mélanges of the Karakaya Complex and the Ankara Mélange, as well as micaschists and amphibolites from the ophiolitic mélange and the Sakarya basement, and rhyolitic lava flows from the Sakarya magmatic arc.

Towards the end of the Middle Eocene, the turbiditic depositional areas of the Haymana Basin began to shrink rapidly. Eocene turbidites graded vertically and laterally into shallow marine nummulitic limestones of the Çayraz Formation and the terrestrial clastic sediments of the Kartal Formation. Both the mélange nappe and the units underlying it were later covered unconformably by terrestrial conglomerates, sandstones, marls, evaporates, and the tuffs of the Mio-Pliocene Cihanbeyli Formation.

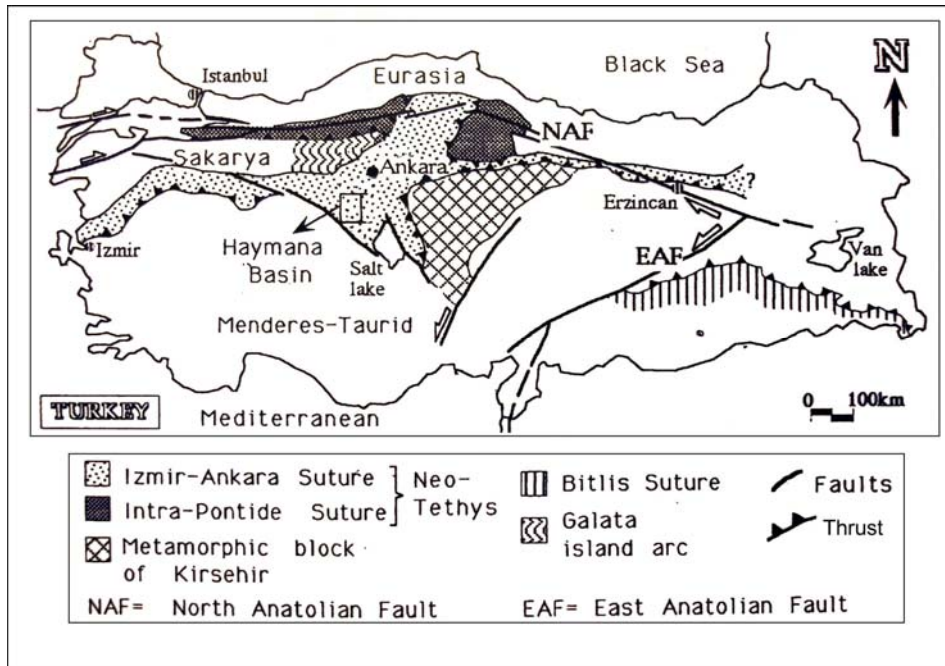


Figure 4. Main structural features of Turkey and location map of Haymana Basin (modified Koçyigit, 1991).

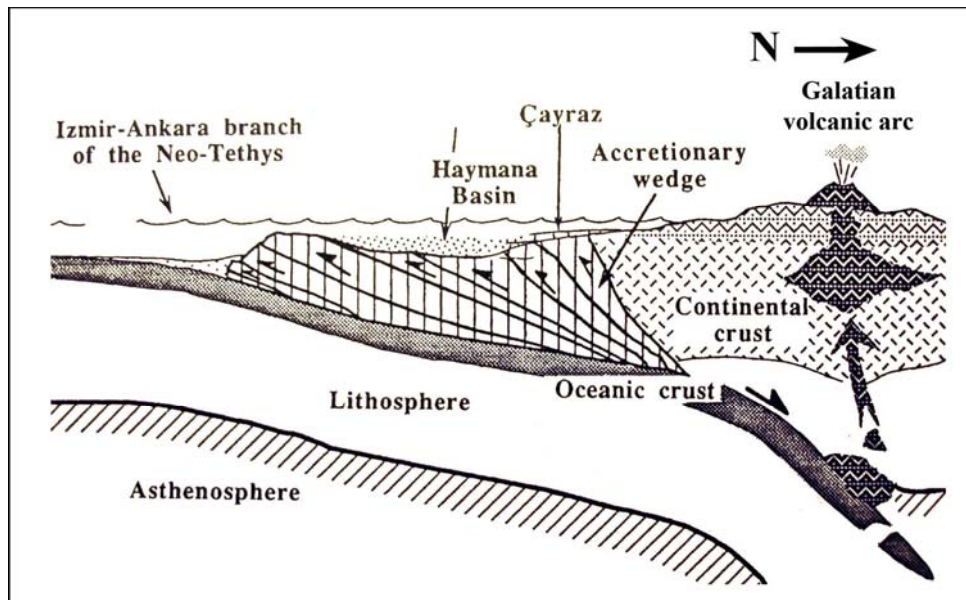


Figure 5. Schematic cross section (not to scale) showing the structural setting of the Haymana Basin during the Campanian to the Lutetian time interval (from Koçyigit, 1991).

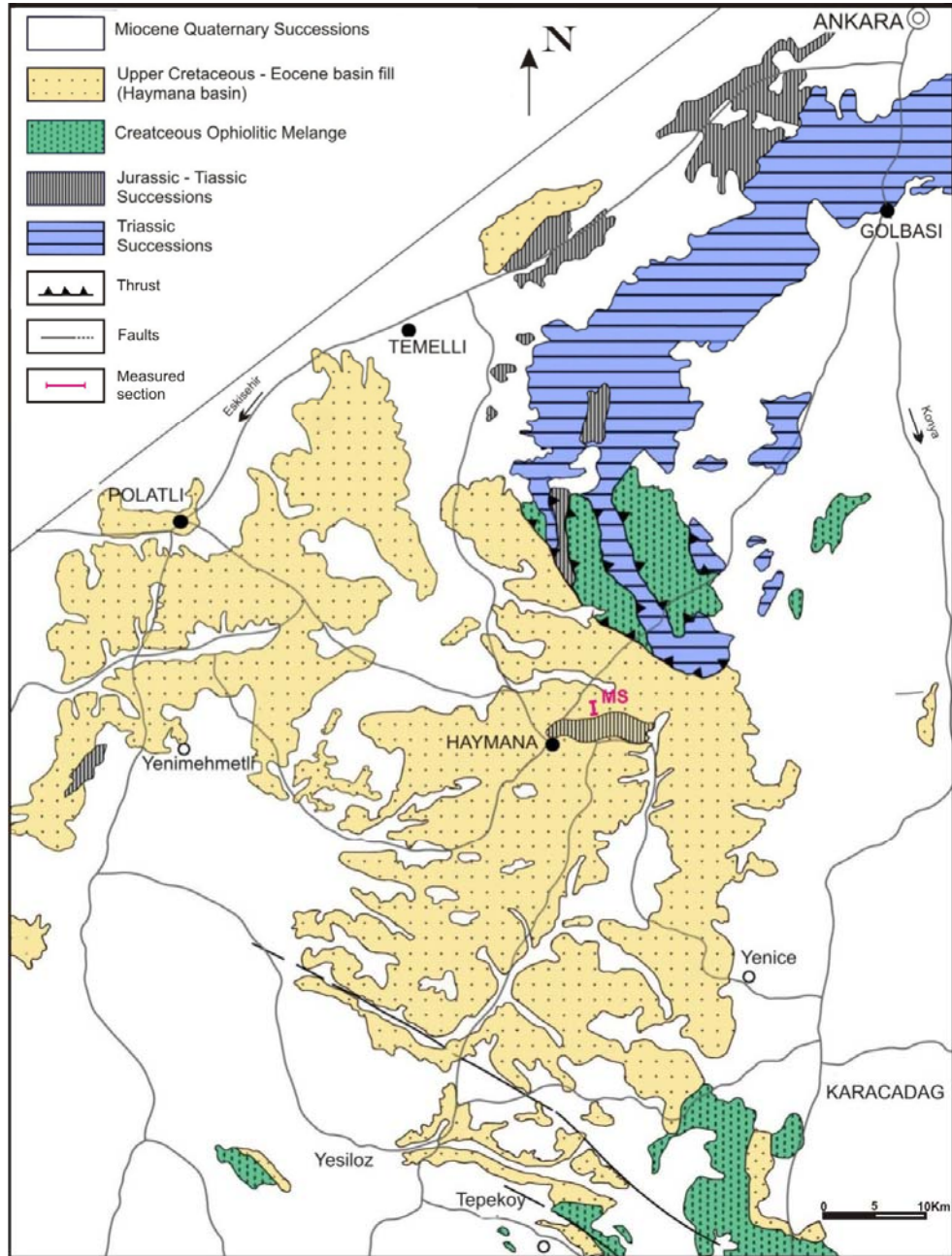


Figure 6. Simplified geologic map of Haymana Basin from 1:500 000 map of Ankara (MTA maps).

CHAPTER II

LITHOSTRATIGRAPHY AND BIOSTRATIGRAPHY

2.1 Lithostratigraphy

Haymana Basin deposits are mainly characterized by Upper Cretaceous to Eocene marine sequences and the total thickness of these deposits is about 5000 m (Koçyigit 1991). The Upper Cretaceous part of these deposits, which we are mainly dealing with this thesis work, is characterized by deep sea sediments consisting turbiditic successions and other mass flow deposits and their total thickness is around 1500 m.

The lower boundary of the Haymana basin deposits has been disputable for a long time and it has been modified in this study. According to our new observations in the field, the base of the Haymana Formation, contrary of what has been defined in Ünalán et al. (1976), rests on the reddish to pinkish beds of the Kocatepe Formation which overlies the Seyran Formation unconformably comprising limestones, shales and breccias (Yüksel, 1970). The Seyran Formation overlies in turn unconformably the thick bedded limestones of the Çaltepe Formation which is probably a block embedded within the matrix of the ophiolitic melange (Figure 7).

At the upper contact, the Haymana Formation is overlain by the Beyobasi Formation consisting of conglomerate and sandstones (Figure 7).

Based on Ünalán et al. (1976) studies, the Haymana Formation consists of shale and sandstone intercalations with frequent conglomerates and debris flow deposits. In the sandstone facies, some sedimentary structures like laminations, normal and reversed grading and erosional bottom structures have also been documented. Conglomeratic deposits are lens like and laterally pass into fine grained deposits. All these deposits have been interpreted to be deposited in the

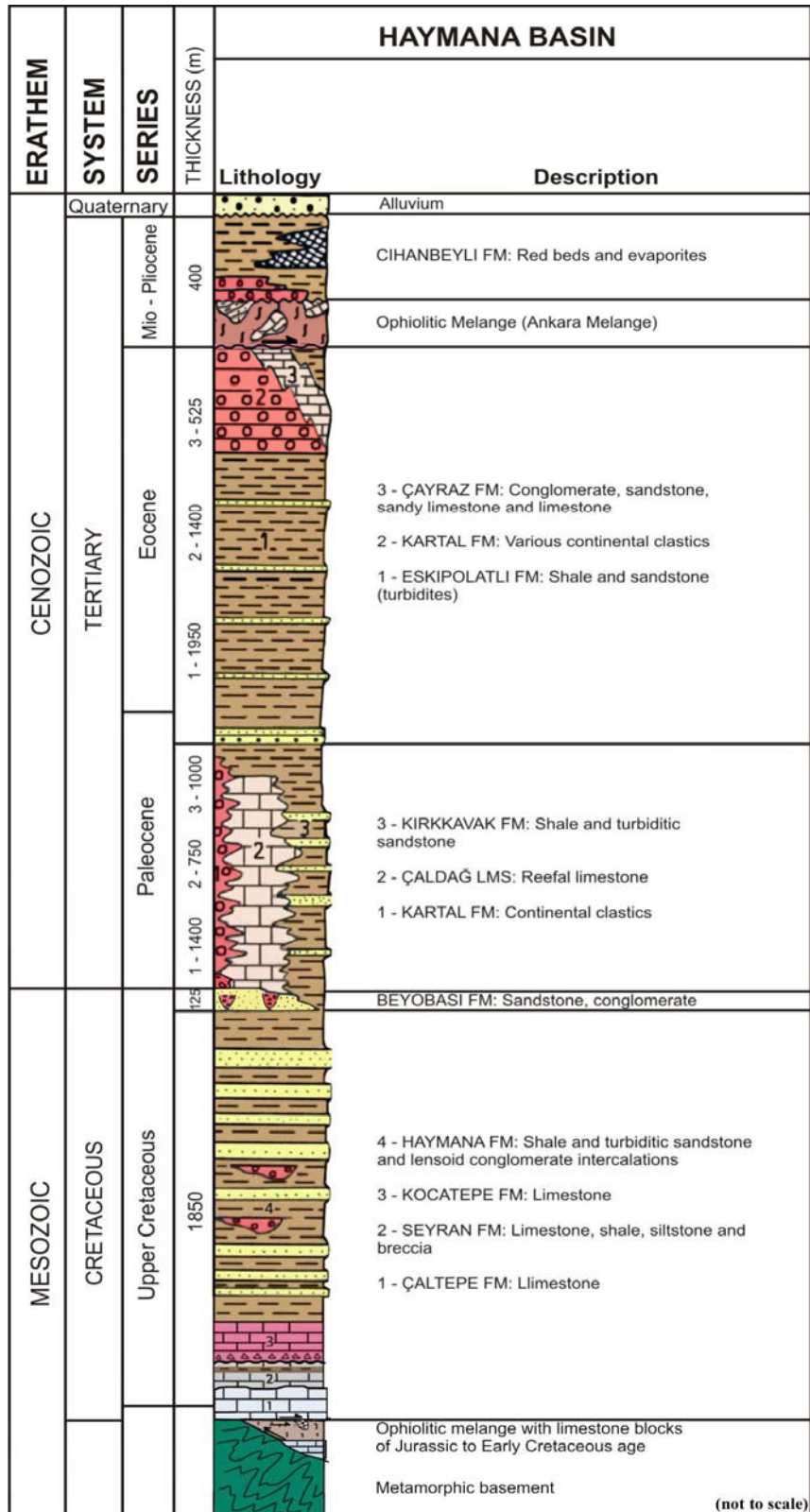


Figure 7. Modified tectonostratigraphic columnar section of the Haymana basin (modified from Unalan et al., 1976).

slope to basin setting within turbiditic systems where active deposition has continued from Late Cretaceous till Early Tertiary time.

In the studied area, the Upper Cretaceous succession of the Haymana Basin is widely exposed. Approximately 250 m thick lithological section has been measured in the field and 150 m of this section has been studied in detail.

The studied section starts at the base with purple to pinkish colored limestones of the Kocatepe Formation of Yüksel (1970) (Figures 7, 8) (Samples 1 - 6). The upper 2 m portion of the formation has been studied and the Haymana Formation starts right after the limestone. This interval is characterized by pinkish to reddish, thin to medium bedded limestones. Limestones are sometimes laminated and interbedded with thin mudstone to shale intervals. The limestone facies is mainly composed of wackestone to mudstone alternations (Appendix B) and silt to sand sized fossil fragments consisting mainly of planktonic foraminifera are abundant. It gradually grades upward into an interval composed of mudstones and shales (Figures 8, 9).

Mudstones are more frequent in the lowermost part of the measured section. They look like massive but at closer look, they consist of thin to medium and thick mudstone layers (Figure 8 and samples 7-8). Their color varies from dark brownish to greenish. The thickness of this fine grained succession in the lower part of the section reaches up to 12 m. Upward along the section mudstone facies grades into shale and sandstone alternations, however in the interval comprising samples and 22, another mudstone interval is observed along the section (Figures 8, 9). Mudstones of this interval are almost identical to lower mudstones except the color and thickness. The color is relatively darker and the thickness, measuring 11 m, is markedly less than that of the lower mudstone. Shales start right after the mudstone bed alternating with sandstone or siltstone in the lower part of the measured section. They are laminated and fissile and the color is mainly greenish. The thickness of the shaly intervals in the lower part of the section reach as sometimes up to 3 m in thickness (samples 13, 19, 24), whereas the thickness decreases to 10 cm in the upper most part of the measured section

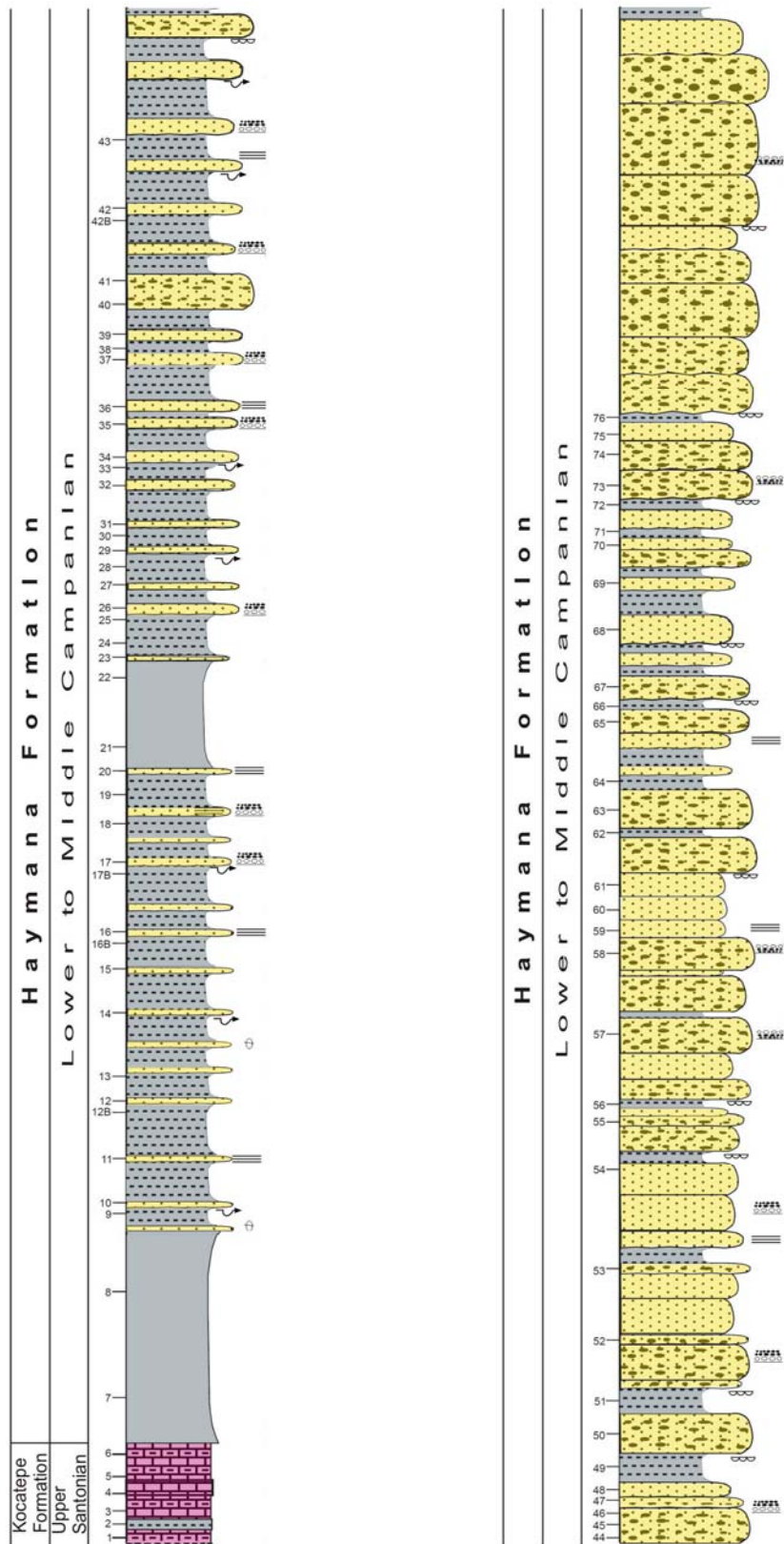


Figure 8. Simplified measured section (for detailed section see appendix A).

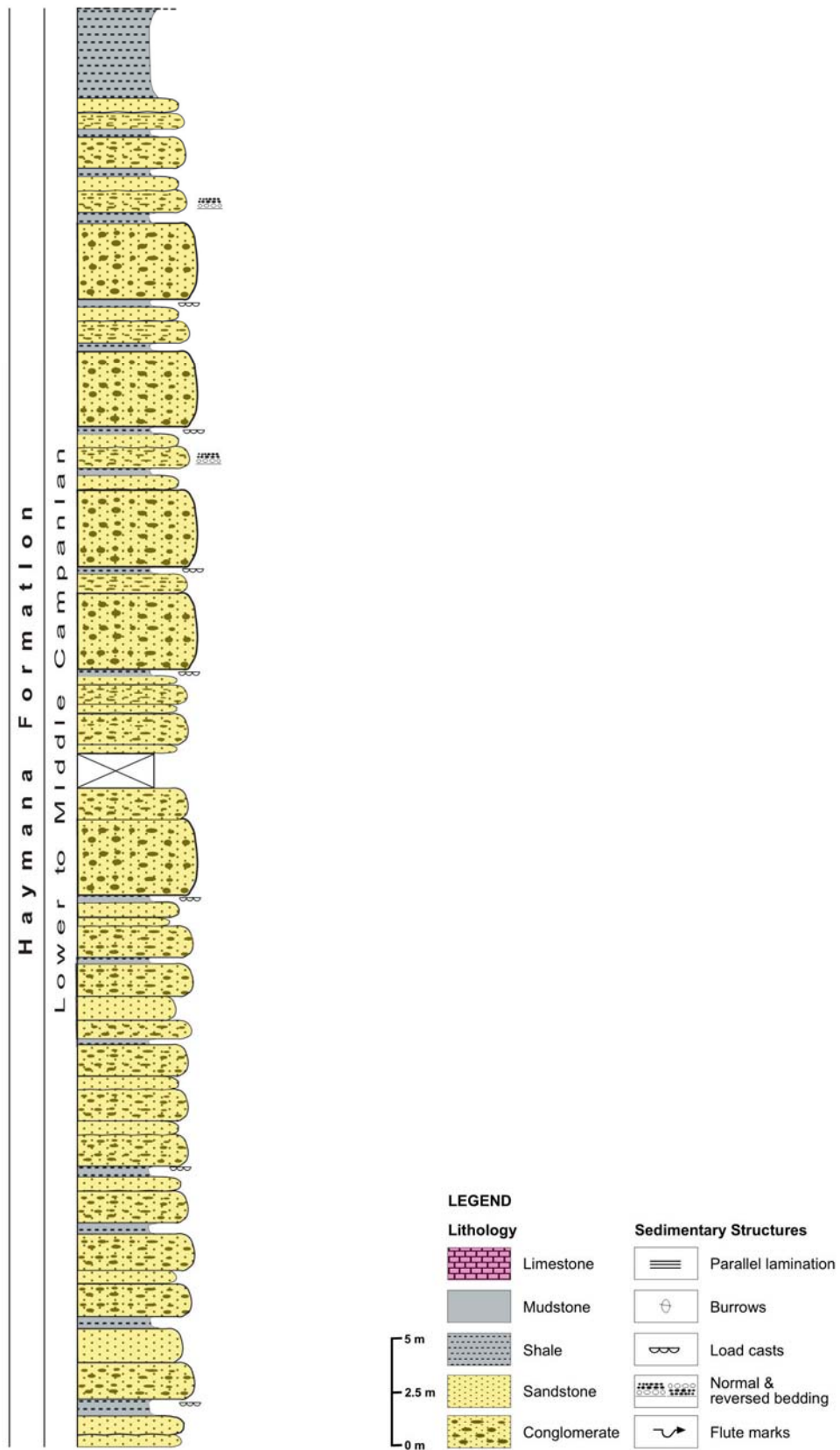


Figure 8. Continued.

where they alternate usually with conglomerates (samples 56, 66, 71,72, 76). The lowermost shale beds (samples 9, 13, 18, 19) are more laminated due to variations in grain size, whereas shales above the level 25 are more fissile and coarser in grain size. There is a clear sandstone - shale alternation along the lower half of the measured section and upward this alternation is getting more frequent (see the interval between the samples 9 to 43).

In the lower parts of the measured section, sandstone beds are thin, 2 - 4 cm (Figures 8 and 9; samples 10, 11, 12, 14)), but upward there is a gradual increase in their thickness which reaches up to 70 cm (Samples 20 – 27; 31 - 39). Their color is mainly greenish. The grain size of sandstones increases upward along the succession. Sandstone beds in the lowermost part of the studied section are laminated and at their bases erosional sedimentary structures have been observed (Figure 10, samples 10, 11, 12, 14, 15, 16, 17, 20). Sandstone beds observed in the upper part of the section are characterized by normal grading and where there are thick, load structures are can be observed (Samples 32, 37). In general, sandstone facies are composed of lithic greywackes, which are abundant in the lower parts of the studied section and litharenites which are mainly observed in the upper most part of the section (Samples 54, 60, 61).

Upward in the studied succession along with sandstone – shale alternations, conglomeratic units are getting common (Figure 11). Conglomeratic successions begin nearly in the middle part of the measured section (Figure 8 (samples 40 - 41). Most of these conglomerates consist of pebble to cobble size grains, however boulder size were also observed in the upper most part of the section in the field (Figure 9). Compositionally these pebbles and cobbles comprise sedimentary (limestone, chert and shale) and metamorphic rocks fragments (slate and schist). The thickness of conglomeratic levels in the middle part of the sections is nearly 1 m in average but the thickness increases along the section. The color of the beds is generally greenish to grey. At closer examination, some textural differences can be observed in the conglomerates. Conglomeratic beds observed in the middle part are matrix supported and no grading can be seen in most of them (Samples 41, 42, 44 - 46), whereas in the upper part of the section conglomerates are grain

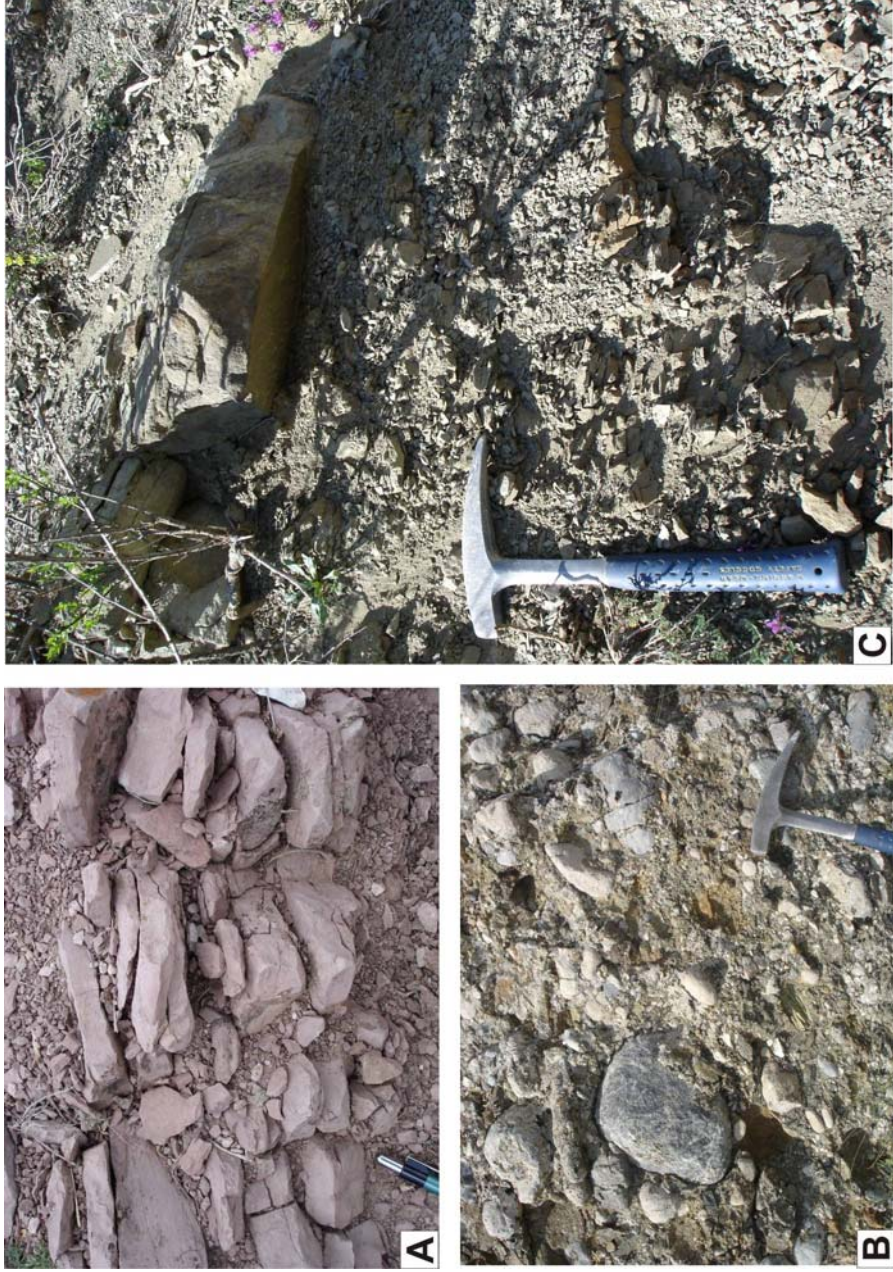


Figure 9. Field photographs of the rock units recognized along the measured section. **A** – Pinkish limestones of the Kocatepe Formation (Upper Santonian), level HAH – 3 – 4 pen for a scale; **B** – Conglomerates of the Haymana Formation, level HAH – 73 (hammer for a scale). **C** – Sandstone - shale alternation in the lower part (HAH - 17) of the Haymana Formation.



Figure 10. Field photographs of erosional sedimentary structures at the bottom of the sandstone beds. **A-** Load casts and groove marks, level: HAH – 32; **B** – Flute marks. Flow from top to bottom, level: HAH – 10.



Figure 11. Field view photograph of the sandstone – shale – conglomerate alternations, levels: HAH 40 to 52.

supported and some normal and reversed grading can be observed (Samples 47, 52, 58, 63 and). Some conglomeratic beds, especially in the upper part of the section, are characterized by multiple grading. At the bottom of almost all conglomeratic beds load structures can be observed. Above the conglomeratic units the measured section finishes with a shale interval. Thickness of this shaly interval is nearly 7 m, and the color is mainly greenish.

In the previous studies the age of the Haymana Formation has been defined as Maastrichtian, based on *Tritaxia trilatera* Cushman, *Dorothia bulletta* Carsey, *Blumina carseyae* Plummer, *Globotruncana arca* Cushman, *Globotruncana conica* White, *Globotruncana stuarti* De Lapparent etc. (Ünalán et al.1976). However our studied portion of the Haymana Formation has been divided into two chronozones and attributed to the early to middle Campanian age (see biostratigraphy chapter).

2.2 Biostratigraphy and chronostratigraphy

Based on the biostratigraphic data obtained from the samples collected along the measured section, the studied sequence has been divided into two chronozones. These are the lower *Dicarinella asymetrica* chronozone and the upper *Globotruncanita elevata* and *Globotruncana ventricosa* chronozones (Fossils were identified by Demir Altınar, METU). The lower chronozone contains several marker species of globotruncanids including *Dicarinella asymetrica*, *Dicarinella concavata*, *Marginotruncana coronata*, *Muricohedbergella flandrini*, etc (Figure 12 Plate-1) and corresponds to the *Dicarinella asymetrica* biozone. This zone indicates a Late Santonian age for the interval of the section (samples 1 - 6) represented by the pinkish to reddish limestones of the Kocatepe Formation of Yüksel (1970). *Dicarinella asymetrica* biozone has been recently redefined by Silva and Verga (2004) as one of the planktonic foraminifera biozones of the Cretaceous system corresponding to the late Santonian. However, the upper chronozone, comprising *Globotruncana hilli*, *Globotruncana linneiana*, *Globotruncana orientalis?*, *Heterohelix globulosa* and

some other species of Cretaceous (Figure 12, Plate-1), is devoid of the main markers *Globotruncanites elevata* and *Globotruncana ventricosa*. In Premoli Silva and Verga (2004), *Globotruncanites elevata* and *Globotruncana ventricosa* biozones have been defined between the *Dicarinella asymerica* and *Globotruncanites calcarata* biozones corresponding to the Upper Santonian and Upper Campanian, respectively.

In this study, the *Dicarinella asymerica* zone has been recognized in the lower most part of the section indicating the presence of Upper Santonian. Yüksel (1970), has reported the *Globotruncanites calcarata* biozone from the northern flank of the Haymana anticline just above the conglomerates of the Haymana Formation corresponding to the uppermost part of our measured section. Therefore, we assign the interval comprising the samples 7 – 76 to the *Globotruncanites elevata* - *Globotruncana ventricosa* chronozones equating with the Lower to Middle Campanian. This chronostratigraphic assignment also confirms that the base of the Haymana Formation is lying very close to the Santonian – Campanian boundary and the main conglomeratic interval of the Haymana Formation is in Early to Middle Campanian age.

In the upper chronozone starting with the sample 20, we have recognized several fossil groups in the reworked limestone clasts in the samples collected along the measured section. These limestone clasts can be categorized into four groups:

1) This group of clasts comprises calpionellids which have been identified in the sample 20. Calpionellids indicate a Tithonian – Valanginian age interval.

2) The second group of limestone clasts contains several planktonic foraminifers. In the sample 37, *Hedbergella infracretacea* indicates an interval from Valanginian to Albian. In the sample 41, the association with *Heterohelix moremani* is assignable to an interval Albian – Coniacian whereas in the sample 58 the assemblage with *Ticinella* sp is probably Albian in age.

3) This group of clasts is characterized by the benthic fossil assemblages. In the sample 57, the clasts include Cretaceous type Miliolidae, however in the sample 37, *Tubiphytes morronensis* is present in clasts indicating an age spanning

from Kimmeridgian to Valanginian. In the sample 74, large limestone clasts contain a well diverse assemblage including *Trocholina alpine*, *Trocholina delepeini*, *Quinqueloculina robusta*. These type of clasts are probably Berriasian – Valanginian age based on the biozonation frame introduced by Altner (1991).

4) This group includes Radiolaria – type pelagic organism and has been identified in the samples 66 and 67.

As a summary, all these reworked clasts indicate ages older than the age of the succession spanning from Late Santonian to Early to Middle Campanian. The clasts of the second group suggesting age Albian or younger than Albian in the interval from the Albian to the Coniacian are most probably derived from the Seyran Formation of Yüksel (1970). This further suggests that an unconformity should be present separating the Kocatepe (Santonian) and Seyran (Turonian - Coniacian) Formations of Yüksel (1970).

PLATE – 1

All specimens x150

Figure 1 – 2. *Marginotruncana pseudolinneiana* Pessagno, 1967. 1: Sample HAH – 1; 2: Sample HAH – 3

Figure 3. *Marginotruncana coronata* (Bolli, 1945). Sample HAH – 3

Figure 4. *Globotruncana linneiana* (d'Orbigny, 1839). Sample HAH – 23

Figure 5. *Globotruncana hilli* Pessagno, 1967. Sample HAH – 23

Figure 6 – 7. *Dicarinella concavata* (Biotzen, 1934). 6: Sample HAH – 3; 7: Sample HAH – 1

Figure 8 – 9. *Dicarinella asymetrica* (Sigal, 1952). 8: Sample HAH – 3; 9: Sample HAH – 1

Figure 10. *Muricohedbergella flandrini* (Porthault, 1970). Sample HAH – 1

Figure 11. *Heterohelix globulosa* (Ehrenberg, 1840). Sample HAH – 3

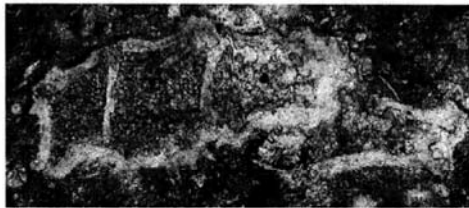
PLATE - 1



1



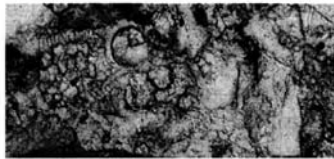
2



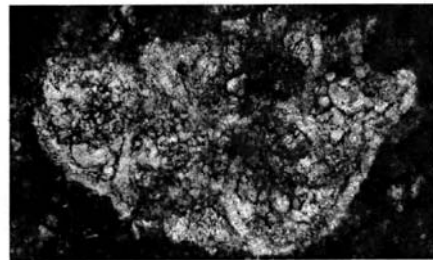
3



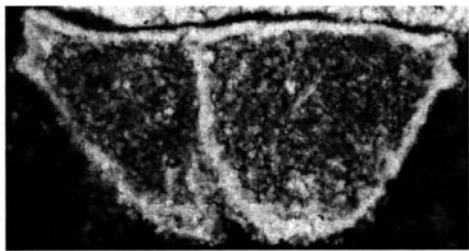
4



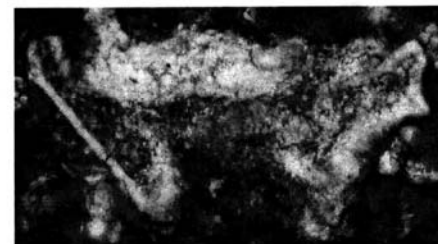
5



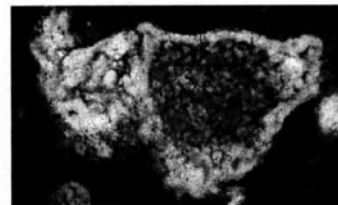
6



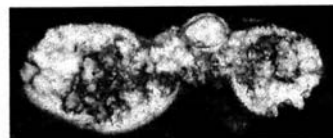
7



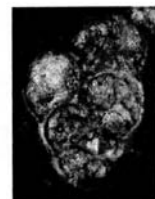
8



9



10



11

CHAPTER III

SEQUENCE STRATIGRAPHY

3.1 Historical Background

Sequence stratigraphy is a subdiscipline of stratigraphy and most recent paradigm in geological thought. Sequence stratigraphy is often regarded as a relatively new science, evolving in the 1970s from seismic stratigraphy. Seismic stratigraphy emerged in 1970's with the work of Vail et al. (1977). The seismic stratigraphic analysis stimulated a revolution in stratigraphy. This new method together with the global cycle chart was published by Vail et al. (1977). Seismic stratigraphy is a geologic approach to the stratigraphic interpretation of seismic data (Vail and Mitchum, 1977). Seismic sequence analysis is based on the depositional sequences. Depositional sequence is defined as a stratigraphic unit composed of a relatively conformable succession of genetically related strata and bounded at its top and base by unconformities or their correlative conformities (Mitchum et al., 1977). However, in 1963 Sloss had defined the sequence as an unconformity bounded rock-stratigraphic units of higher rank.

Sequence stratigraphy provides a powerful tool for stratigraphic analysis of deep – marine clastic systems when it is combined with an appreciation of the variability in processes and depositional products of deep marine settings. This combined approach based on sequence stratigraphy and sedimentary processes has advanced from early studies of the late 1970s, which emphasized simple model-driven interpretations of deep – marine clastic systems based on seismic data (Mitchum et al., 1977; Vail et al., 1977; Mutti, 1985; Posamentier and Vail, 1988; Van Wagoner et al., 1990; Walker, 1992; Posamentier and Weimer, 1993). Turbidity currents are most important transporters of coarse – grained sediments into deep water and, while they were not been observed in deep – marine settings, they have been inferred observations of sequential breaks in submarine telegraph

cables (Heezen & Hollister, 1971). Mutti, (1979, 1985) identified three types of turbidite depositional systems (Figure 13), which he related closely to the volumes of gravity flows and he believed that they were largely a function of sea-level position.

Type 1 turbidite depositional systems consist of thick, extensive lobe deposits that are correlated with large –scale erosional features cut into adjacent shelf edges (Mutti, 1992). They compare with ‘efficient’ mud – rich fan systems (Mutti, 1979).

Type 2 turbidite depositional systems consist of channel – lobe transition deposits that grade basinwards into subordinate lobe deposits. They compare with ‘efficient’ sand-rich systems (Mutti, 1979).

Type 3 turbidite depositional systems are very small. They are formed entirely of thin bedded and graded ‘mud-laden’ units, deposited in small sandstone – filled channels that are restricted to the inner parts of the system.

Our studied turbiditic system can be classified as *Type 2* turbidite depositional system (Mutti, 1979).

Sequence stratigraphy is defined as the study of rock relationships within a chronostratigraphic framework of repetitive, genetically related strata bounded by surfaces of erosion or nondeposition, or their correlative conformities (Van Wagoner et al., 1988). Sequence is the fundamental unit of sequence stratigraphy. A sequence can be subdivided into system tracts which are composed of depositional systems, 3D assemblages of lithofacies (Van Wagoner et al., 1988). System tracts are defined by stacking patterns of parasequence sets or cycles. Cycle is defined as a relatively conformable succession of genetically related beds or bed sets bounded by marine flooding surfaces and their correlative surfaces (Van Wagoner et al., 1988). Meter scale depositional cycles are fundamental stratigraphic units. Cyclicity is defined by the stratal repetition of physical and chemical characters of sedimentary rocks, such as, lithofacies and biofacies (Yang et al., 1998). This stratal regularity is the basis for establishing a high resolution cyclostratigraphy (Yang et al., 1998).

This study documents a detailed study of cyclic sedimentation in the deep – marine siliciclastic deposits of the Upper - Cretaceous successions of the Haymana Formation.

In order to define cyclic sedimentation in the turbiditic depositional system of the studied area, firstly detailed vertical lithofacies association have been carried out and documented in the field. Secondly more detailed microfacies analyses have been performed in the laboratory based on thin section analyses, which will be discussed in the sedimentology chapter.

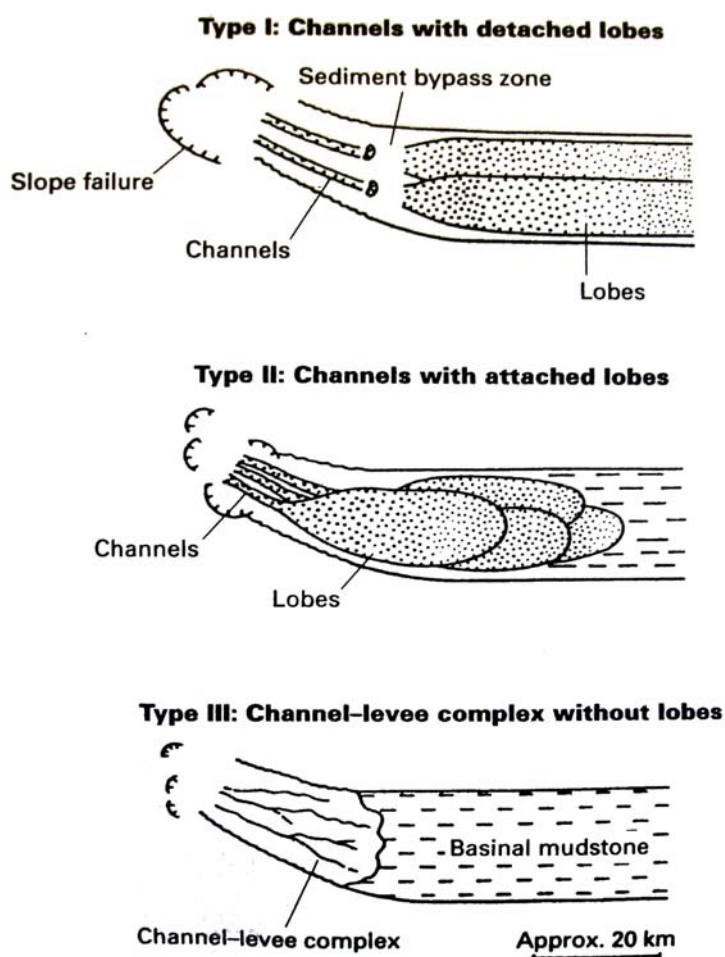


Figure 13. Plan views of the three main types turbidite depositional systems of Mutti (1985).

3.2 Meter – Scale Fining and Coarsening Upward Units

The parasequence is a relatively conformable succession of bed or bedsets bounded by marine flooding surfaces and their correlative surfaces (Van Wagoner et al., 1988). Because a parasequence is bounded by flooding surfaces, recognition of flooding surfaces is the key for establishing a parasequence. In shallow - water environments, it is possible to recognize flooding surfaces because small changes in water depths (i.e., a few m) are reflected in the deposits. However in deep - marine settings minor changes in water depths cannot be easily recognized in all cases and care must be taken in definition of these surfaces (Shanmugam, 1997). However, although in various parts of the basin (such as fluvial, shoreface or submarine fan) cyclic sedimentary patterns are observed, they are not always limited by a marine flooding surface and do not always show coarsening – up tendency. In order to integrate these field observations, the elementary cyclic units is used, which were proposed by Çiner (1996). Elementary or basic cyclic unit is defined as a shallowing or deepening – up unit of several to several tens of meters thick and is environmental dependent contrary to parasequences.

In our study area, where the Upper Cretaceous succession of the Haymana basin is well exposed, perfect repetition of meter scale units (cycles) can be seen and mudstone intervals within studied section were interpreted as an increase in water depths. A section was measured to define the fining and coarsening upward cyclic units. The total thickness of the measured section is 250 m and it contains depositional systems and its smaller subdivisions (Figure 14).

3.2.1 Types of fining and coarsening upward cyclic units

According to detailed lithofacies analyses and their vertical association, the whole section, which is 250 m thick, can be interpreted as one turbiditic system based on hierarchical scheme of Mutti and Normark (1987, 1991), which made up of sandstone and conglomeratic deposits overlain by mudstone deposits. Within this turbiditic system three depositional and basic sequences have been identified,

latter is mainly related with turbidites irrespective of system tracts. To integrate these field observations, each depositional sequence has been subdivided into a medium-scale (5 – 10 m) and small-scale (1 - 3 m) cyclic basic units (Figure 14, 15). Basic units, which were defined on the basis of lithofacies association and their stacking patterns are the building blocks of the basic sequences, and were subdivided into fining upward A – type and coarsening upward B – type cyclic units (Figure 15).

3.2.1.1 Basic sequence no. 1

Basic sequence no. 1 is a 15 m thick fining upward unit. Basic sequence is bounded at the lower part by limestones of the Kocatepe Formation and at the upper part by mudstone deposits of the Haymana Formation. In the lowermost part of this basic sequence, which is mainly characterized by hemipelagic – pelagic deposits, clear limestone – mudstone alternations have been observed. A pervasive feature of both pelagites and hemipelagites is cyclicity (Schwarzacher and Fischer, 1982; Einsele and Ricken, 1991), and the basic cyclic units in within this basic sequence have been defined on the basis of limestone and mudstone alternations (Figure 14, Appendix - A). In general, the first basic sequence is composed of mainly A1 –type basic cyclic units (cycles), which starts with limestone deposits and ends with mudstones (Figure 15).

3.2.1.2 Basic sequence no. 2

Basic sequence no. 2 is a nearly 20 - 25 m thick fining upward unit. This basic sequence (BS) is bounded at the lower and upper parts by massive mudstones and characterized by sandstone and shale alternations, which are defined as cyclic basic units (cycles) and could be interpreted as a low density turbidity currents. In general whole BS no. 2 consist of A 2 – type cycles (Figures 14, 15), which are starting with sandstone beds and finishing with shales. The sandstone bed thicknesses slightly increase upward from 2 to 5 cm. Grading and parallel laminations can be observed in some sandstone beds and Bouma sequences T_{bd} are present. Erosional sedimentary structures like flute and groove

casts 2 - 3 cm in length, are observed on many of the flat soles of the sandstone beds of these cycles.

3.2.1.3 Basic sequence no. 3

Basic sequence no. 3 is a nearly 30 m thick composed also fining upward units. It has the following parts: a lower part of massive mudstones and an upper part composed of laminated shale interval. This BS is also characterized by sandstone shale alternations, which were defined as A2 – type cycles, represented by sandstone at the base and shale deposits at the top (Figures 14, 15, 17). The thickness of sandstones is increasing upward from 2 to 30 cm, whereas thickness of cyclic units is decreasing. These cycles are also represented by Bouma's T_{bd} sequences and characterized by erosional sedimentary structures, and graded beds which are typical characteristics of the turbidites. These cyclic units can also be interpreted as low – density turbidity currents.

3.2.1.4 Basic sequence no. 4

Basic sequence no. 4 is the thickest sequential unit with a thickness nearly 140 – 160 m coarsening and thickening upward sequence. The lower and upper contacts are marked by abrupt changes from sandstone – conglomerate beds to silty mudstones. In contrast to previous two BS, this sequence can be distinguished with its thinner lower muddy part, thicker and coarser sandstone and conglomeratic units, especially in the upper part and thick gravel rich units, which are generally associated with channel fills. There is also decrease in erosional sedimentary structures and increase in load cast structures. Normal - reversed and multiple-grading along with some parallel lamination structures are also presented in the BS 3. The thickness of the sandstone beds normally varies between 0.2 and 1.2 m. Within BS 4 more than seventy basic cyclic units (cycles) have been defined, based on vertical lithofacies association and stacking. At the lower part of BS 4 these cycles are commonly starting with A2 type and A3 type fining upward cycles. In previous two BSs, A2 type – cycles described, and now I would like to

pay your attention on A3 type cyclic units. A3 type fining-upward cyclic units are starting with conglomeratic deposits changing upward into in some cases parallel laminated sandstone deposits and finishing with fine-grained silty deposits. This type of cycles is dominant in the middle and especially in the upper part of the section. A3-type cycles corresponds to Bouma's T_{abcd} , but in some cases complete Bouma's turbiditic sequences are also were observed in the field (Figure 16). Starting from the level of HAH – 51, fining upward cyclic units are changing upward into coarsening upward cyclic units. These coarsening upward cycles are starting with B2 - type cycles, which is starting with shale and finishing with conglomeratic deposits (Figure 17). B3 type coarsening upward cycles are interpreted to become dominant from the level of HAH -57, which are characterized by sandy in the lower part and conglomeratic in the upper part. B1 type cycles are represented by silty in the lower part and sandy in the upper part and this type of cyclic units are abundant in the middle part of the BS 4 (Figure 14). Starting from the level of the HAH – 76, coarsening and/or shallowing upward cycles are changing upward into fining upward cyclic units. These fining upward cycles are also represented by the A2 and A3 type cycles.

3.3 Sequence Stratigraphic Interpretation

Sequence stratigraphic interpretation is based on lithofacies association of fining and coarsening upward cycles. The vertical evaluation of lithofacies, their bounding surfaces, packing and interaction of cycle types within the section is examined to define system tracts and possible sequence boundaries in the measured section. Whole measured section can be interpreted as one turbidite system divided into three depositional sequences (Vail et al., 1977). Within these depositional sequences, system tracts and four basic sequences (fourth-order), and two sequence boundaries have been defined. At the same time, each basic sequence has been divided into smaller sequential subdivisions basic cyclic units (Figure 14).

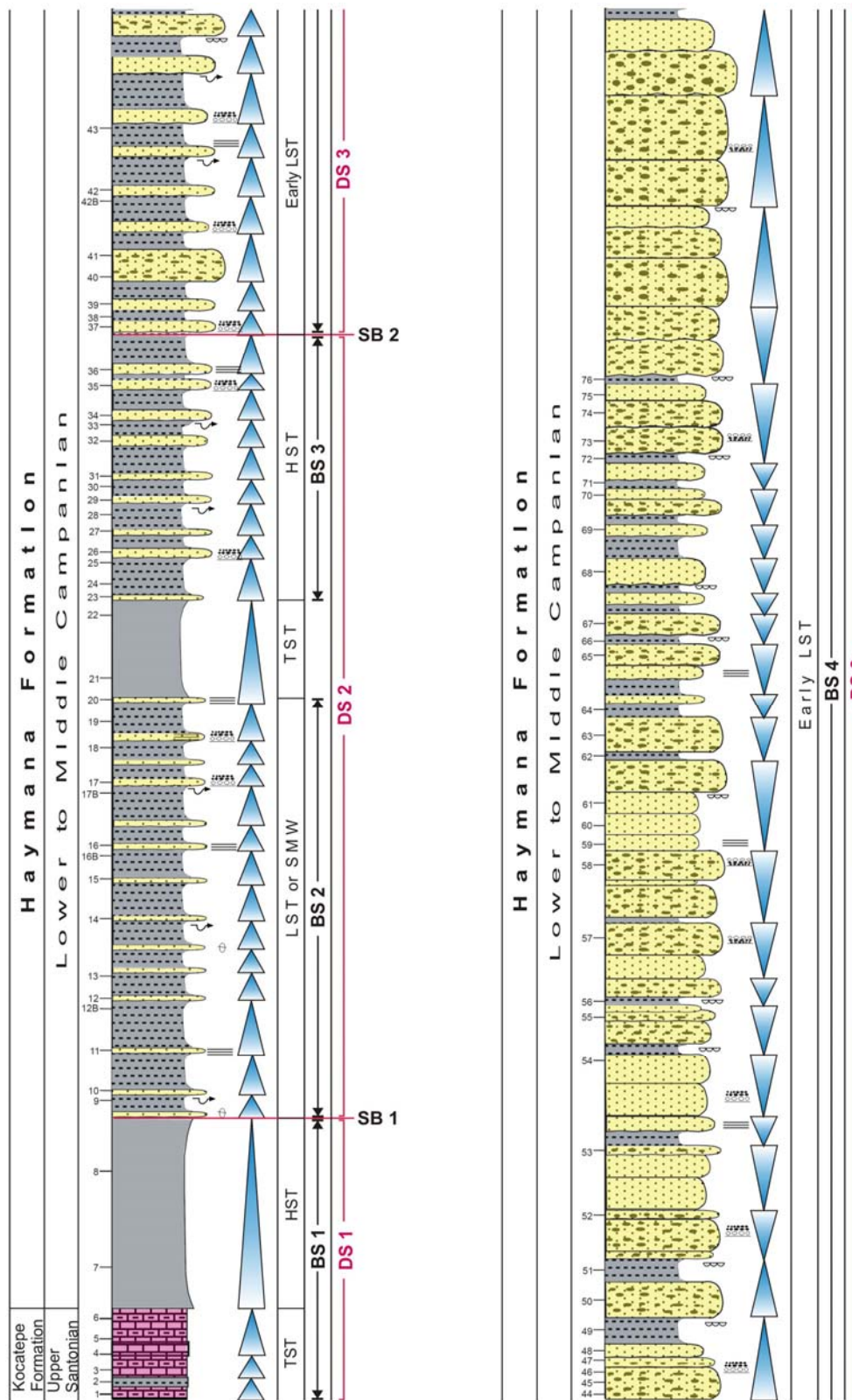


Figure 14. Simplified measured section showing cyclic units and sequence boundaries.

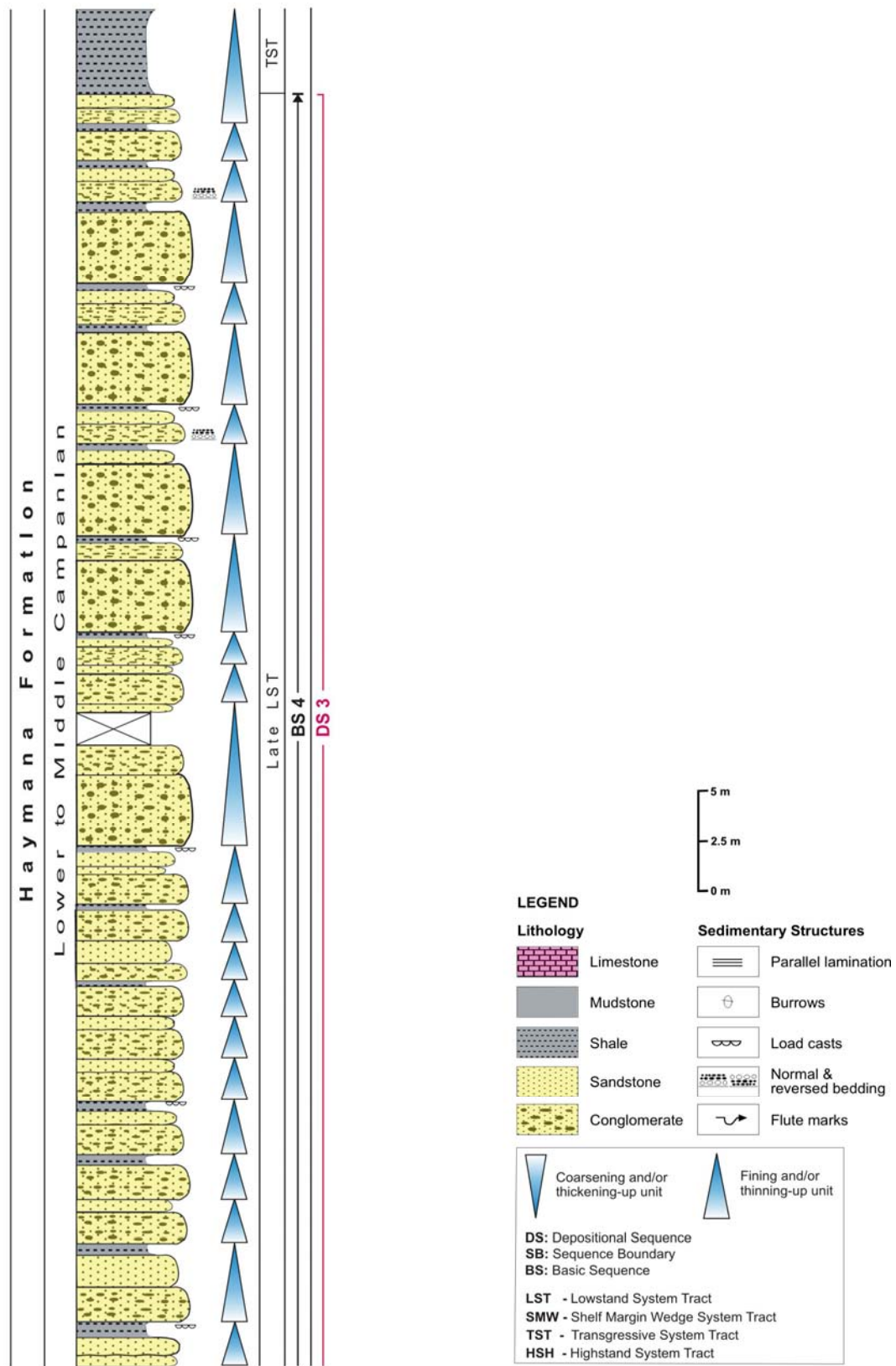


Figure 14. Continued.

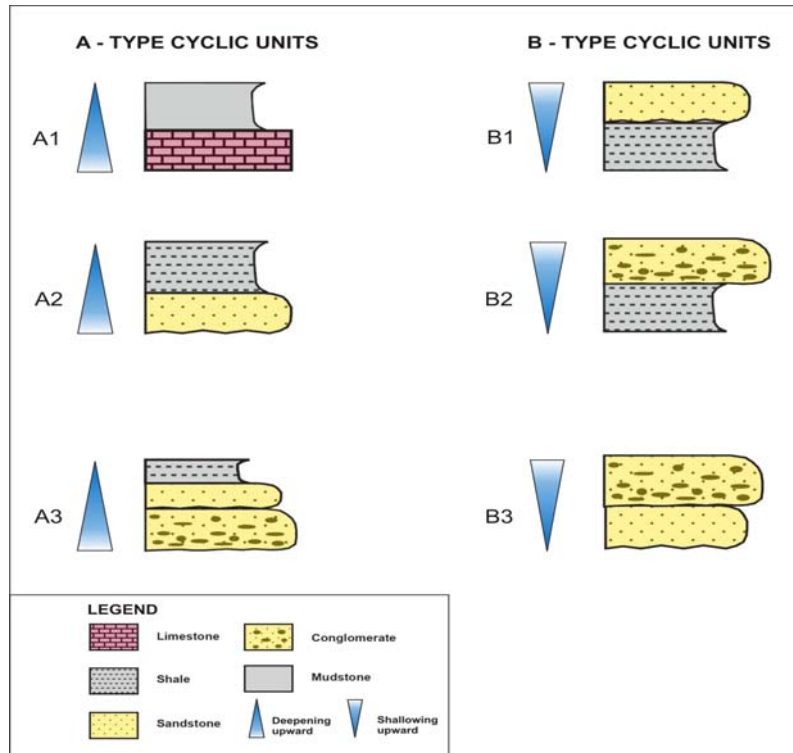


Figure 15. Illustration of A and B-type basic cyclic units and sub-cycles defined within them.

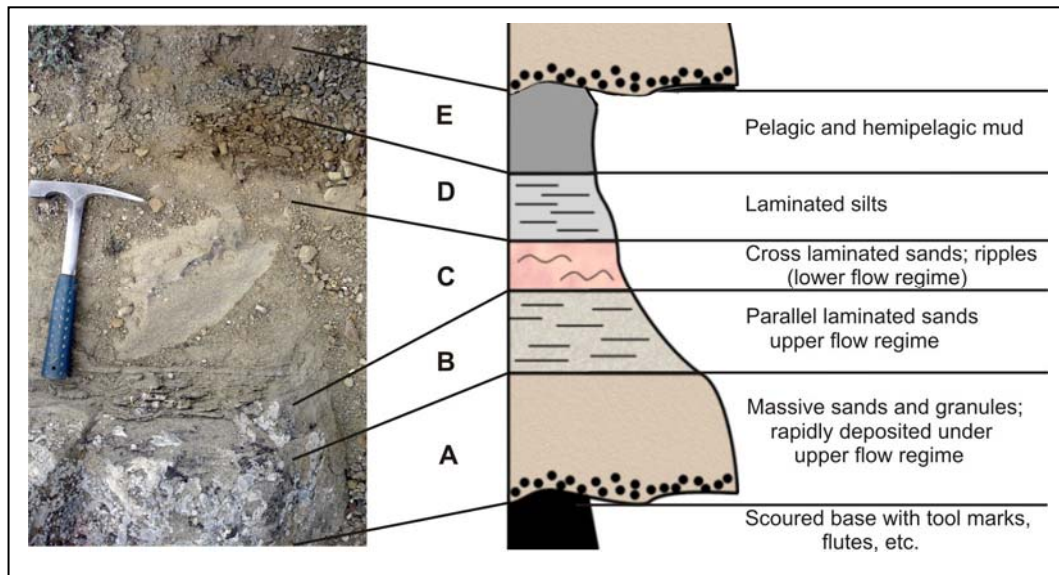


Figure 16. Illustration of complete Bouma's sequences observed in the field and interpreted as A3-type sub-cyclic units (HAH – 55 – 56).



Figure 17. Photographs of coarsening and fining upward cycles (**A** – **B2** type sub-cycles, **B** – **A2** type sub-cycles).

These basic cyclic units are building blocks of the basic sequences and the latter can and/or cannot be correspond to system tracts (Figure 14). Consequently, A - type fining upward cyclic units are mainly related with transgressive system tract (TST) and highstand system tract (HST), whereas B-type coarsening upward cyclic units mainly corresponding to the lowstand system tract (LST) (Figure 14).

Based on our interpretations, the first depositional sequence is incomplete and it is represented by transgressive and highstand system tract. TST of this depositional sequence is characterized by pinkish to reddish hemipelagic to pelagic limestone and mudstone deposits and A1 – type basic cyclic units (Figure 14). Taking into account that it is difficult to define the maximum flooding surface in the deep-marine sequences, which is the surface separating the underlying TST from the overlying HST, we chose this surface at the upper part of the limestone facies (above HAH - 6) (Figure 14). When no turbidities can reach the basin due to relative sea-level high, mudstones are relatively getting dominant. These mudstones are therefore corresponding to the HST. HST continues till level HAH – 9 (Figure 14) and here we defined our first sequence boundary. The first sequence boundary might be interpreted as the type-2 sequence boundary, and probably formed when the rate of sea-level fall was less than the rate of subsidence at the depositional shoreline break.

The second depositional sequence is complete and represented by LST or shelf margin system tract, TST and HST. LST or shelf margin system tract of this depositional sequence is corresponding to basic sequence 2 and characterized by A2 – type fining upward basic cyclic units. LST continues till level HAH – 20, here TST takes over (Figure 14). TST of the second depositional sequence is represented by available finest material within sequence, mudstones corresponding to relative sea – level rise. TST continues till level HAH – 23 (Figure 14). HST is starts above level HAH – 23 and characterized by A2 – type basic cyclic units and corresponds to basic sequence 3, which continues till the level HAH – 37. At the level HAH – 37, the second sequence boundary has been defined (Figure 14). The second sequence boundary can be interpreted as the type 1 sequence boundary, which forms when the rate of sea-level fall exceeds the rate

of subsidence at the depositional shoreline break (usually at base level or at sea level).

The third depositional sequence is again incomplete and consists of LST and partially recognized TST deposits. Although deposition in deep –marine settings can occur any time when sediments are transported by gravity flows towards the basin, the highest sand/mud ratio and coarse grained conglomerates probably occurs during lowstand sea - level, when rivers bypass the shelf and deposition takes place on the slope or by distribution through channels into the deep-sea fan system. In comparison previous two depositional, this sequence is thicker and characterized by various types of basic cyclic units consisting of A2, A3, B1, B2, B3 - type cycles available the coarsest conglomeratic deposits (Figure 14). Conglomerates observed in this depositional sequence are thick and amalgamated. LST of the third depositional sequence corresponds to basic sequence 4 and finishes at the uppermost part of the measured section, where system is changing to mud-rich again; the latter has been interpreted as TST deposits of the third depositional sequence.

3.4 Origin and Duration of Cycles

In the studied interval of the Haymana Formation, the vertical succession of the lithofacies delineates fining and coarsening upward cyclic units. Vertical basic sequences and cyclic unit analyses are made by the fact that facies, stratal thickness and correlative conformities in deep marine siliclastic rocks are systematically grouped within a hierarchy of chronostratigraphic units.

The sedimentary record has stratigraphic cycles of different orders, defined by duration, first order (>100 my), second order (10-100 my), third order (1-10 my), fourth order (0.1-1 my) and fifth order (0.01-0.1 my) (Vail et al., 1977; Goodwin and Anderson, 1985; Van Wagoner, 1988; Cross, 1988 etc.) Causes of these cycles are primarily eustatic and tectonic events. The first-order cycles relate to plate reorganization (Vail et al., 1977), second-order cycles are driven by glacio – eustatism and change in ocean basin volumes (Vail et al., 1977). The

mechanism responsible for the third and fourth order cycles is most probably glacio-eustatism and intraplate stresses (Goodwin and Anderson, 1985; Van Wagoner, 1988) (Table 1).

At the same time, high frequency, 4th, 5th or higher order, depositional cycles are the building blocks of large scale lower frequency (3rd order) depositional sequences. These high frequency cycles are climatically driven sea level changes and their amplitude depends on the global ice volume, the records of ocean volume changes, climate, subsidence and compaction (Fraizer, 1974; Busch and Rollins, 1984; Mitchum and Van Wagoner, 1991). These short periods lie within the range of the Milankovitch frequency band and glacio-eustasy caused by drastic climatic change (Einsele et al., 1991). These higher order cyclic patterns can be identified as Milankovitch cycles. These climatic variations are resulted from cyclic changes in the orbital parameters of the Earth. These orbital parameters are the eccentricity, the obliquity and the precession.

Based on biostratigraphy, studied interval in the Haymana Formation indicates a time interval from Early to Middle Campanian. When we look at the chronostratigraphic chart (Harland et al., 1989), this period corresponds to approximately 3.5 My in duration. From this, by counting the number of depositional sequences, basic cyclic units (Appendix - A) presented in the studied interval, we can roughly estimate the duration of these cycles. Then, if we assume an allocyclic origin for above described cyclic origin for the above described cycles, we may consider a possible correlation with other allocyclic sequences proposed in literature (Table 1).

The 1 – 5 My duration of third – order cycles may correspond to our depositional sequences. When compared with global sea – level chart, we may observe that defining our depositional sequences as a third – order, coincides with sequence boundaries and global - cycles defined by Haq et al. (1988) within studied time interval (Figure 18).

Accordingly, the fourth – order cycles may correspond to our basic sequences, with a time interval span estimates between 0.1 and 1 My. Vail and Hardenbol (1979) considers glaciations as the only mechanism capable of

producing rapid sea – level fluctuations such as those involved in third – and fourth – order cycles. However, several authors (e.g., Cloetingh, 1986; Watts et al., 1982; Allen, 1990) think that tectonic processes are at least as important and claim that intraplate stresses as well may create similar fluctuations. However, in active

Table 1. Possible correlation of cyclic units observed in the studied interval with other cyclic sequences proposed in literature.

Order		Estimated duration	Comparable to	Causes
2 nd		5 to 50 My	Transgressive – Regressive Cycles Supercycles (Vail et al. 1977)	Plate motions
3 rd	Depositional sequence	1 to 5 My	Depositional Sequences (Vail et al. 1977)	Glacio-eustatism and intraplate stresses
4 th	Basic sequences	0.1 to 1 My	Parasequence sets (Van Wagoner, 1988) PACs sequences (Goodwin & Anderson, 1985)	
5 th	Basic cyclic units (cycles)	10 000 to 100 000 years	Parasequences (Van Wagoner et al. 1988) PACs (Goodwin & Anderson, 1985) Progradational events or Baselevel transit cycles (Cross, 1988) Transgressive – Regressive Units (Busch & Rollins, 1984) Genetic stratigraphic sequences (Frazier, 1974; Galloway, 1989) Genetic sequences (Busch, 1971) 5 th order sequences (Mitchum & Van Wagoner, 1991)	Milankovitch Cycles

margins, where the frequency of tectonic events is greater than of eustatic changes, sequence may development responds to the integrated effects of both these parameters (Posamentier et al., 1991). Taking into account, the absence of glaciations in the fore-arc setting of Haymana Basin during the Campanian, collisional tectonics, rather than eustasy, seems to be a better candidate for an origin of our depositional sequence (turbidite system) and basic sequences in the Upper Cretaceous successions of the Haymana Basin.

Consequently, the fifth – order cycles, which are thought to be developed over intervals of between 10 000 and 100 000 years. In the studied section, nearly 130 basic cyclic units have been defined (Appendix A).

Assuming that our studied section is 3.5 My, when we divide it by our basic units, roughly estimation of these cycles will be 27 000 years (all cycles are not in the same hierarchy). Consequently, basic cyclic units might correspond to fifth – order cycles, which could be related to Milankovitch cycles.

CHAPTER IV

SEDIMENTOLOGY

Sedimentological investigations of the measured section include petrographic, and sedimentary analyses such as interpretation of sedimentary structures, provenance, grain size and sphericity. Measurements of the sedimentary structures were carried out in the field using hand lens. Petrographic study was performed on thin sections of the samples collected along the measured section. Grain size analyses include sphericity, sorting and calculation of median and mean grain size parameters. Additional sedimentary analyses include provenance and palaeocurrent studies were also carried out.

4.1 Petrography and Classification of Lithofacies

Seventy six thin sections were examined in detail for the petrographic study. Standard petrographical techniques using a polarising microscope were employed to describe the thin sections. Thin sections were also point-counted using a Swift automatic point counter. A total of 750 - 1000 points were counted per thin section. These quantitative data were used to establish the composition and also classify the rocks. Based on these laboratory analyses performed on each sample collected from the field, five types were defined in the studied interval comprising the Kocatepe and the Haymana Formation. These are 1) limestones, which are classified as wackestones and mudstones; 2) mudstones; 3) shales; 4) sandstones classified as litharenites and lithic greywackes, and 5) conglomerate, which are orthoconglomerates (clast - supported) and paraconglomerates (matrix - supported).

4.1.1 Limestones

Limestones were classified by using R. J. Dunham (Figure 19) classification (Tucker, 2001). R. J. Dunham divides limestones on the basis of texture into: *grainstone*, grains without matrix; *packstone*, grains in contact with matrix; *wackestone*, coarse grains floating in a matrix; and a *mudstone*, micrite with few grains. By using this classification, limestone interval in the lower portion of the measured section, was classified as either wackestone or mudstone (Appendix B).

4.1.1.2 Wackestones

This rock type contains an average of 78% and a maximum of 87% matrix, which is mainly composed of lime mud and stained with iron oxide. Bioclasts constitute 12 – 28 % of the rock volume, which are commonly represented by planktonic foraminifera, 0.5 - 2% of silt to clay size quartz fragments and some 0.3% accessory minerals (opaque) (Appendix B). In general, this lithofacies is matrix supported and grains are floating in the matrix (Figure 20). Matrix contains few iron oxides in the fissures.

4.1.1.3 Lime Mudstones

This rock type was interpreted only in three levels (samples HAH – 2, 4, 6) and contain an average of 90% of matrix, which is again composed of lime mud and stained with iron oxide. Bioclasts constitute less than 10% and an averaging 5% of the rock volume. Accessory minerals, including mica (muscovite), are present in all samples in minor amount (0.5%). Silt to clay size quartz fragments constituting 1 - 2% of the rock volume.

4.1.2 Mudstones and Shales

Mudstone and shale rocks were classified during the field works by visual estimation and using hand lens. Mudstones have been defined by its indurated, massive and non-fissile structure, whereas shales were laminated and fissile.

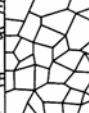
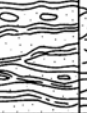
Original components not bound together during deposition				Original components bound together	Depositional texture not recognizable Crystalline carbonate	Original components not organically bound during deposition		Original components organically bound during deposition			
Contains lime mud		Grain-supported	Lacks mud and is grain supported			>10% grains >2mm	Matrix supported	Supported by > 2mm components	Organisms act as baffles	Organisms encrust and bind	Organisms build a rigid framework
Less than 10% grains	More than 10% grains										
Mudstone	Wackestone	Packstone	Grainstone			Boundstone	Crystalline	Floatstone	Rudstone	Baffle stone	Bindstone
											

Figure 19. Classification of limestones based on depositional texture, Embry A. F. and Klovan J. E., 1971 (after Dunham R. J., 1962).

4.1.2.1 Mudstones

This type of rocks have been documented only in four intervals (HAH- 7, 8, 21, 22) within the studied section. Mudstones contain an average of 86% and a maximum of 96% matrix, which is mainly silt-clay sized quartz and clay minerals and sometime stained with iron oxide. Quartz minerals comprise of average of 10% and range from 2% to 21% by rock volume. Accessory minerals, including mica are minor 1 – 2%.

4.1.2.2 Shales

Shales are abundant in the studied interval of the Haymana Formation (Appendix - B) relatively to mudstones and represented mainly by siltstones . This type of rock contains an average 90% and range from 60% to 94% clay matrix and several silt size minerals. These are quartz, mica and accessory minerals (Figure 21). Presence of quartz is the most common ones among the mentioned minerals and their percentage value ranges 10 – 15%. All samples contain, micas and heavy minerals, in minor or trace amounts. Both muscovite and biotite occur in all samples 0.5 - 1%, but muscovite is more abundant. Heavy minerals, present which is commonly opaque iron oxides (0.1 – 0.5%).

4.1.3 Sandstones

Sandstones were classified either litharenite or lithic greywacke by using Pettijohn et al. 1987, classification (Figure 22 and Appendix - B). The classification scheme is based on a triangular diagram with end members of quartz (Q), feldspar (F) and rock fragments (L). Sandstones are divided into two major groups based on relative amount of grains and matrix, that is, whether the sandstones are composed of grains only, the *arenites*, or contain more than 15% matrix, forming the *wackes*. Litharenite is applied where the rock – fragments content exceeds 25% and is greater than feldspar and lithic greywacke refers to a wackes with more than 15% matrix and/or cement and rock fragments exceeds feldspar.

4.1.3.1 Litharenites

This type is not prevalent relatively to lithic greywackes and only interpreted in seven levels (Appendix - B). Minerals or mineral groups, identified in the sandstones, are quartz (polycrystalline was common with minor monocrystalline), feldspar, calcite, (mainly as cement), heavy minerals, mica, amphibole and pyroxene. The quartz component of these samples is an average of 16% and a maximum of 32% and dominated by mainly polycrystalline and some monocrystalline quartz showing straight extinction. The grains are sub-angular to angular with angularity generally increasing up-section. Plagioclase feldspar comprises the majority of the feldspar component 0.5 – 1%, with only minor orthoclase in most of the samples. Mica minerals are dominated by biotite, which contains an average 2% and range from 1% to 6%. The cement is calcite comprising an average 10% of the whole rock volume. Litharenites contain an average of 15% matrix. It consists of silt-sized quartz and clay minerals. Igneous and metamorphic minerals are minor, comprising of average of 0.5 - 2%, which are mostly amphiboles and pyroxenes. There are huge amount of rock fragments in sandstone lithofacies, which will be discussed later.

4.1.3.2 Lithic greywackes

This type of rocks is the most abundant in the measured section and defined in 27 levels. Following minerals were identified in these samples, quartz, feldspar, calcite, mica, amphibole, pyroxene and minor clay minerals, chlorite/glaucanite (Figure 23). The most common mineral is quartz (polycrystalline was common), and, in average, lithic greywackes contain 20 – 35% quartz in the lower parts of the succession. However, the amount decreases down to 10 – 15% upward in the succession. These samples are also dominated by mainly polycrystalline and minor monocrystalline quartz showing straight extinction. The grains are sub-angular to angular with angularity generally increasing up-section. Plagioclase feldspar is ranging between 0.5 – 1%. Biotite comprises the majority of the mica minerals 2 – 3%, with minor amount of muscovite in most of the samples (Appendix B). Cement is mainly calcite, and constitutes in average 25 – 30% of the rock volume and shows slight decrease upward along the section. Pyroxene and amphibole minerals are also observed.

4.1.4 Conglomerates

Conglomeratic beds are abundant in the middle and in the upper parts of the studied section. These beds are composed of pebble, cobble and boulder size clasts of sedimentary, metamorphic and volcanic origin and almost in all samples sedimentary clasts are dominant. Conglomerates are polymictic and have been classified by using clast – matrix relationships and they were separated into two types, which are orthoconglomerates (clast-supported) and paraconglomerates (matrix – supported) based on the classification Tucker (2001).

4.1.4.1 Orthoconglomerates

This type of rock is matrix poor (80% or more framework grains) and has an intact, stable, grain supported matrix. These lithofacies were interpreted only in four levels (HAH – 44, 46, 55 and 57). Among the minerals recognized in the orthoconglomerates, quartz ranges in average of 6 - 8%; mica minerals 1 – 1.5%, which consist of biotite. Accessory minerals, are extremely rare but still observed

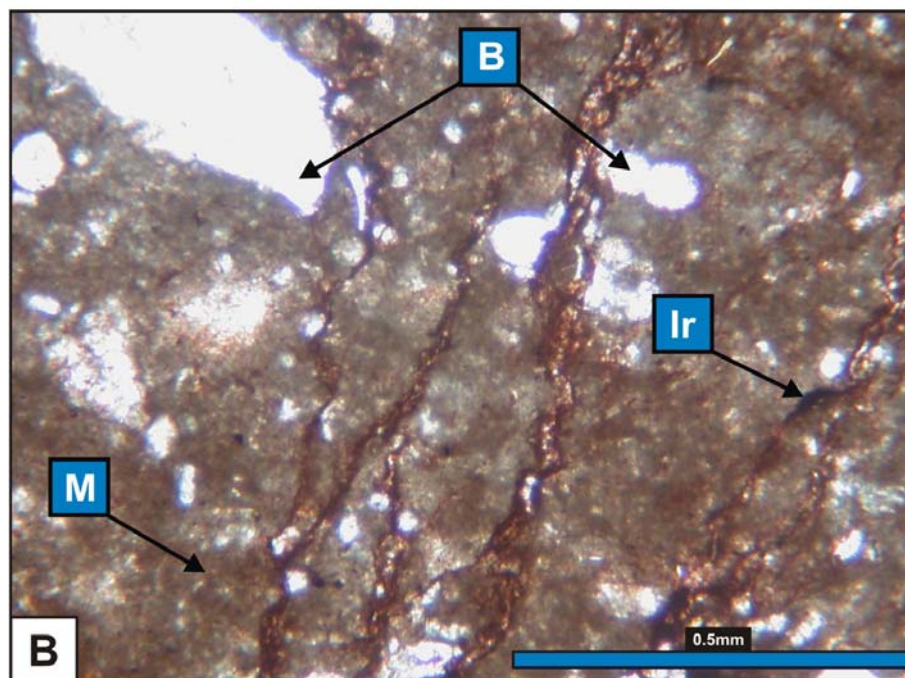
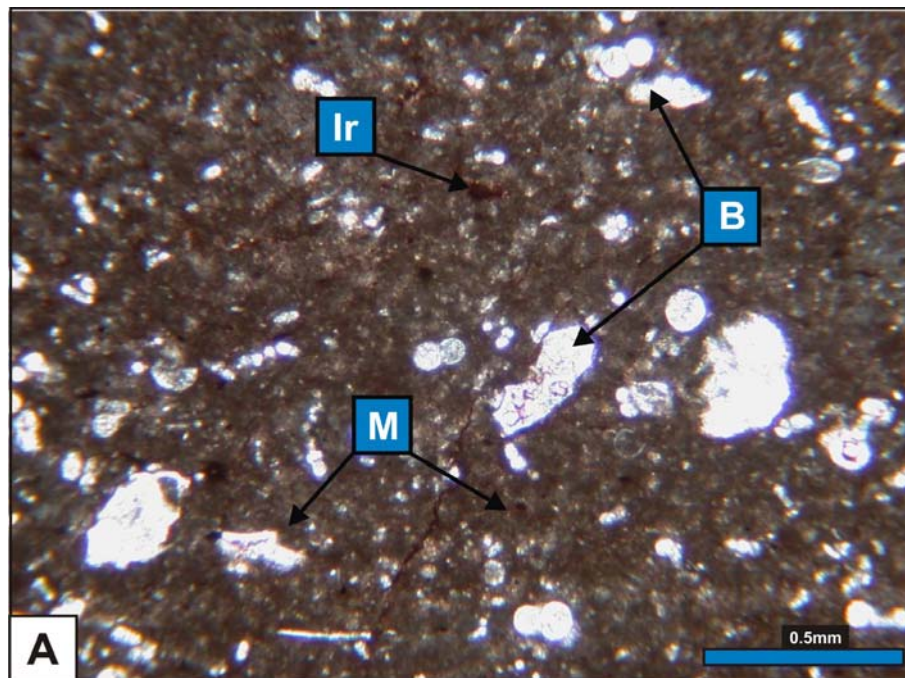


Figure 20. Photomicrographs of the limestones - wackestones, (**M** – matrix (limy mud), **Ir** – iron oxide in the fissure, **B** – bioclast (planktonic foraminifera)), (**A, B**: HAH – 1)

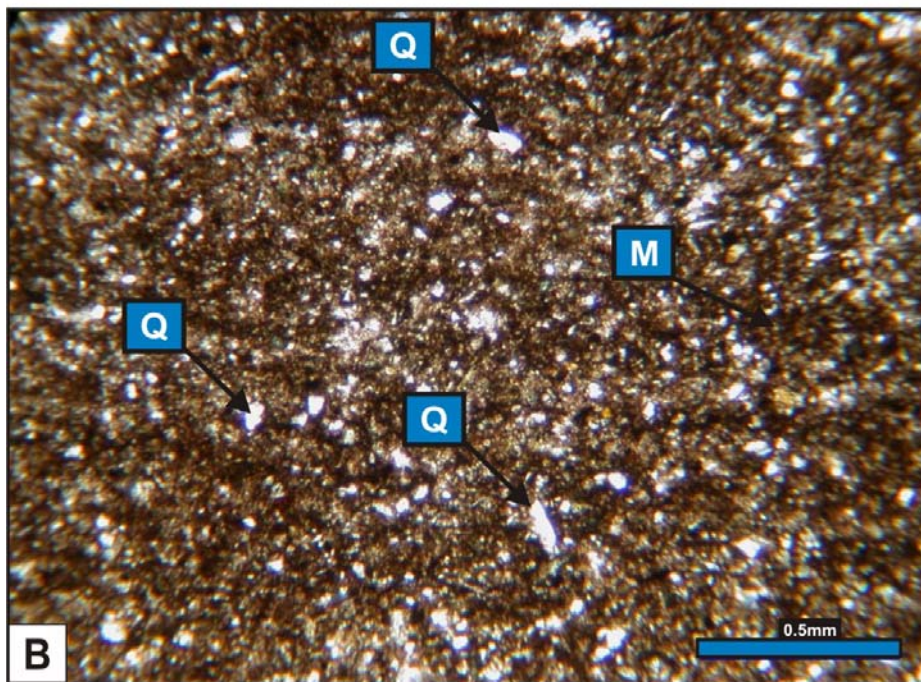
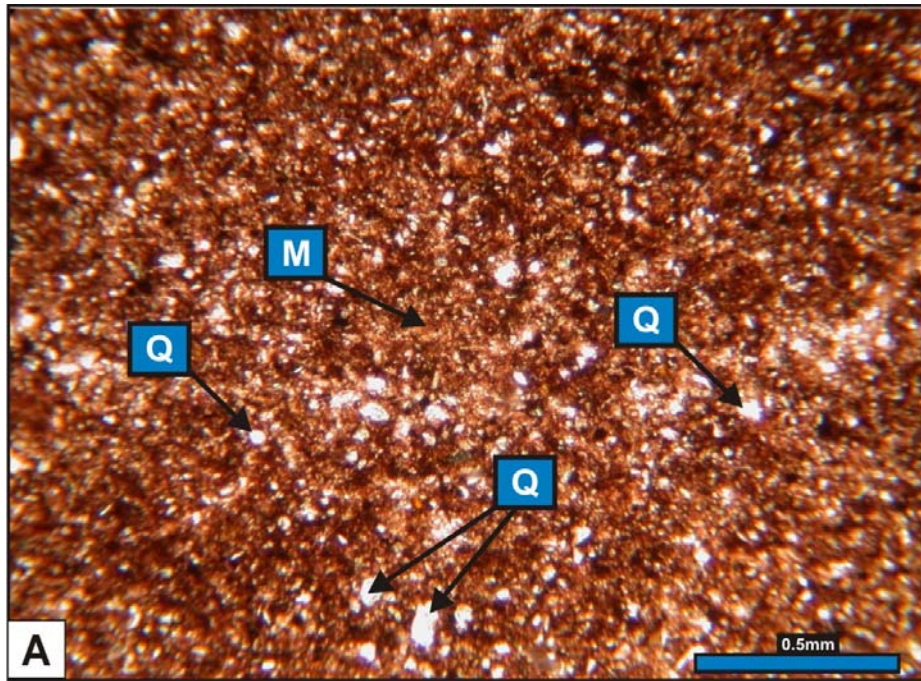


Figure 21. Photomicrographs of silty shales, (Q – quartz, M – matrix (silt-sized quartz and clay minerals)), (A: HAH – 7; B: HAH - 16B).

an average 10% and range from 6% to 20%. The grains are sub-angular to angular and they display overall coarsening upward trend along the section, and they are typically long, concavo – convex and with rarely sutured contacts, indicating at least moderate compaction. Plagioclase feldspar comprises the majority of the feldspar component again and ranging in average 1% of the rock volume. Calcite is the major cement type and occurs as calcite spar (finely crystalline mosaic) and as poikilotopic crystals enveloping several grains. Orthoconglomerates contain an average of 15 - 20% cement by volume. Accessory minerals, including mica, are minor latter comprising on average 1 – 2% of the rock volume. Matrix contains silt/fine sand and fine – gravel 5-10%. Conglomerates show, in overall, coarsening upward along the succession and clear shale–sandstone–conglomeratic alternations are seen along the succession. A huge amount of rock fragments were observed in conglomeratic lithofacies, which will be discussed later.

Additional thin section views of minerals and rock fragments observed in the studied samples are given Appendix F.

4.1.5 Rock fragments

The most abundant material in sandstones and conglomerates is rock fragments. Rock fragments are sedimentary, metamorphic and igneous in origin, and their quantitative analyses were performed in order to detect their change along the succession (Appendix C).

Amount of rock fragments in sandstone facies is in average 30 – 40%, but this value reaches up to 70% in some samples. A common rock fragment in sandstones is the metamorphic type consisting in average 60- 65% of the rock volume and consisting of quartzite, slate and schist fragments (Figure 23). The second common type is sedimentary rock fragments varying between 15 – 20% and consisting of mainly limestones. It should be noted that chert fragments were also encountered rarely among sedimentary rock fragments. Igneous rock fragments constitute around 10 – 15% and they mainly consist of pyroxene and

amphibole group minerals. In most samples, the pyroxene was altered to epidote, probably due to low – grade metamorphism (Appendix F, Figure F4).

Lithic fragments in conglomerates constitute 60 – 70% of whole rock volume and most of them are metamorphic ranging from 70% to 90% and averaging 80% of whole rock volume (Figures 24, 25). The second abundant rock fragments are again sedimentary in origin (average 14%) include limestone and minor chert fragments. Igneous rock fragments are mafic and ultramafic and consist mainly of pyroxene and amphibole group minerals (average 5%).

The distribution of rock fragments along the section for sandstones and conglomerates was shown in Figure 25. As we may observe from this chart the rock fragments in the lower portions of the measured section between intervals HAH – 10 and 14 the sedimentary fragments are prevailing (60% at level HAH-10), whereas and igneous rock fragments ranging between 20 - 40% (Figure 25). However, we observe that, upward along the section there is a significant decrease in sedimentary and igneous rock fragments and increase in metamorphic fragments (Figure 25). It was noted above that, studied section shows coarsing - upward trend, and hence increase in energy. Decrease in igneous rock fragments content along the section most probably due to the change in tectonic setting of source area provenance (change in a rock petrography due to change in stream transportation direction – shift of streams). However, decrease in sedimentary rock fragments are most probably related with source area supply of these sedimentary fragments.

Additional views of minerals and rock fragments observed in the studied thin sections are given Appendix F.

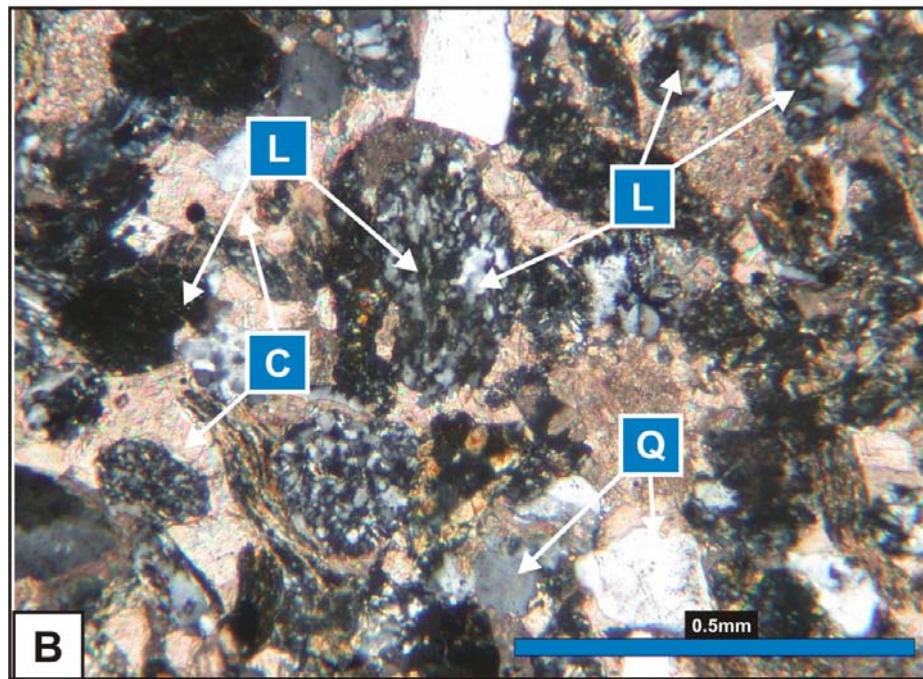
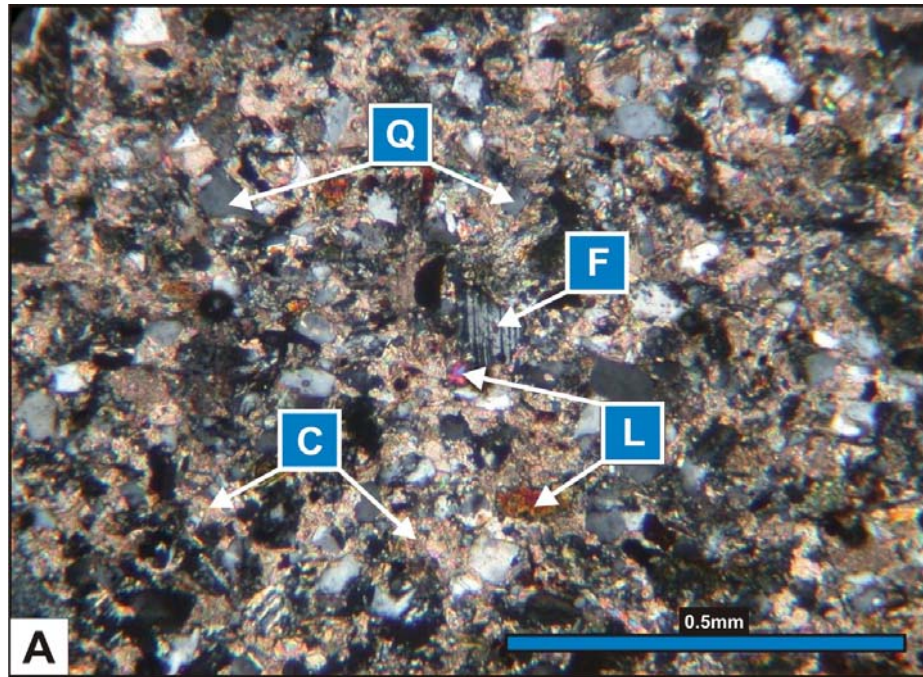


Figure 23. Photomicrographs of sandstones – litharenites (**Q** – quartz, **L** - rock fragments (mainly metamorphic), **C** - calcite cement, **F** - feldspar), (**A**: HAH – 15, **B**: HAH – 23).

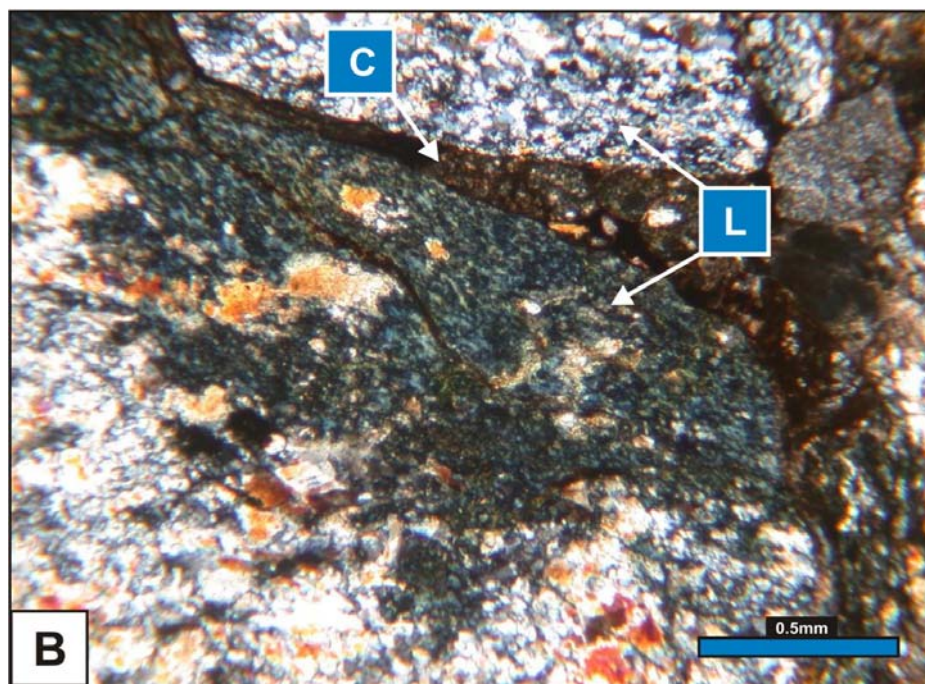
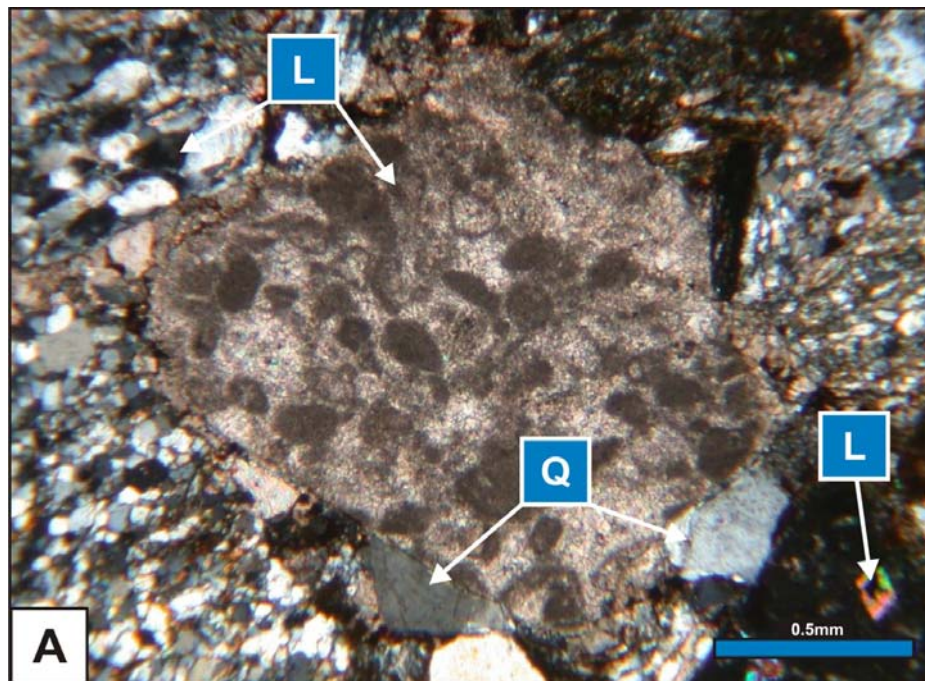


Figure 24. Photomicrographs of conglomerates (**Q** – quartz, **L**- rock fragments (sedimentary and metamorphic), **C** - cement), (**A**, **B**: HAH-45).

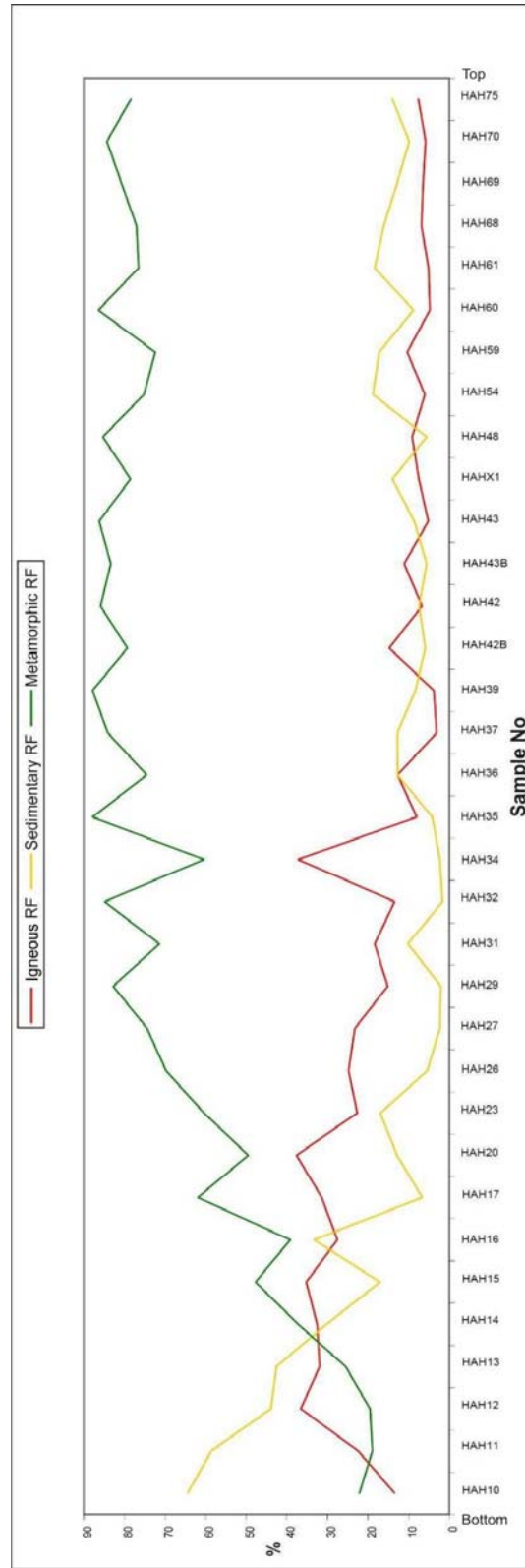


Figure 25. Illustration of rock fragment distribution along the measured section.

4.2 Sedimentary structures

In the field, more than 50 sedimentary structures have been observed and they are documented along the measured section. In the lower part of the measured section, where shale - sandstone intercalations are common, mainly erosional and rarely burrow structures were observed (Figure 26C,D). At the base of most sandstone beds, flute marks were recognized (Figure 26 A) and they are characteristic structures of turbidites and give a reliable indication of the flow direction (Tucker, 2001). Along with erosional sedimentary structure, some parallel laminations also were recognized in the lower and middle intervals of the studied section (Figure 27).

In the middle and upper part of the measured section, where sandstone and conglomeratic successions are getting thicker, graded beds have been observed (Figure 27). The feature relates to the grain – size changes upward through a bed and mostly develops in response to changes in flow conditions during sedimentation. Along the measured sections, many different types of graded bedding have been observed, which is typical for the turbidites (Bouma, 1962). These are normal grading, reverse grading and even multiple grading, where there are several graded subunits in a bed (Figure 27). Massive bedding without any apparent internal structures is also common. Additionally in the middle and upper part of the section, mainly at the base of coarse grained successions, load casts have been observed (Figure 26 B). These load structures are downward – directed protuberances of sandstone and conglomeratic beds into underlying mudrocks. In homogeneous thick beds, 30 – 50 cm in diameter sandstone balls are observed (Figure 27). These balls are spherical to ellipsoidal in shape, and are often aligned along the stratification planes. They are darker and harder than surrounding sandstone, but they display no obvious change in petrographic composition.

Along with erosional and depositional sedimentary structures, some post depositional structures also have been recognized in the lower intervals of the section. Grazing traces, which are produced by mobile, deposit – feeding epibenthic organisms that feed at or near the sediment surface (after Benton and Harper, 1997). These grazing traces observed in the field, most probably belongs

to *Nereites* ichnofacies, which are common in deep – water sequences (Figure 26 C, D).

4.3 Provenance analysis

Modal compositions can be used to infer the tectonic setting of the basin and source rocks (Dickinson and Suczek, 1979). In order to perform this, nearly 20 selective sandstone samples (Figure 28) were used and after gaining all data from the laboratory analysis (point counting), we have used Dickinson (1985) triangular diagram, which is a plot of Qm (monocrystalline quartz), F (total feldspar), Lt (total lithic fragment), include Qp (polycrystalline quartz) with lithic grains and so give weight to the source rock. In the work of Dickinson (1985) on ancient sands, four major provenance terranes were distinguished: stable craton, basement uplift, magmatic arc and recycled orogen. Detritus from the various provenance terranes generally has a particular composition and the debris is deposited in associated sedimentary basins, which occur in a limited number of plate – tectonic settings. In this modal analysis of sandstone samples, the percentages of various combinations of grains are plotted on triangular diagram. It should be noted that more precise results can be reached by measuring at least 300 samples from different places within one layer. Due to time saving, in our studies nearly 20 samples were selected (Figure 28), in order to give at least some information about tectonic setting of source rock. Sandstone samples for this analysis have been selected from lower, middle and upper intervals of the studied section. The main criteria in selecting these samples were their low content of matrix, because care must be exercised where there is more than 15% matrix in sandstone (Cox and Lowe, 1996).

Thin – section analyses of the samples show that the sandstones are mainly composed of polycrystalline quartz, rock fragments and minor quantity of feldspars. As long as there were considerable amount of rock fragments in each sample and few feldspar, when we plot these data on ternary diagram, the

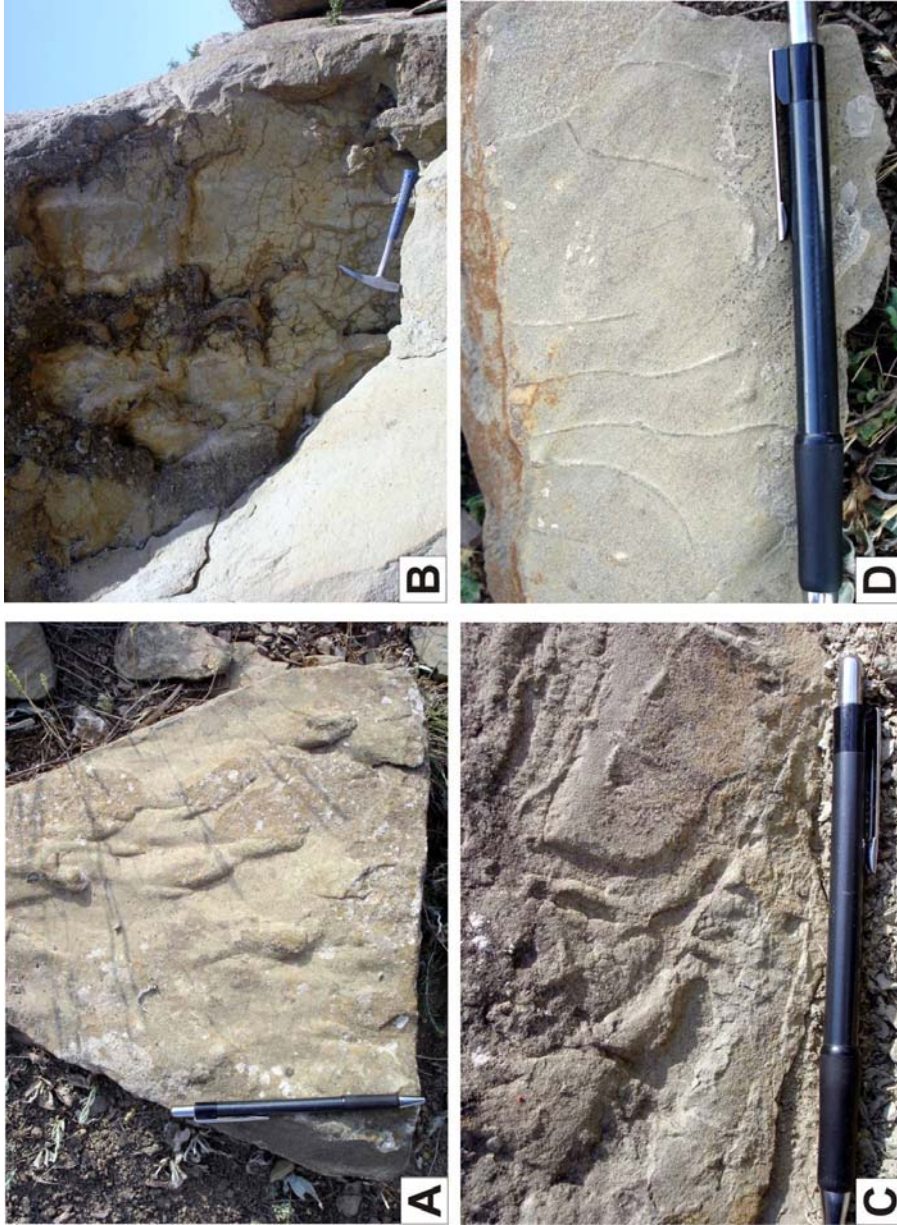


Figure 26. Photographs of sedimentary structures observed in the field. **A** – flute marks at the base of sandstone bed (flow from bottom to the top) (HAH-10); **B** – Pseudo mudcrack structures at the base of conglomerate (HAH-73); **C** and **D** – Grazing traces (*Nereites* ichnofacies?) (HAH-14)

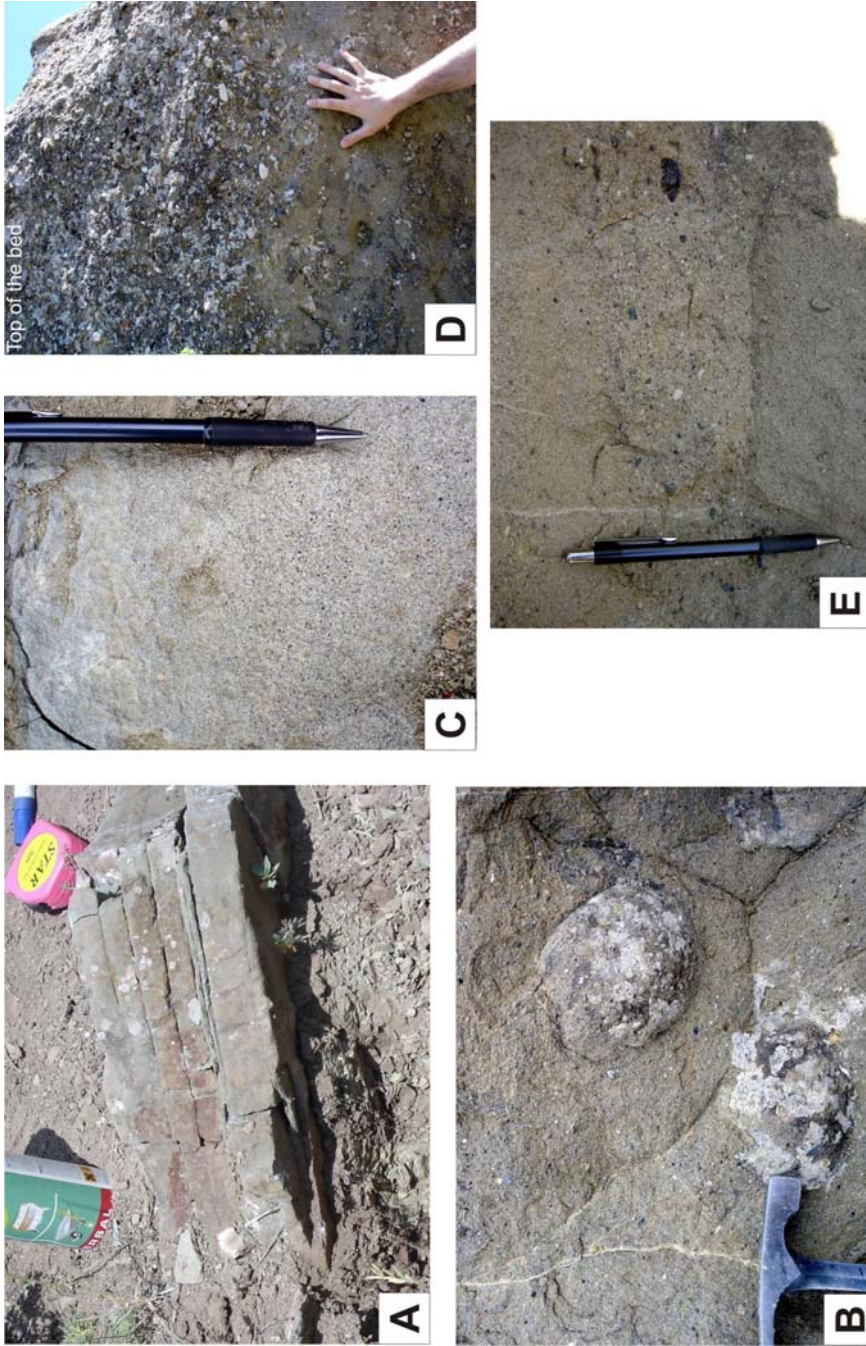


Figure 27. Photographs of sedimentary structures observed in the field. **A** – laminated sandstone bed, HAH – 11; **B** – ball structures, HAH – 74; **C** – normal graded bed, HAH – 54; **D** – reversed graded bed, above HAH – 76; **E** – multiple graded bed, HAH – 69

results of almost all samples fall into section related recycled orogen terranes (Figure 28). Among these fragments, metamorphic rock fragments are dominant, and most probably these fragments including composite quartz derived from the basement of the Sakarya Continent (Ünalán et al., 1976; Görür and Derman 1978; Norman et al., 1980).

In summary, when we plot our data on ternary diagram of Dickinson (1979) all data fall in section related to recycled orogen. The sandstones have large lithic components consisting mainly of sedimentary and metasedimentary fragments, and are low in feldspar and volcanic-derived fragments, typical of rocks derived from a continental collision orogen.

Sediments derived from the recycling of orogenic belts are varying in composition, reflecting the different types of orogen. Lithic grains dominate in many recycled - orogen sandstones, and in those derived from continental collision mountain belts, quartz plus sedimentary rock fragments dominate, and then the metamorphosed equivalents of the latter as deeper levels of the orogen are uplifted (Zuffa, 1985). These sands thus tend to be more quartzo-lithic, with little feldspar. Detritus from an uplifted subduction complex in a continent – ocean orogen, by way of contrast, will have a high igneous rock – fragments content, as well as fine grained sedimentary rock fragments such as chert (Zuffa, 1985), feldspar will be more abundant too.

4.4 Palaeocurrent Analysis

The measurement of palaeocurrents is a vital part of the study of sedimentary rocks, since they provide information on the palaeogeography, palaeoslope, current and wind directions and they are useful in facies interpretation. Many erosional and depositional structures can be used to deduce the direction or trend of the currents that formed them.

In the previous years, palaeocurrent studies in the Haymana Formation have been performed by various researches in different years, Gökçen and Kelling (1983) and Çiner (1996). For this purpose, they mainly used erosional

Samples No	Quartz %	Rock fragments %	Plagioclase %
HAH10	44.3	55.5	0.3
HAH17	46.1	53.1	0.8
HAH20	49.7	49.2	1.2
HAH29	22.6	76.7	0.6
HAH35	21.0	78.8	0.3
HAH37	16.5	83.5	0.0
HAH39	15.3	84.7	0.0
HAH42	18.8	80.8	0.5
HAHX1	44.3	55.7	0.0
HAH48	16.6	83.4	0.0
HAH54	12.0	87.3	0.7
HAH59	25.8	70.4	3.8
HAH60	21.1	77.5	1.4
HAH61	16.3	83.7	0.0
HAH68	19.5	79.4	1.2
HAH11	76.9	23.1	0.0
HAH15	61.3	36.5	2.2
HAH26	21.6	78.0	0.4
HAH32	26.3	73.7	0.0
HAH46	11.9	88.1	0.0

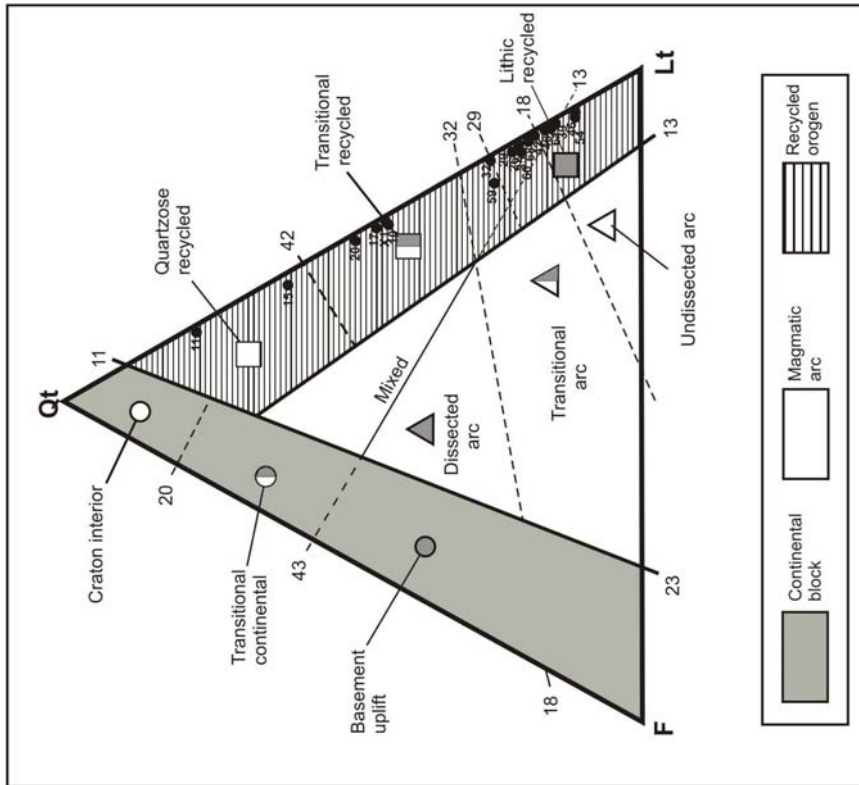


Figure 28. Triangular diagram showing average compositions of sand derived from different provenance terranes (After Dickinson, 1985).

sedimentary structures such as flute and groove casts and major transportation direction was towards NNW.

In our study, we used pebbles orientation from two individual conglomeratic beds in order to predict paleocurrent direction. Although the more data give more accurate palaeocurrent picture, approximately 100 measurements have been performed from each bed (Figure 29) and results of these measurements were plotted on rose diagram (Rose diagram, version 2.1.0 by Thompson) Compositionally these pebbles consist of sedimentary (limestone, chert, shale) and metamorphic fragments (schist and slate).

The first measured conglomeratic bed is located approximately in the middle part of the measured section (HAH - 55) and thickness of this bed is 160 cm, at coordinates $36^{\circ} 46' 12''$ E – $43^{\circ} 66' 645''$ N. Collected measurements (Appendix D) have been plotted on rose diagram and result is shown in Figure 30. As we may observe from this diagram the major transport direction was towards NE (unidirectional).

The second conglomeratic succession is located at the upper most part of the measured section (last conglomeratic succession). The thickness of this bed is 345 cm and coordinates of this bed is $36^{\circ} 46' 12''$ E – $43^{\circ} 66' 851''$ N. The readings taken from this succession are shown in Figure 31. As we may observe, the major transport direction was towards SE (unidirectional).

One common fabric of oblate pebbles in waterlain deposits is *imbrication*, where the pebbles overlap each other, dipping in upstream direction (Figure 29). Consequently transport direction for the first bed is SE, and for the second bed it is towards W. Additionally measurements taken from erosional structures like flute mark indicate major transport direction SW. As we observe there is a discrepancy between palaeocurrent directions derived from pebble analyses and imbrication patterns. This discrepancy is most probably due to tectonic tilting. Because these conglomeratic successions are dipping in northward direction at 43° (bed one) and 63° (bed two).

In normal conditions, if strata are tilted to any extent (greater than 25°) the beds must be brought back to the horizontal by using stereogram.



Figure 29. Photographs of pebbles and cobbles in conglomeratic successions, used for palaeocurrent direction (**A** – layer one, palaeocurrent direction is SE; **B** – layer two, palaeocurrent direction is W; red arrows show imbrication).

Parameter Value

Name: Bed one
Type of Rose: Unidirectional
Number of Points: 100
Number of Classes: 72 (5°)
Maximum Class: 6%
Compass Direction: 51.58 (NE)

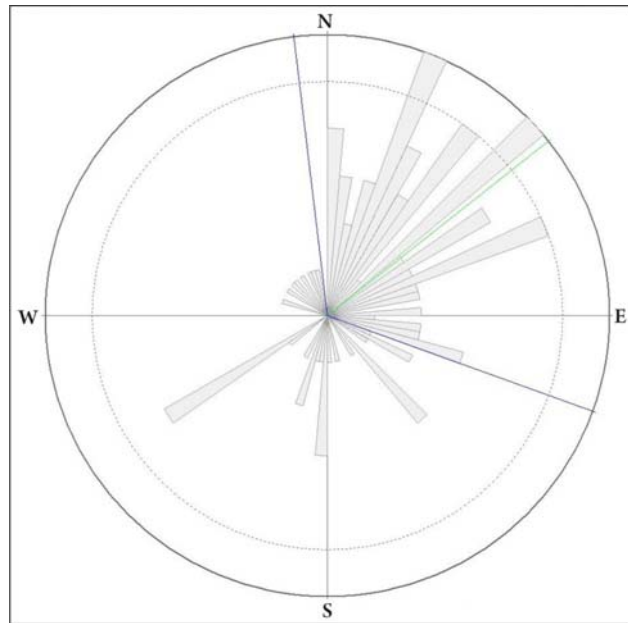


Figure 30. Rose diagram illustrating palaeocurrent direction for the first bed (HAH - 55)

Parameter Value

Name: Bed two
Type of Rose: Unidirectional
Number of Points: 100
Number of Classes: 72 (5°)
Maximum Class: 11%
Compass Direction: 164.87 (SE)

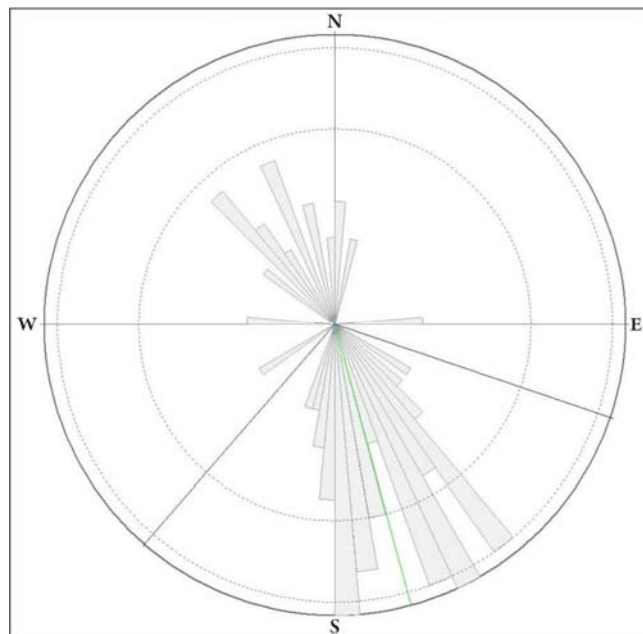


Figure 31. Rose diagram illustrating palaeocurrent direction for the second bed (last conglomeratic bed in the studied interval)

But in this study we have not performed any corrections due to factors shown below:

- Fault induced deformation
- Oblique section correction
- Tectonic tilt correction due to not only dipping rate but also overturning.
- Differential compaction rate of shales and sandstones
- Plung correction for the plunging anticline

Consequently these conglomeratic successions are too tectonically complicated for precise palaeocurrent analyses, but from rose diagrams it can be seen that, transportation direction between lower and upper conglomeratic unit is different indicating possibility of faulting, which were not observed in the field.

4.5 Grain size and sphericity analyses

The basic descriptive element of all sedimentary rocks is the grain size. In this study, grain size and sphericity analyses have been performed in two conglomeratic successions, where it was possible to measure pebbles in 3 dimensions, which is important for deducing exact grain size parameters and sphericity analyses. Approximately 100 pebbles in each bed have been measured (Appendix E). For graphic presentation of grains sizes, the histogram and cumulative frequency curve were plotted (Figures 32 and 33). It should be noted that, all grain size units are given phi units.

The median grain size, simply the grain size at 50%, is not as useful as the mean grain size that is an average value taking into account the grain sizes at the 16th, 50th and 84th percentiles. Where a grain – size distribution is perfectly normal and symmetrical, then the median, mean values are the same. Sorting is a measure of the standard deviation i.e. spread of the grain – size distribution. It is one of the most useful parameters because it gives an indication of the effectiveness of the depositional medium in separating grains of different classes.

By using cumulative frequency log (Figure 32 B and 33 B) and formulae (Table 2), the grain size parameters have been calculated and results are shown Table 3.

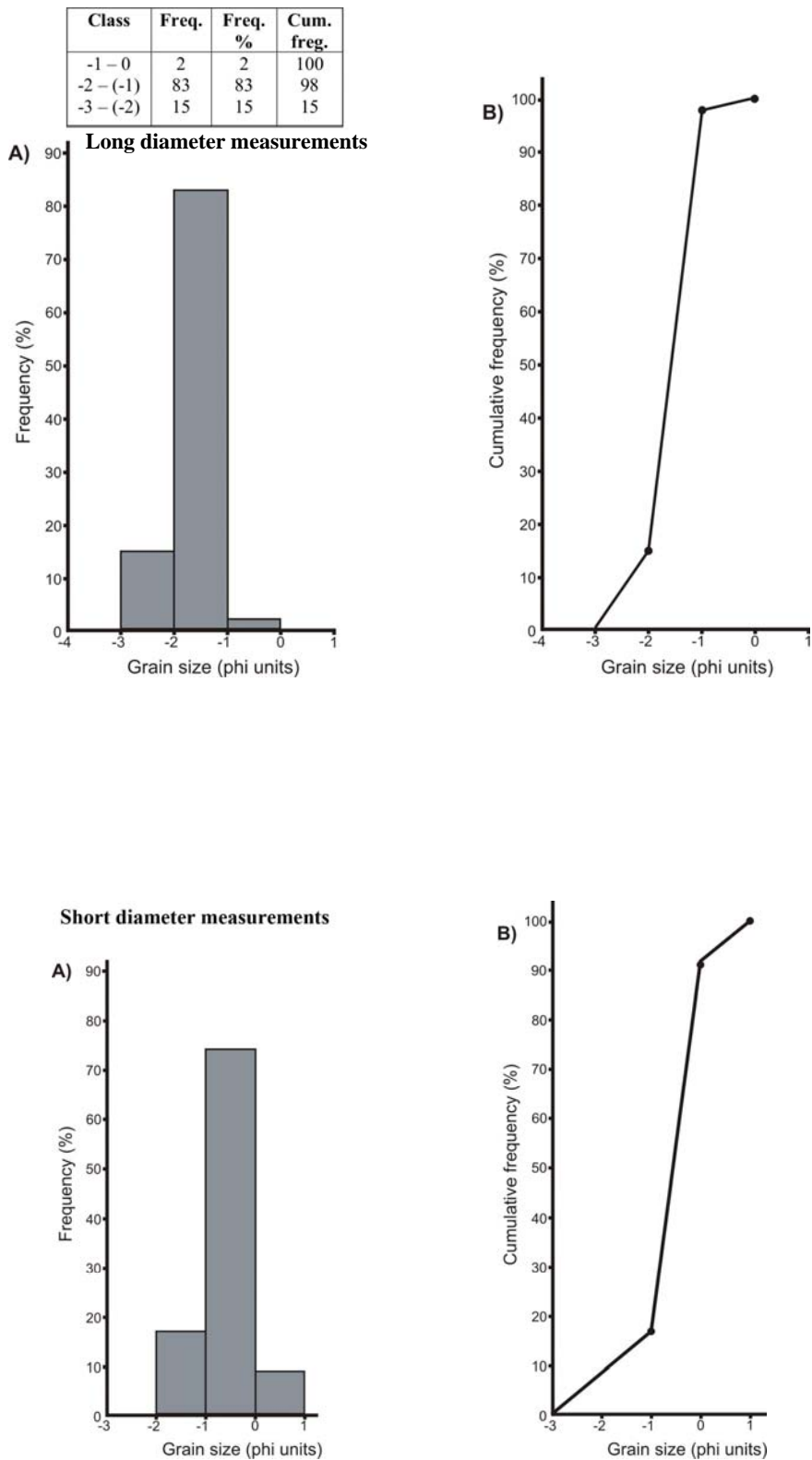
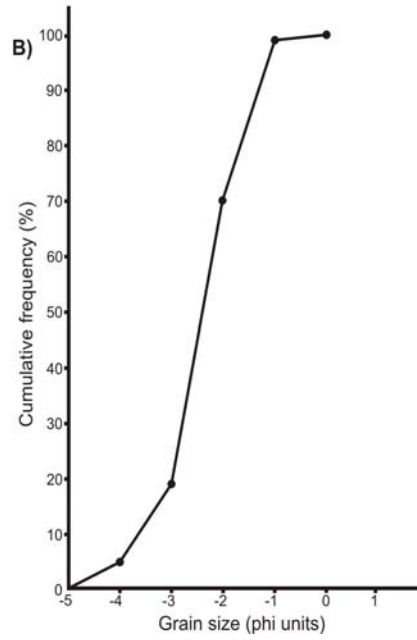
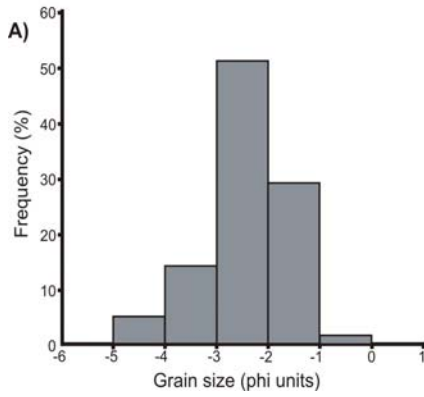


Figure 32. Graphic presentation of grain size data for bed one (HAH-55) (A-histogram, B –cumulative frequency curves plotted with an arithmetic scale).

Class	Freq.	Freq. %	Cum. freq.
-1 - 0	1	1	100
-2 - (-1)	29	29	99
-3 - (-2)	51	51	70
-4 - (-3)	14	14	19
-5 - (-4)	5	5	5

Long diameter measurements



Short diameter measurements

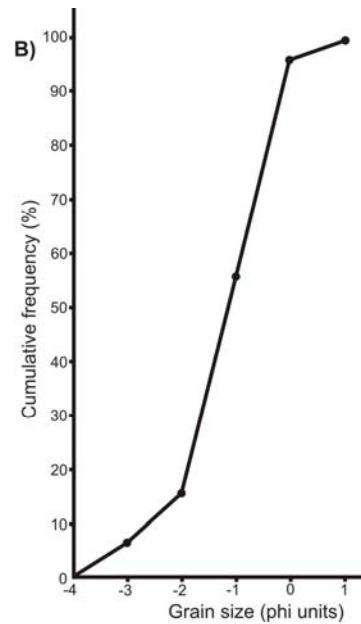
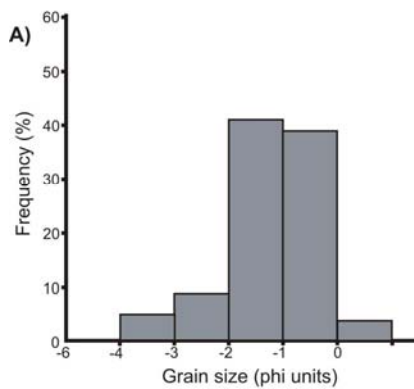


Figure 33. Graphic presentation of grain size data for bed two (last conglomeratic unit in the studied interval) (A-histogram, B –cumulative frequency curves plotted with an arithmetic scale).

Table 2. Formulae for the calculation of grain – size parameters from a graphic presentation of the data in a cumulative frequency plot. The percentile measure ϕ_n is the grain size in phi units at the n^{th} percentage frequency

Parameter formula	Folk & Ward (1957)
Median	$Md = \phi_{50}$
Mean	$M = \frac{\phi_{16} + \phi_{50} + \phi_{84}}{3}$
Sortin	$\sigma\phi = \frac{\phi_{84} - \phi_{16}}{4} + \frac{\phi_{95} - \phi_5}{6.6}$

Table 3. Grain size parameters derived graphically, Folk and Ward formulae.

Bed No	Grain size parameters		Sorting
	median	mean	
1	-1.58	-1.59	0.46 (well)
2	-2.39	-2.37	0.86 (moderately)

Sphericity analyses have been performed also for two conglomeratic successions shown above and studied for palaeocurrent analysis. Form based on ratios of the long (L), intermediate (I) and Short (S) axes of a pebbles collected from the field (Appendix E). In our analyses sphericity were calculated based on Sneed and Folk formulae shown below:

$$SPH = \sqrt[3]{S^2 / LI}$$

Results of these calculations are shown in (Appendix - E) and in average the sphericity is 0.65 for both beds which means shape of the particles are

compact. Additionally Oblate – Prolate index (OP index) have been performed for these beds. OP index is closely related to Form; however, it's obtained by a different formula shown below:

$$OP = (10L (L-I)/S (L-S)) - (5L/S)$$

The results of OP index data is plotted on diagram proposed by Dobkins and Folk (1970), which developed the OP index of shape, for recognizing Beach gravel and Stream gravel (Figure 34 and 35). As it can be observable from the OP index diagrams, in the first bed slightly beach environments gravels dominant, whereas for the second bed this number slightly changes to river gravels. But for sure, none of these beds is indicating particular environment (beach or river gravel). In general, as we may observe, gravels in these beds more likely mixture of beach and river. This might be explained because of multiple sediment supply from different sources. Roundness for these two conglomeratic beds has been interpreted by visual estimation and they are rounded to well - rounded indicating transportation was far enough. When sediment is transported, it gets abraded due to contact with other sediment and bedrock, and as roundness is a function of abrasion, it can infer the time or distance in transport.

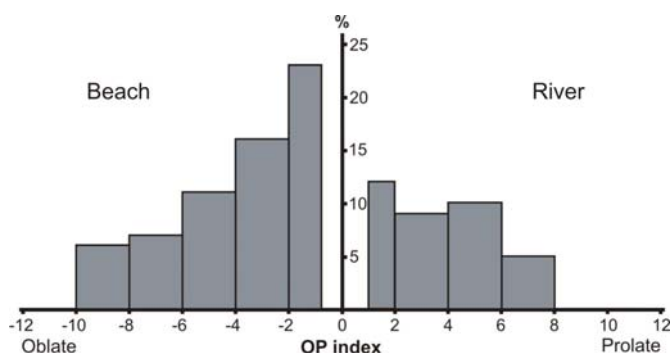


Figure 34. OP index diagram for bed one

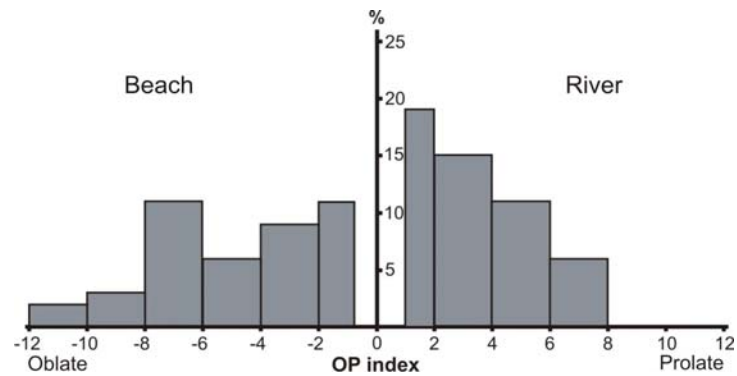


Figure 35. OP index diagram for bed two

Additionally grain size analyses have been performed for six selective samples. In these samples, it was possible to measure up to 300 individual grains under microscope in each sample. A histogram and cumulative frequency curves have been prepared for each sample (Figure 36 - 41) and grain size parameters have been calculated by using Folk and Ward (1957) formulae. Results of grain size parameters are shown in Table 4. In general they show grain size increase and decrease in sorting along the selected samples. As we may observe, their sorting is moderate to poor, fluctuating depositional process energies (Sahu, 1964).

The distinct S – shaped curve, is often plotted on probability paper, where a sediment population of normal distribution is displayed as a straight line (Figure 42, Friedman and Sanders, 1978). Sediment distributions usually exhibit a series of straight line segments, which represents the influence of different modes of sediment transport on the deposits. Consequently, all our grain – size cumulative frequency plots (Figure 36 - 41 (B)) in comparison with transportation modes proposed by Friedman & Sanders (Figure 42) (1978), show that main transportation mechanism was saltation. In turbiditic succession, transportation mechanism can be rolling, saltation and suspension depending upon mainly on grain size and energy of the flow.

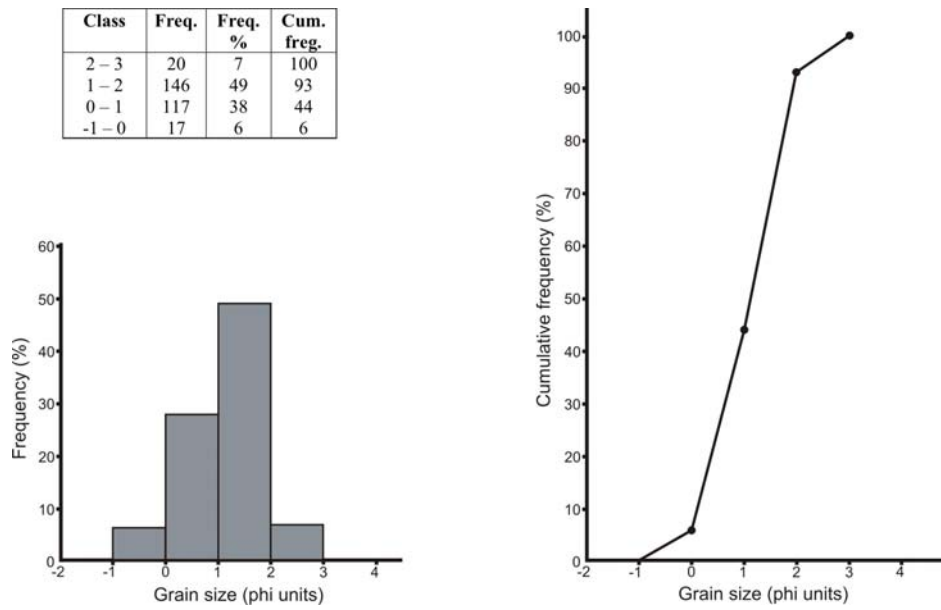


Figure 36. Graphic presentation of grain size data for a sample HAH - 39 (A-histogram, B –cumulative frequency curves plotted with an arithmetic scale).

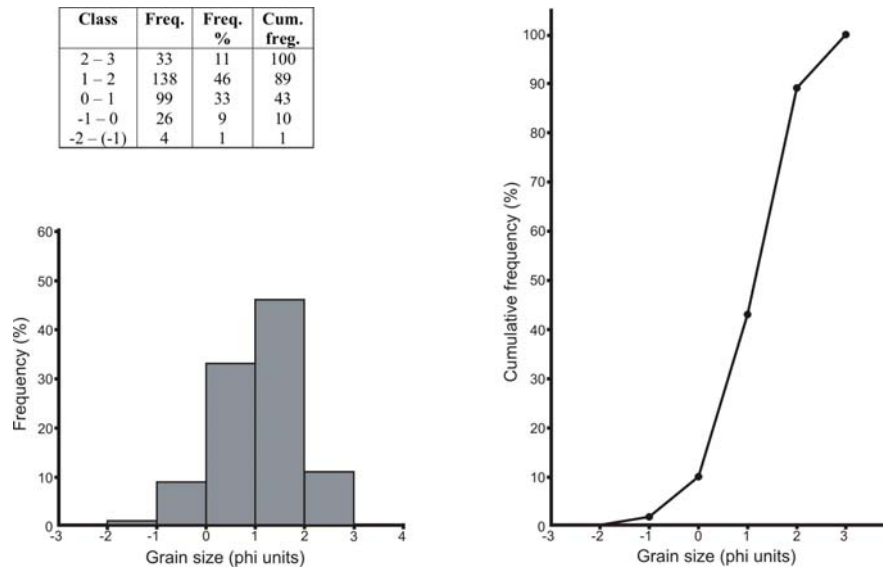


Figure 37. Graphic presentation of grain size data for sample a HAH - XI (A-histogram, B –cumulative frequency curves plotted with an arithmetic scale).

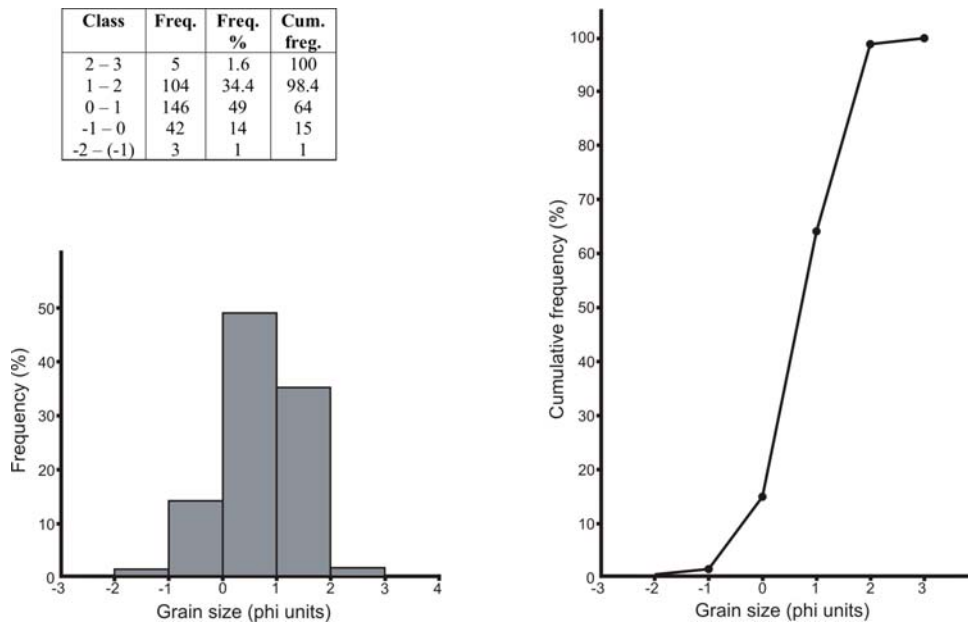


Figure 38. Graphic presentation of grain size data for sample a HAH - 42 (A-histogram, B -cumulative frequency curves plotted with an arithmetic scale).

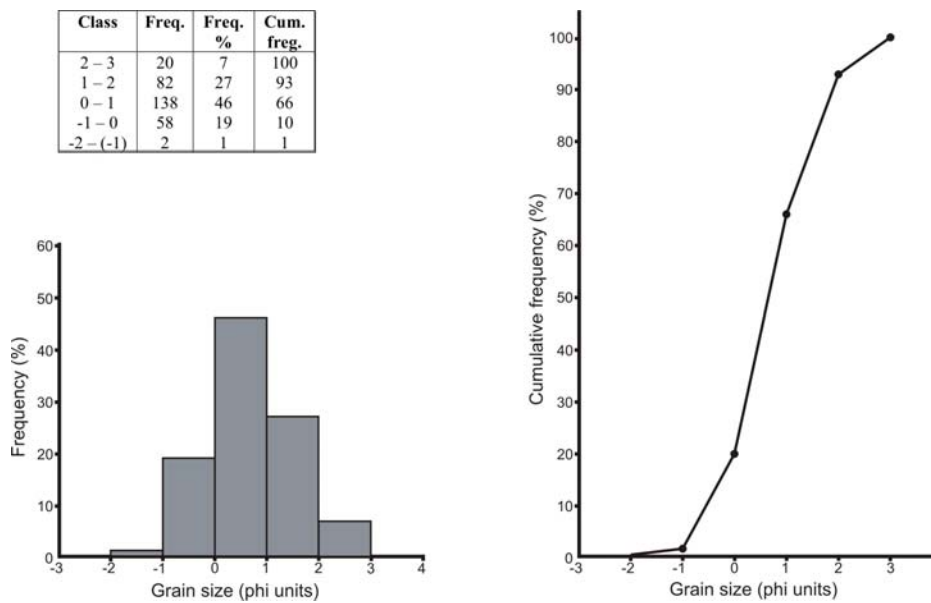


Figure 39. Graphic presentation of grain size data for sample a HAH - 43 (A-histogram, B -cumulative frequency curves plotted with an arithmetic scale).

Class	Freq.	Freq. %	Cum. freq.
2 - 3	31	10	100
1 - 2	110	37	90
0 - 1	101	34	53
-1 - 0	40	13	19
-2 - (-1)	18	6	6

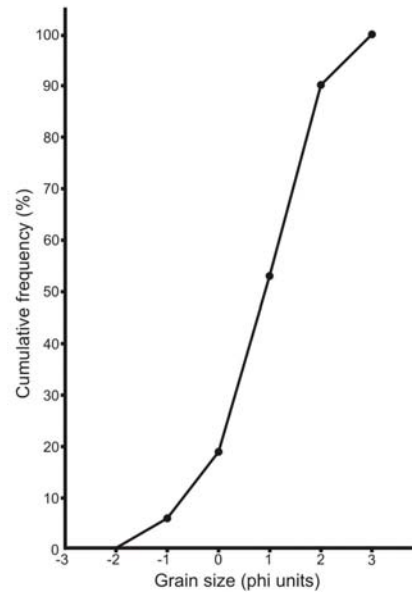
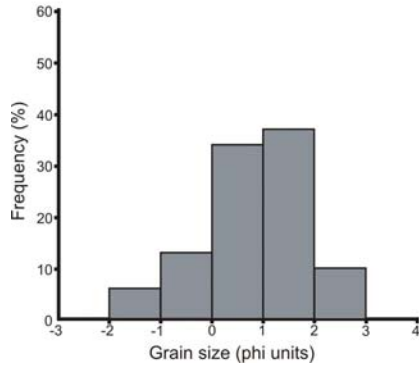


Figure 40. Graphic presentation of grain size data for sample a HAH – 48 (A-histogram, B –cumulative frequency curves plotted with an arithmetic scale).

Class	Freq.	Freq. %	Cum. freq.
3 - 4	7	2	100
2 - 3	43	14	98
1 - 2	115	38	84
0 - 1	89	30	46
-1 - 0	33	11	16
-2 - (-1)	11	4	5
-3 - (-2)	2	1	1

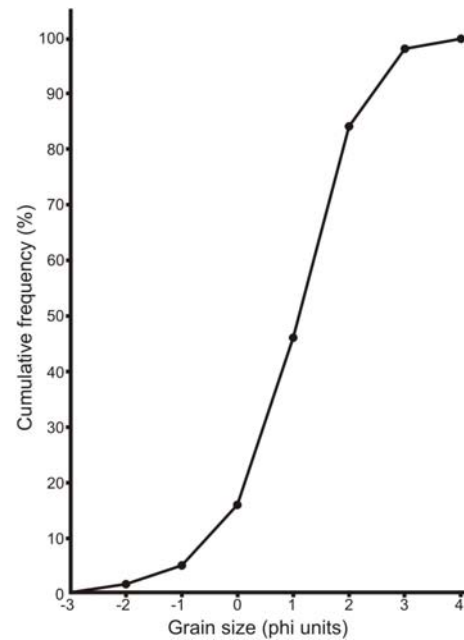
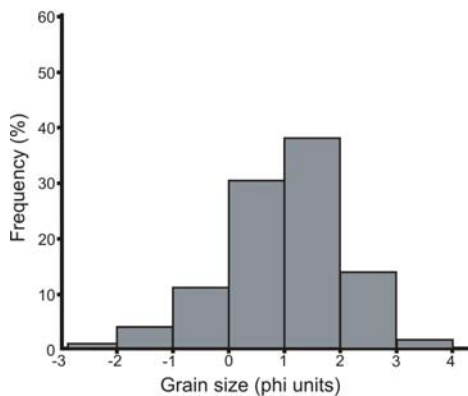


Figure 41. Graphic presentation of grain size data for sample a HAH – 45 (A-histogram, B –cumulative frequency curves plotted with an arithmetic scale).

Table 4. Grain size parameters derived graphically, Folk and Ward formulae.

Sample No	Grain size parameters		Sorting
	median	mean	
HAH – 39	1.1	1.06	0.75 (moderately)
HAH – X1	1.12	1.06	0.90 (moderately)
HAH – 42	0.71	0.80	0.77 (moderately)
HAH – 43	0.64	0.70	0.95 (moderately)
HAH – 48	0.92	0.85	1.07 (poorly)
HAH – 45	- 1.1	- 1.77	1.09 (poorly)

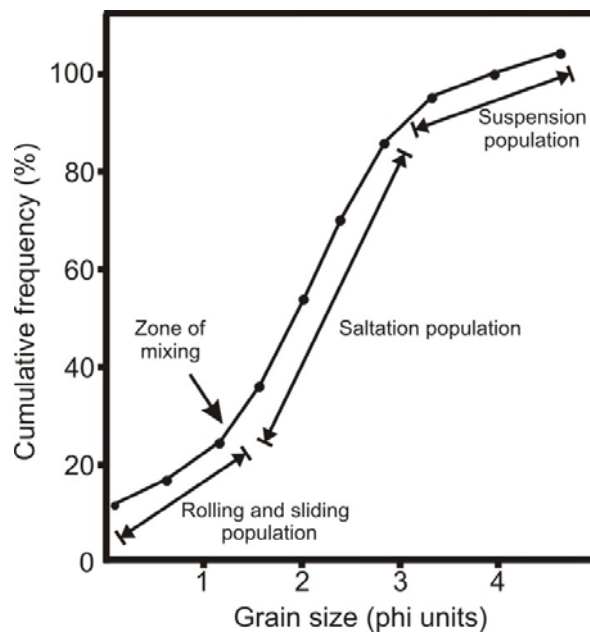


Figure 42. Transport modes in relation to size distributions (Friedman & Sanders, 1978).

4.6 Depositional environment

Important factors when analyzing depositional environment are field and laboratory data on the sedimentary constituents, their shape and grain size and the structures and textures which the rocks acquired during sedimentation, as observed on different scales (Herve Chamley 1990). Together with the physical and biological modification undergone by the sediments following deposition, and with the general sedimentary mechanisms, these data allow the reconstruction of the depositional environments of a given sediment and the understanding of its history.

The overall deep - marine nature of the siliclastic successions of the Haymana Formation has previously been documented in geodynamic reconstructions (Ünalán et al. 1976; Koçyigit and Lunel 1987; Koçyigit 1991). Deep – water basins are the depositional sites of sandstones and conglomerates derived from adjacent slopes and shelves.

In general studied interval of the Haymana Formation might be interpreted as a prograding lower and middle portion of submarine – fan. Deep – water environments are primarily the sites of pelagic and hemipelagic deposition. Pelagic to hemipelagic limestones and sandstones observed in the lowermost part (levels 1 – 20, Figure 14) of the measured section is most likely basin plain deposits due to their composition and fossil content. The impressive regularity and lateral persistence of bedding and depositional structures, combined with the association of thin hemipelagic intercalations are typical characteristics of the basin plain thin - bedded turbidites. The grain size of these thin sandstone beds is fine – to medium sand size. Sedimentary structures observed in these beds are commonly erosional (fute mark), some parallel laminations, and very rarely burrow structures, which are interpreted to be a grazing traces, most probably belongs to *Nereites* ichnofacies, which are common in deep – water sequences (Figure 26). Palaeocurrent transport direction of these sandstone beds towards NNW, based on measurements taken from flute marks.

The depositional environments of the lower - middle intervals (levels 22 – 43, Figure 14) of the measured section may be interpreted as lobes of

a lower submarine fan and/or to overbank deposits of channels located in middle to upper fans (Mutti and Rucci – Lucchi 1972) (Figure 43). A fan occurs in a lower slope/basin – rise setting and usually is fed by one major channel, which divides into smaller and shallower channels on the fan itself (Tucker 2001). The presence of Bouma sequences and erosional sedimentary structure (flute marks and groove casts), are characteristics of lobes of a lower submarine fan depositional environment, which were observed in the middle part of the studied section. The boundary between sandstone and muddy deposits is sharp, stepwise upward-fining consists of rapid grain-size changes at fixed heights (grain-size breaks), which divide a bed into sandy, silty, and muddy zones. Transportation mode of these deposits is mainly saltation (Figure 42), and they are moderate to poorly sorted indicating change in flow energy.

The middle - upper part (level - above 43) of the studied section might be interpreted as a succession of sandy conglomeratic channels and muddy interchannel deposits. Conglomeratic facies with their sharp erosional contact with mudstones, which were clearly seen in the field, the most frequently observed conglomeratic sediments can be interpreted as erosional channel - fill deposits (Mutti and Normark 1987). Decreasing pebble sizes towards the margins, which were observable in the field, indicate probable channel margin slumps, which are thought to be controlled by high density debris flows. Palaeocurrent data shows the main transport direction in the middle conglomeratic succession towards NE, whereas transport direction of upper conglomeratic bed towards SE, based on pebble orientation analyses. In particular, petrographic and sedimentology analyses of samples collected along the section, show that sandstones and conglomerates are texturally immature due to their cement/matrix content, moderate to poor sorting and angular grains. Immature to submature textural maturity, corresponding to neritic depositional environment, which is also indicating deep – water setting (Folk 1980).

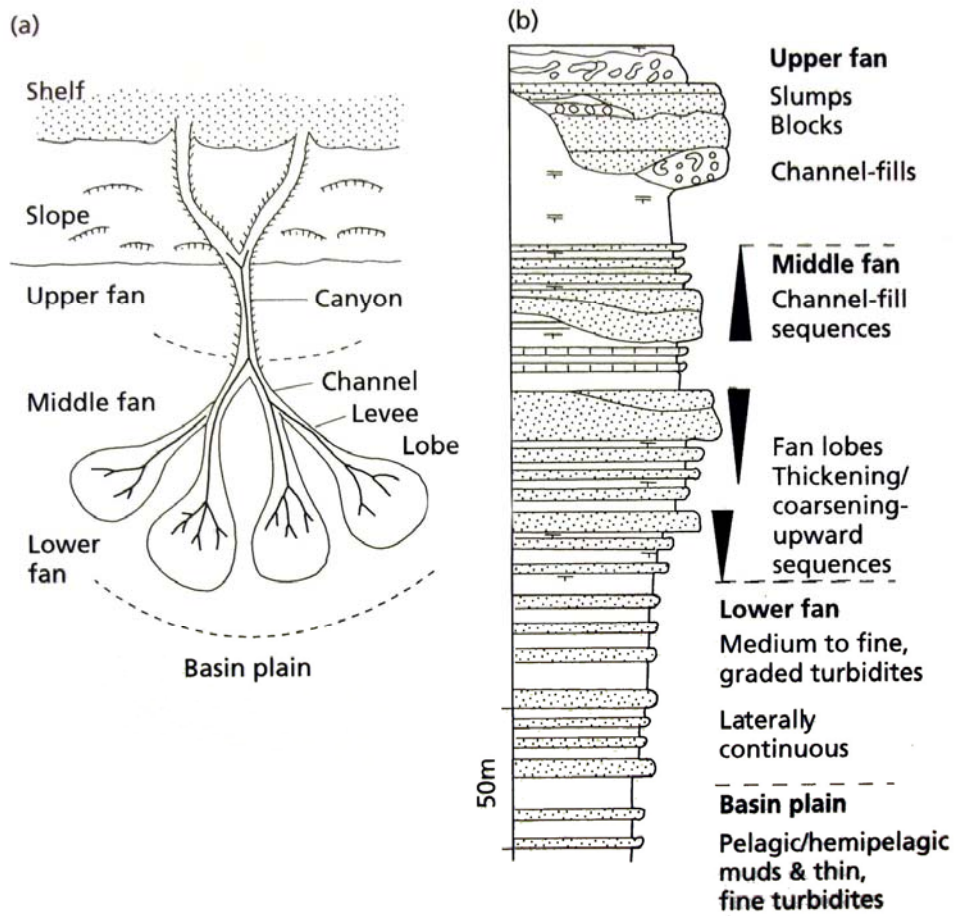


Figure 43. Submarine-fan facies model. (a) Classic model of fan with suprafan lobes, some active, some abandoned. (b) Succession produced through fan growth and lobe progradation (Tucker, 2001).

CHAPTER V

CONCLUSION AND RECOMMENDATION

1. In the Haymana Basin, a 250 m thick stratigraphic section has been measured within the Haymana Formation, which is mainly composed of carbonates and sandstone – shale – conglomerate alternation.

2. The lower boundary of the Haymana Formation has been disputable for a long time and it has been modified in this study. Based on the field works and detailed lithofacies analyses, our new observations suggest that, the base of the Haymana Formation, contrary of what has been defined in Ünalán et al. (1976), rests on the reddish to pinkish beds of the Kocatepe Formation which overlies the Seyran Formation unconformably comprising limestones, shales and breccias (Yüksel, 1970).

3. Detailed petrographic, sedimentologic and biostratigraphic analyses were carried out in 150 m (starting from the base) of the total measured section. The measured section starts with the purple to pinkish colored wackestone and mudstone lithofacies of the Kocatepe Formation. Upward, these muddy and limy deposits grade into sandy and conglomeratic deposits. Actually sandstone–shale–conglomerate alternations are evident observed along the measured section. According to biostratigraphic studies, two chronozones were recognized based on planktonic foraminiferal zonations. These are the lower *Dicarinella asymetrica* (Upper Santonian) chronozone and the upper *Globotruncanita elevata-Globotruncana ventricosa* (Lower to Middle Campanian) chronozone.

4. During the detailed petrographic analysis, several minerals or mineral groups have been recognized in the studied section. These are quartz, plagioclase, muscovite, biotite, opaque, chlorite/glaucanite. Cement in the siliciclastic rocks is commonly calcite and found either in form of calcite spar (finely crystalline mosaics) or as poikilotopic crystals enveloping several grains. The quantitative

data of minerals and rock fragments have been used to establish the composition and also classification the rocks. Among rock fragments the most abundant type is metamorphic, which is composed of quartzite, schist and slate fragments. The sandstones and conglomerates examined from the studied section exhibit evidence of diagenesis resulting from near-surface processes such as cementation and compaction. However, there is no evidence of pressure dissolution or grain replacement due to deeper burial. Compaction appears to have been a fairly minor process judging from the preservation of most point contacts between grains and only a few long contacts between quartz grains. However, sedimentary and metasedimentary lithics are commonly compacted and deformed between quartz grains. Mica grains are also in most cases deformed by compaction. Feldspar grains are only partially altered along cleavages indicating dissolution was not a major process.

5. Modal analysis of 20 sandstone samples has been used to infer the tectonic setting of the basin and source rocks. When plotted on Dickinson (1978) ternary diagram, these results fall into the section corresponding to the subduction and recycled orogen.

6. High resolution sequence stratigraphic study within the studied section has resulted in the recognition of three depositional sequences. Two 2 sequence boundaries have been identified in the sequential deposition of the clastic rocks. The first depositional sequence is incomplete and represented by only TST and HST and composed of A1 type fining and deepening upward basic cyclic units. A1 type cycles are characterized by limestone deposits at the base grading upward into muddy deposits. The second depositional sequence is complete and represented by LST or SMW systems tract, TST and HST deposits, consisting of several smaller sequential subdivisions of basic cyclic units. Cyclic units of the second depositional sequence are mainly composed of A2 fining and deepening upward type cycles, which are represented by sandstone deposits at the base changing upward into muddy to silty deposits. The third depositional sequence is again incomplete and consists of LST and partially recognized TST deposits. In comparison with previous two depositional sequences, this sequence is thicker

and characterized by various types of basic cyclic units, consisting of A2 and A3 fining and/or deepening upward cycles and B1, B2, B3 type coarsening and/or shallowing upward basic cyclic units. Additional turbiditic basic sequences have also been defined within depositional sequences, where turbiditic deposits are abundant.

7. Paleontologic investigations in the measured section indicates a time interval from the late Santonian and to the early to Middle Campanian. From this, by counting the numbers of depositional sequences and their smaller sequential subdivisions, we can roughly estimate the duration of these cycles. The depositional sequences recognized in the study correspond to third order depositional cycles of Haq et al. (1988). Our systems tracts are distinct parts of these third – order cycles and their building blocks are the basic cyclic units corresponding probably to fifth – order Milankovitch cycles.

8. Allocyclic and/or autocyclic origin of the units in the studied section stays problematic. Although the general progradational character of each depositional sequence is clearly shown by the upward evolution of the basic sequences and cyclic units, the cyclic alternation of sandstone units and mudstones, particularly well shown in the second depositional sequence, strongly suggests the intervening effects of external factors on the control of sediment input, rather than autocyclic environmental shifts. At the same time, cyclic units of third depositional sequence, which are characterized sandy – conglomeratic channel fill deposits, could have been controlled by autocyclic factors such as channel shifts, lateral accretion and/or lateral shift of a lobe. However, an alternative allocyclic origin for these units is also possible. During a small – scale relative sea - level fall, the coarse material transported from the platform will bypass the upper parts of the channels and will eventually fill them forming erosional channel fills. In this case, lobes will be fed by the finer material which is available in the system. On the other hand, during a small scale relative sea-level rise, the sand in the system will not have the necessary energy to be transported down to the lobes of the lower fan and therefore will fill the channels of the upper and middle fan environment giving rise to depositional channel – fill sequences.

9. As a summary, all depositional sequences have been thought to be allocyclic origin based on their composition, thicknesses, vertical evolution and estimated durations. Basic cyclic units which are the building blocks of the depositional sequences might be controlled by autocyclic factors.

As a recommendation for further work, continuation of the measurement of the upper part of the Haymana Formation can be suggested. Additional lateral stratigraphic sections could improve the construction of a more detailed sequence stratigraphic framework and to study allocyclic or autocyclic origin of sedimentary cycles. Analyses of additional measured sections could yield precise results on provenance, palaeocurrent directions, grain size etc. leading a better reconstruction of the depositional environment of the Haymana Formation.

REFERENCES

Adams, A.E., MacKenzie, W.S., Guilford, C., 1984. Atlas of sedimentary rocks under the microscope. Longman, 101 p.

Altner, D., 1991. Microfossil biostratigraphy (mainly foraminifers) of the Jurassic – Lower Cretaceous carbonate successions in North – Western Anatolia (Turkey). *Geologica Romana*, 27, 167 – 213.

Benton, M., and Harper, D., 1997. Basic palaeontology. Addison Wesley Longman, 342 p.

Boggs, S. Jr. 2001. Principles of sedimentology and stratigraphy. Prentice-Hall, 726 p.

Chaput, E., 1936. Voyages d'études tectoniques et geomorphogeniques em Turquie. Paris.

Çiner, A., 1996. Distribution of Small Scale Sedimentary Cycles Throughout Several Selected Basins. *Turkish J. of Earth Sciences*, 5, 25-37.

Çiner, A., Deynoux, M., Koşun, E. and Gündoğdu, N. 1993. Sequence stratigraphic analyses of the Beldede braid-delta complex: Polatli-Haymana Basin, (Middle Eocene), Central Anatolia, Turkey, (in turkish). *Bull. of Earth Sciences of Hacettepe University*, 16, 67-92.

Çiner, A., Deynoux, M., Koşun, E., 1996. Cyclicity in the Middle Eocene Yamak turbidite complex of the Haymana basin, Central Anatolia, Turkey. *International Journal of Earth Sciences*, Volume 85 (4), 669-682.

Çiner, A., Deynoux, M., Ricou, S. and Koşun, E. 1996. Cyclicality in the middle Eocene Cayraz carbonate formation, Haymana Basin, Central Anatolia, Turkey, *Paleogeography, Paleoclimatology, Paleoecology*, 121, 313-329.

Coe, L.A., 2003. *The sedimentary record of sea-level change*. Cambridge University Press, 288p.

Cox, R. & Lowe, D.R. 1996. Quantification of the effect of secondary matrix on the analysis of sandstone compositional and a petrographic – chemical technique for retrieving original framework grain models of altered sandstones. *Journal of Sedimentology Research*, 66, 548 – 558.

Dickinson, W.R. 1985. Interpreting provenance relations from detrital modes of sandstones. In: *Provenance of Arenites* (Ed. G.G. Zuffa). Reidel, Dordrecht, 333 – 361.

Dickinson and Suczek, 1979 W.R. Dickinson and C.A. Suczek 1979, Plate tectonics and sandstone compositions, *The American Journal of Petroleum Geologists Bulletin*, 63, 2164–2182.

Dunham, R. J., 1962. Classifications of carbonate rocks according to depositional texture. In: Ham, W. E. (ed.), *Classification of carbonate rocks*. American Association of Petroleum Geologist Memoir, 108 – 121.

Einsele G. 1991. *Sedimentary basins: Evolution, Facies, and Sediment Budget*. Springer, 628 p.

Einsele G. 2000. *Sedimentary Basins: Evolution, Facies, and Sediment Budget*. Springer, 792 p.

Embry, A.F. and Klovan, J.E., 1971. A Late Devonian reef tract on the Northeastern Banks Island, NWT: Canadian Petroleum Geology Bulliten, Volume 19, 730 – 781.

Emery, D., and Myers, K. J., editors, 1996. Sequence stratigraphy: Oxford, Blackwell Science, 297 p.

Emery, D., Myers, K.J., 1996. Sequence stratigraphy. Backwell Science, 304 p.

Folk et al., 1970 R.L. Folk, P.B. Andrews and D.W. Lewis, 1970. Detrital sedimentary rock classification and nomenclature for use in New Zealand, *New Zealand Journal of Geology and Geophysics* 13, 937–968.

Friedman, G.M., and Sanders, J.E., 1978, Principles of sedimentology: New York, John Wiley & Sons, 792 p.

Görür, N., Oktay, F.Y., Seymen, I., Sengör, A.M.C., 1984. Paleotectonic evolution of the Tuzgölü basin complex, Central Turkey: sedimentary record of a Neo – Tethyan closure. In: Dixon, J.E., Robertson, A.H.F., (eds) The geological evolution of the eastern Mediterranean. Geol Soc Lond, 467 - 482.

Grovel, W.K., Silverman, R.M., Rasmussen, R.D., Penfield, T.G., Gurnert, R.W., Grateral, V., 2000. AAPG Regional international conference, Istanbul Turkey.

Graciansky, P. C., de, Hardenbol, J., Jacquin, T., Vail, P.R., 1998. Mesozoic and Cenozoic sequence stratigraphy of European basins. SPEM Spec. Publ. 60, 3-13.

Gürbüz, K., 1999. Regional implications of structural and eustatic controls in the evolution of submarine fans: an example from the Miocene Adana Basin, southern Turkey. *Geol. Mag.* 136, 3, 311–319.

Haq et al., 1987. Chronology of fluctuating sea – level since the Triassic (250 million years to present). *Science*. Volume 235, 1156 – 1167.

Harland et al., 1989. A geologic time scale.

Ito, M., 1997. Submarine fan sequences of the lower Kazusa Group, a Plio-Pleistocene forearc basin fill in the Boso Peninsula, Japan. *Sedimentary Geology*, 122, 69-93.

Koçyigit, A., 1991. An example of an accretionary fore –arc basin from northern Central Anatolia and its implications for the history of subduction of Neo –Tethys in Turkey. *Geol Soc Am Bull*, 103, 22 - 36.

Koçyigit, A., Lunel, T., 1987. Geology and tectonic setting of Alci region, Ankara. *J Pure Appl Sci Ankara*, 20, 35 - 57.

Koçyigit, A., Özkan, S., Rojay, F.B., 1988. Examples from the fore-arc basin remnants at the active margin of northern Neo –Tethys; development and emplacement ages of the Anatolian nappe, Turkey. *J Pure Appl Sci Ankara*, 21, 183 - 210.

Lowe, D.R., 1982. Sedimentary gravity flows II. Depositional models with sepical reference to the deposits of high-density turbidity currents. *J Sediment Petrol*, 52, 279 - 297.

Özcan, E., Özkan, S.A., 1997. Late Campanian – Maastrichtian evolution of orbitoidal foraminifera in Haymana Basin successions (Ankara, Central Turkey). *Revue Paleobiol.*, Geneve, 16, (1), 271 – 290.

Özcan, E., Özkan, S.A., 1999. The genera *Lepidorbitoides* and *Orbitoides*: evolution and stratigraphic significance in some Anatolian basins. *Geological Journal*, 34, 275 – 286.

Özcan, E., Özkan, S.A., 1999. The Genus *Lepidorbitoides*: Evolution and Stratigraphic Significance in some Anatolian Basins (Turkey). *Revue de Micropaleontologie*, 42, 111-131.

Özcan, E., Özkan, S.A., 2001. Description of an early ontogenetic evolutionary step in *Lepidorbitoides*: *Lepidorbitoides bisambergensis asymmetrica* subsp. n., Early Maastrichtian (central Turkey) *Rivista Italiana di Paleontologia e Stratigrafia*, 107, 137-144.

Özcan, E., Sirel, E., Özkan, S.A. and Çolakoğlu, S., 2001. Late Paleocene Orthophragminae (foraminifera) from the Haymana – Polatli Basin, (central Turkey) and description of a new taxon, *Orbitoclypeus haymanaensis* *Micropaleontology*, 47, 339 - 357.

Özkan, S.A., Özcan, E., 1999. Upper Cretaceous planktonic foraminiferal biostratigraphy from NW Turkey: calibration of the stratigraphic ranges of larger benthonic foraminifera *Geological Journal*, 34, 287 – 301.

Pettijohn, F. J., Potter, P.E., & Siever, R. 1987. *Sand and sandstone*. Springer – Verlag, New York.

Posamentier, H.W., Erksine, R.D., Mitchum, R.M., 1991. Models for submarine – fan deposition within a sequence –stratigraphic framework. In: Weimer, P., Link, M.M., (eds) *Seismic facies and sedimentary processes*. Springer, Berlin Heidelberg New York, 137 - 148.

Premoli Silva, I. and Verga, D., 2004. Practical manual of Cretaceous planktonic foraminifera. International School on planktonic foraminifera, 3⁰ Course: Cretaceous. Verga and Retteri (eds) Universities of Perugia and Milan, Tipografia Pontefelcino, Perugia (Italy), 283 p.

Reading, H.G., 1996. Sedimentary Environments: process, facies and stratigraphy. Blackwell Science, 688 p.

Ross, C.A. and J.R.P. Ross 1988. in Wilgus, C.K., Hastings, B.J., Posamentier, H., van Wagoner, J.C., Ross, C.A., and Kendall, C.G. St. C.: *Sea-level Change: an Integrated Approach*, SEPM Spec. Pub. 42, 71 - 108.

Sahu, B. K. 1964, Depositional mechanisms from the size analysis of clastic sediments. *Journal of Sedimentary Petrology*, 34, 73-83.

Şenalp, M., Gökçen, L.S., 1978. Sedimentological Studies of the Oil-Saturated Sandstones of the Haymana Region. *Bull Geol Soc Turkey*, 21, 87 – 94 (in Turkish).

Shanmugam, G., 2000. 50 years of the turbidite paradigm (1950s -1990s): deep –water processes and facies –a critical perspective. *Marine and Petroleum Geology*, 17, 285 - 342.

Sirel, E., 1999. Four new genera (*Haymanella*, *Kayseriella*, *Elazigella* and *Orduella*) and one new species of *Hottingerina* from the Paleocene of Turkey *Micropaleontology*, 42, 113 – 137.

Sirel, E., Gündüz, H., 1976. Description and stratigraphical distribution of the some species of the genera Nummulites, Assilina and Alveolina from the Ilerdian, Cuisian and Lutetian of the Haymana region. *Bull Geol Soc Turkey* 19, 31 - 44 (in Turkish).

Sloss, L. L., 1988. Tectonic evolution of the craton in Phanerozoic time, in Sedimentary Cover - North American Craton, The Geology of North America, Geol. Soc. Am., Boulder, Colo., vol. D-2, 25 - 51,

Stow, D.A.V., and Piper, D.J.W., 1984. Deep-water fine-grained sediments: facies models. In Stow, D.A.V., and Piper, D.J.W. (Eds.), Fine-Grained Sediments: Deep-Water Processes and Facies. Geol. Soc. Spec. Publ. London, 15, 611-645.

Stow, D.A.V. & Johansson, M. 2000. Deep-water massive sands: nature, origin and hydrocarbon implications. Marine Petroleum Geology 17, 145 - 174.

Toker, V., 1979. Upper Cretaceous Planktonic Foraminifera and the biostratigraphic investigations of the Haymana area. Bulliten of the Geological Society of Turkey, 22, 121 – 132.

Tucker, E.M., 2001. Sedimentary petrography. Blackwell Publishing, 262 p.

Tucker, E.M., 2005. Sedimentary rocks in the field. Wiley, 234 p.

Turgut S., Eseller G. 2000. Sequence stratigraphy, tectonics and depositional history in eastern Thrace Basin, NW Turkey. Marine and Petroleum Geology, Volume 17, 1, 61-100.

Ünalın, G., Yüksel, V., Tekeli, T., Gonenç, O., Seyirt, Z., Hüseyin, S., 1976. Upper Cretaceous – Lower Tertiary stratigraphy and paleogeographic evolution of Haymana – Polatlı region (SW Ankara). Turkish Geol Soc Bull 19, 159 - 176 (in Turkish).

Varol B., Özgüner M., Koşun E., İmamođlu Ş., Daniş M., Karakullukçu T., 2000. Western Blacksea glauconite depositional environment and sequence stratigraphy. MTA press, 122, 1-23 (In Turkish).

Visher, G.S., 1969, Grain size distribution and depositional processes, *Journal of Sedimentary Petrology*, Volume, 39, 1074 – 1106.

Wagoner, Van J.C., H.W. Posamentier, R.M. Mitchum, P.R. Vail, J.F. Sarg, T.S. Loutit, and J. Hardenbol, 1988. An overview of the fundamentals of sequence stratigraphy and key definitions. In C.K. Wilgus, B.S. Hastings, C.G.St.C. Kendall, H.W. Posamentier, C.A. Ross, J.C. Van Wagoner, eds., *Sealevel changes: an integrated approach*. Society of Economic Paleontologists and Mineralogists Special Publication No. 42, 39 - 45.

Yüksel, S., 1970. Etude geologique de la region d'Haymana (Turquie Centrale). These Univ Nancy, 1 - 179.

Zuffa, G.G., (Ed.) 1985 *Provenance of Arenites*. Reidel, Dordercht, 408 p.

APPENDIX A

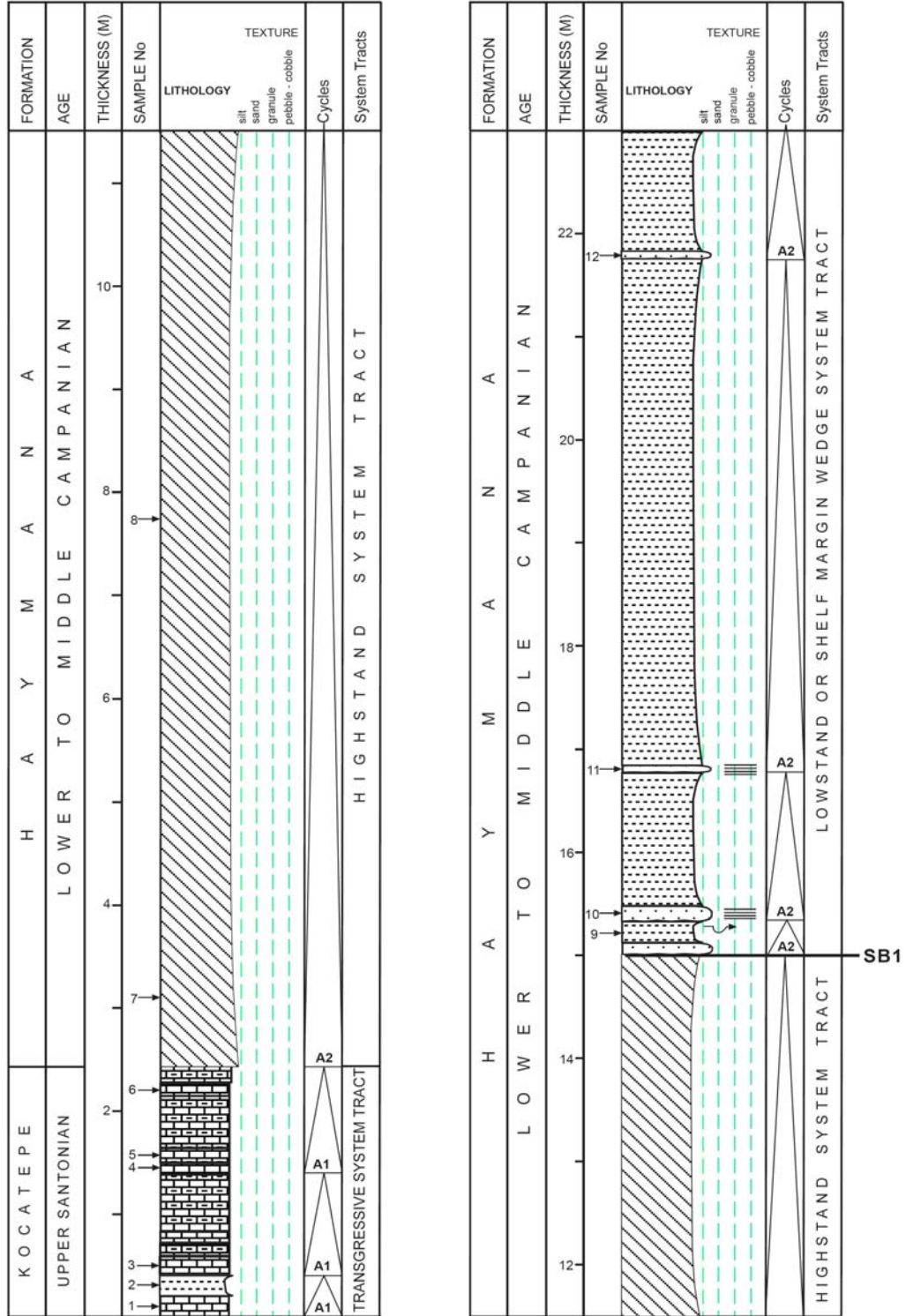


Figure A1. Detailed measured section

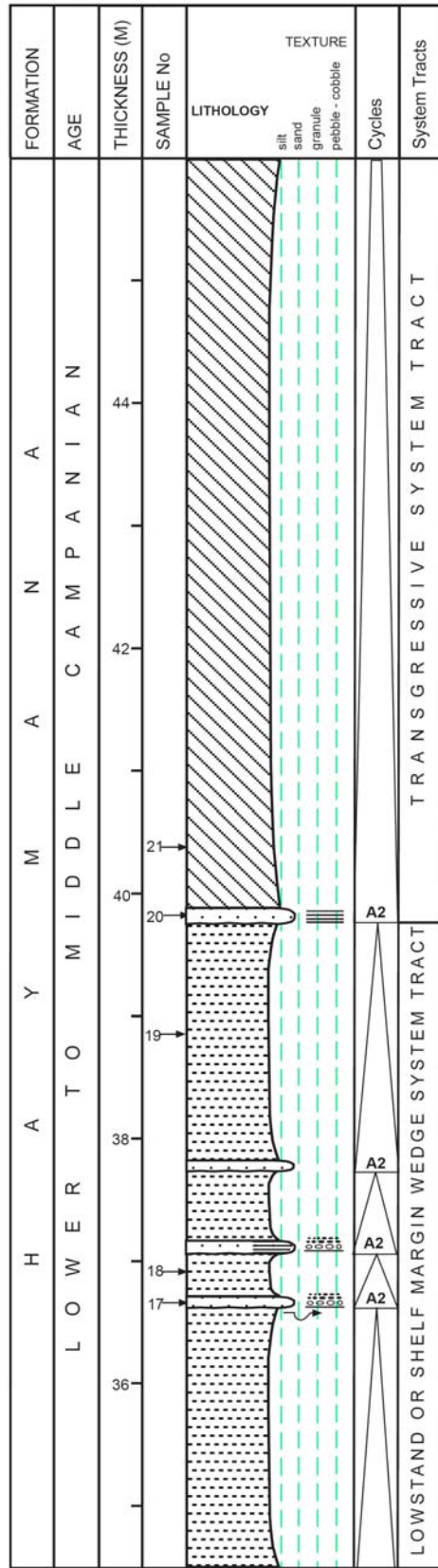
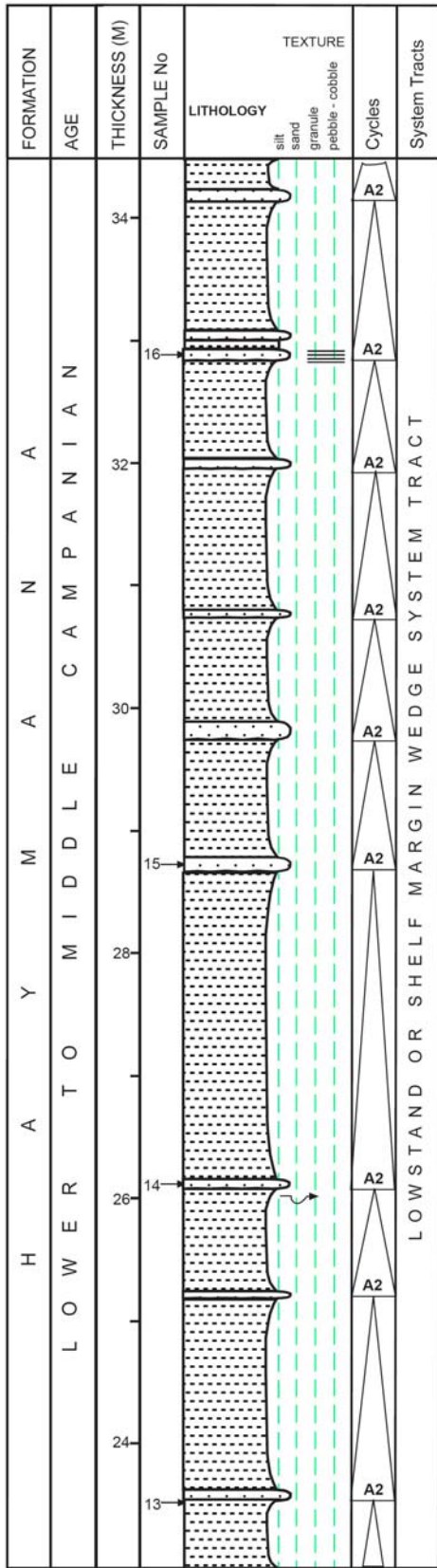


Figure A2. Detailed measured section (continued)

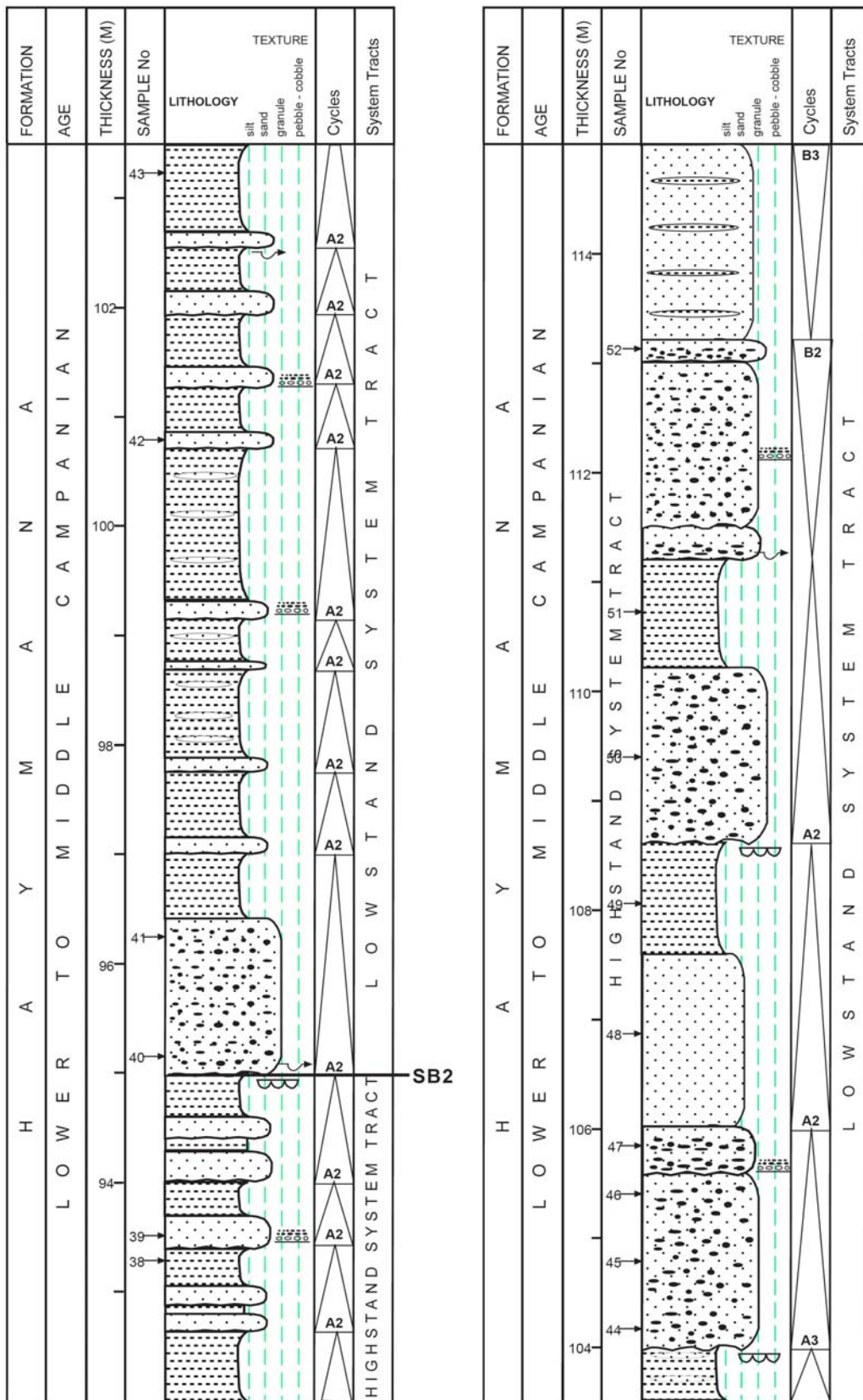


Figure A5. Detailed measured section (continued)

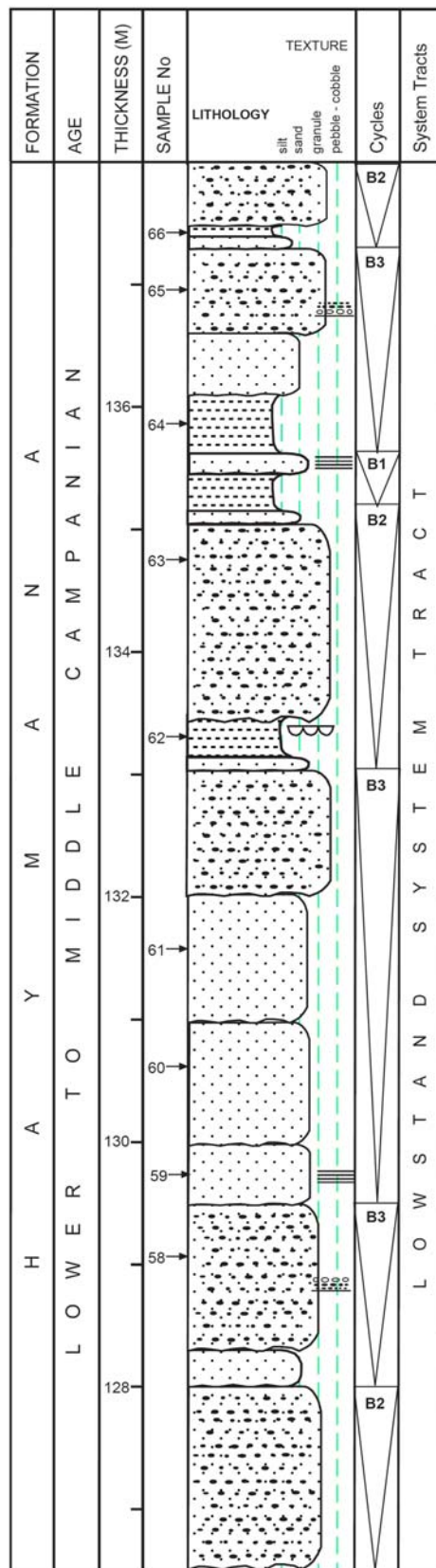
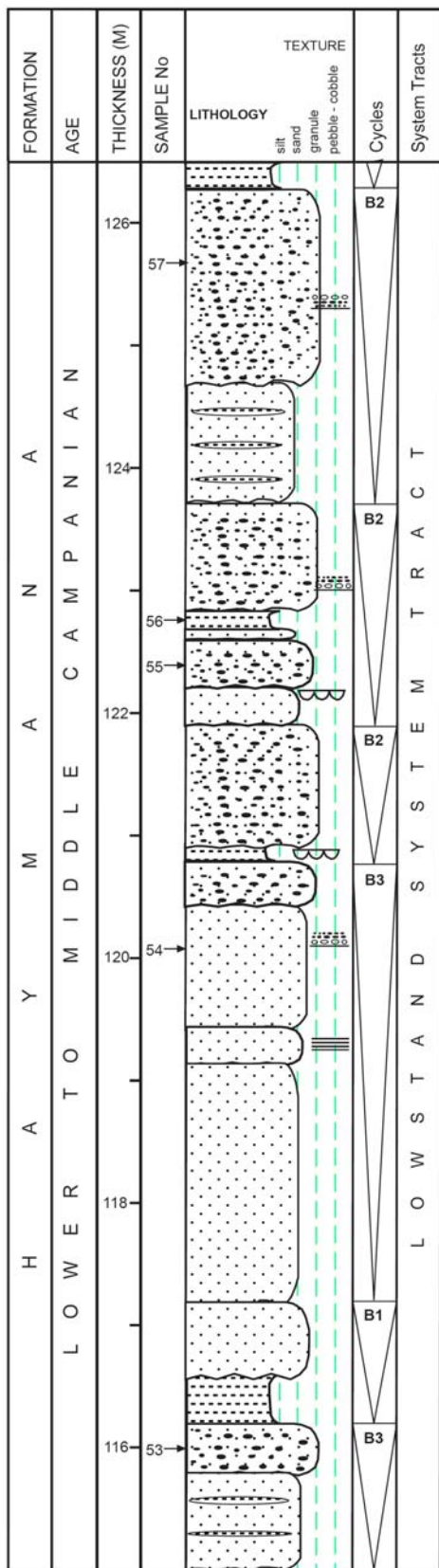


Figure A6. Detailed measured section (continued)

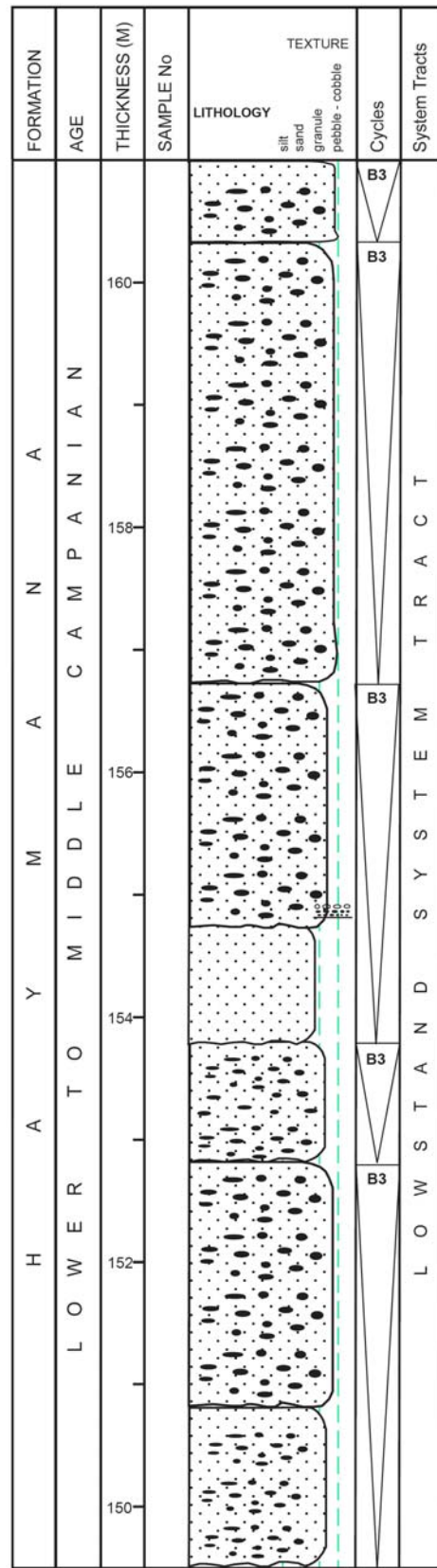
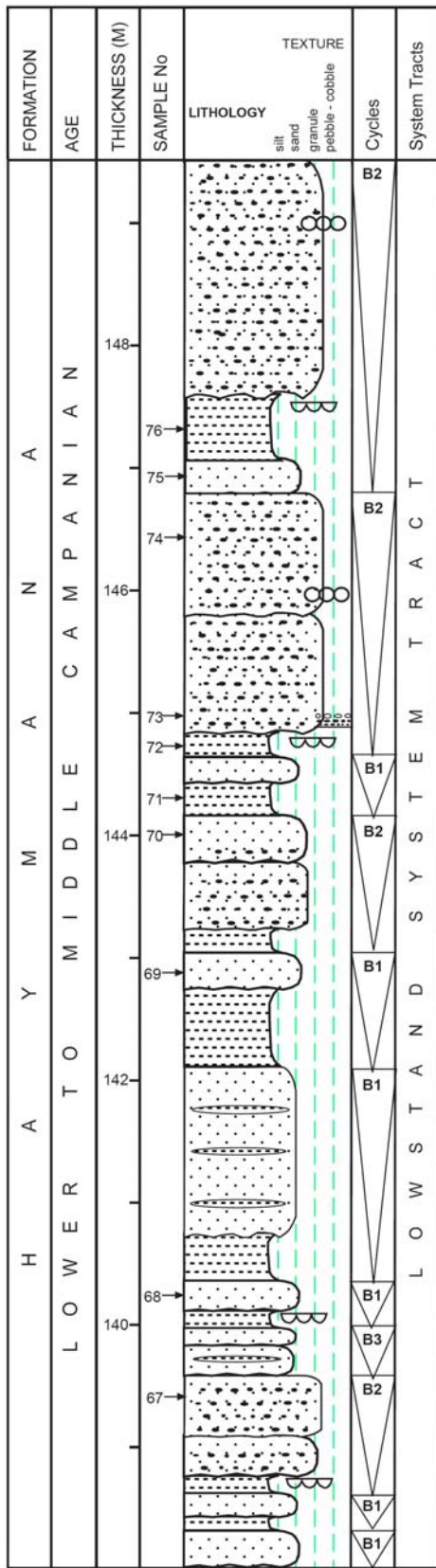


Figure A7. Detailed measured section (continued)

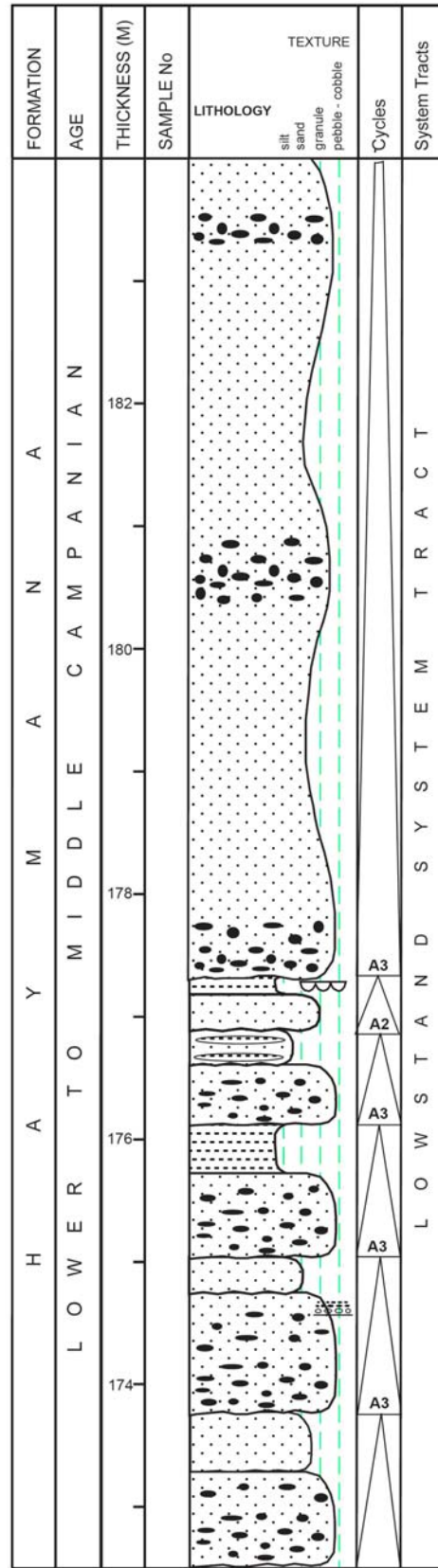
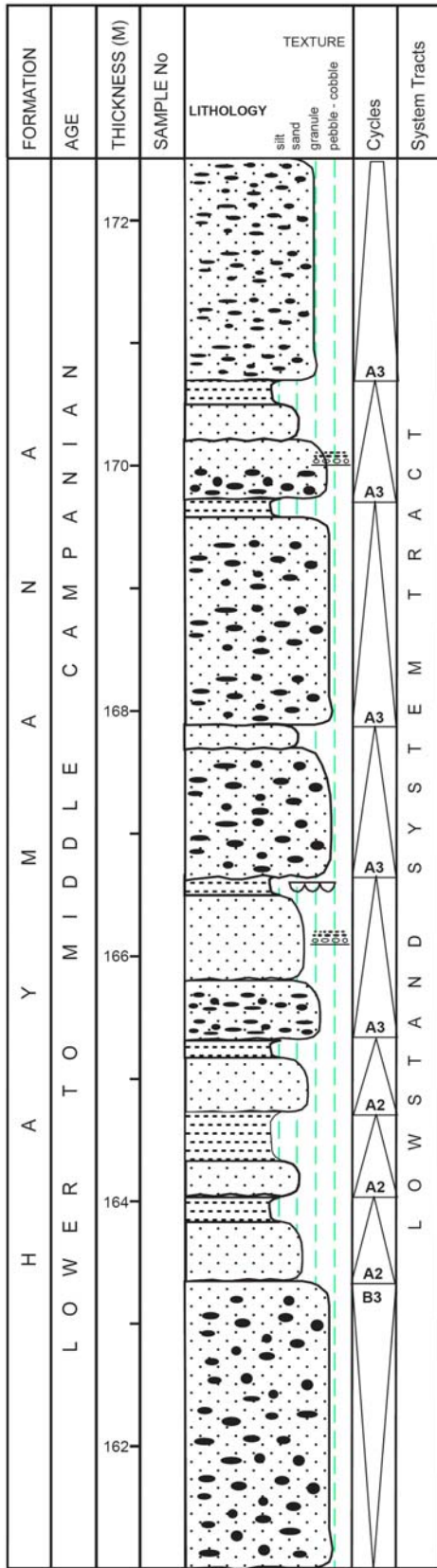


Figure A8. Detailed measured section (continued)

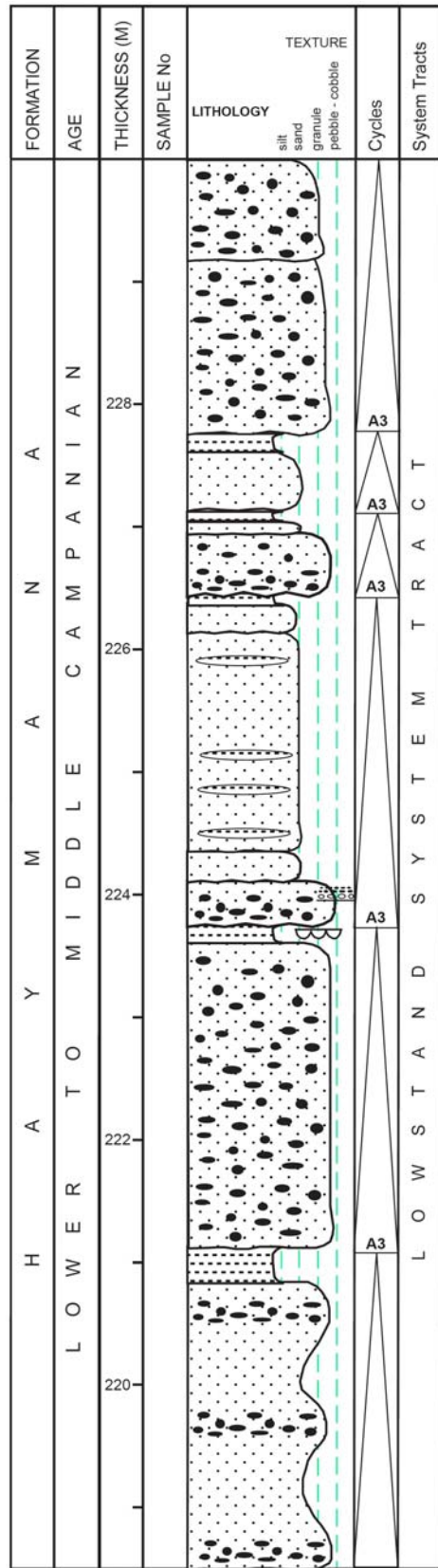
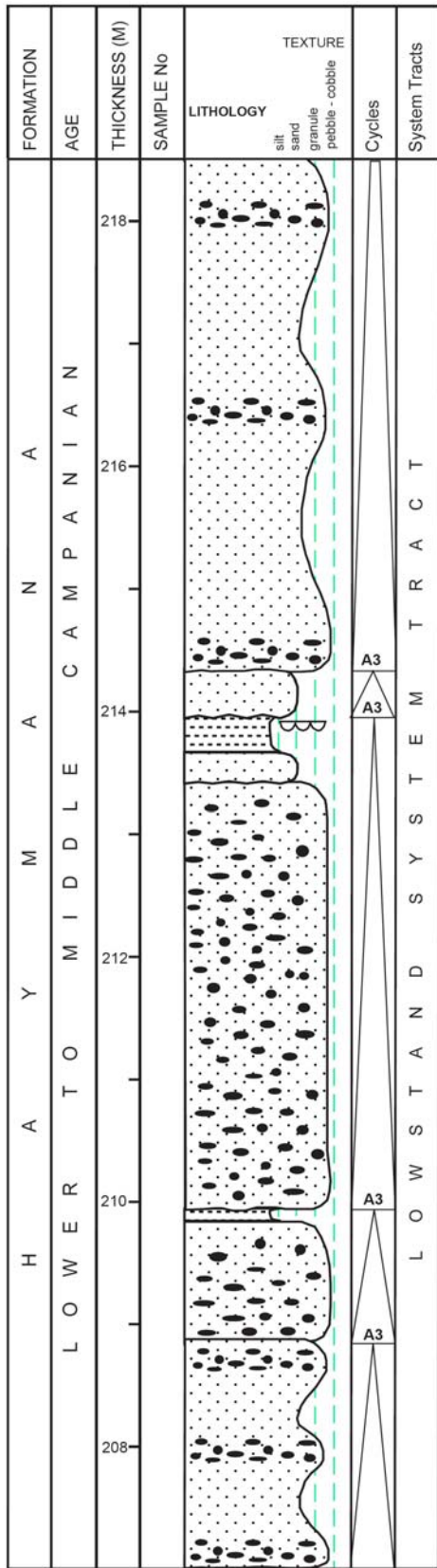


Figure A10. Detailed measured section (continued)

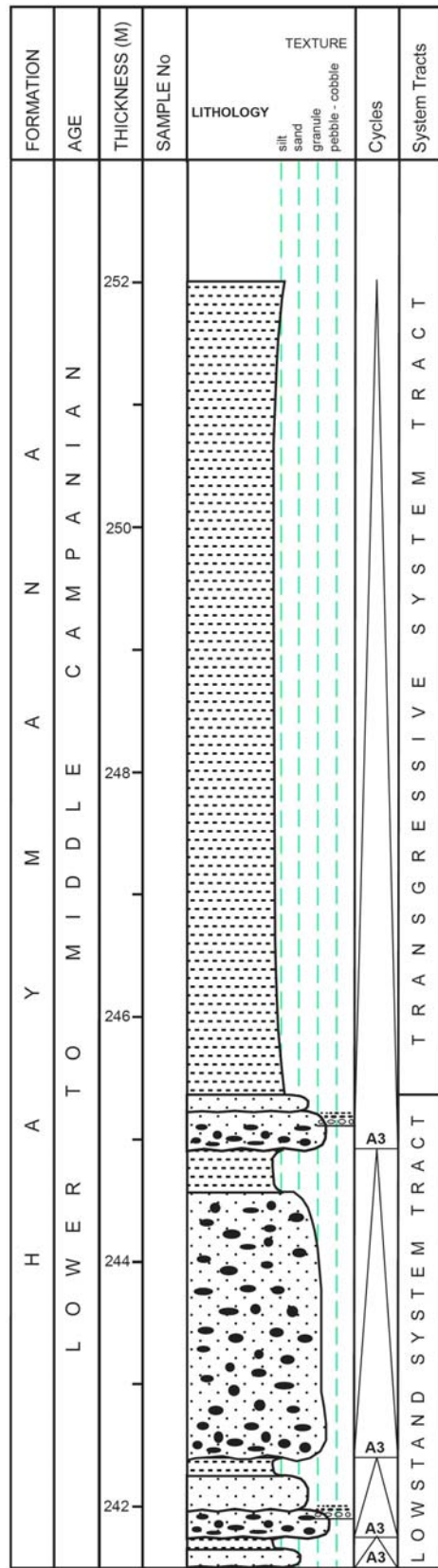
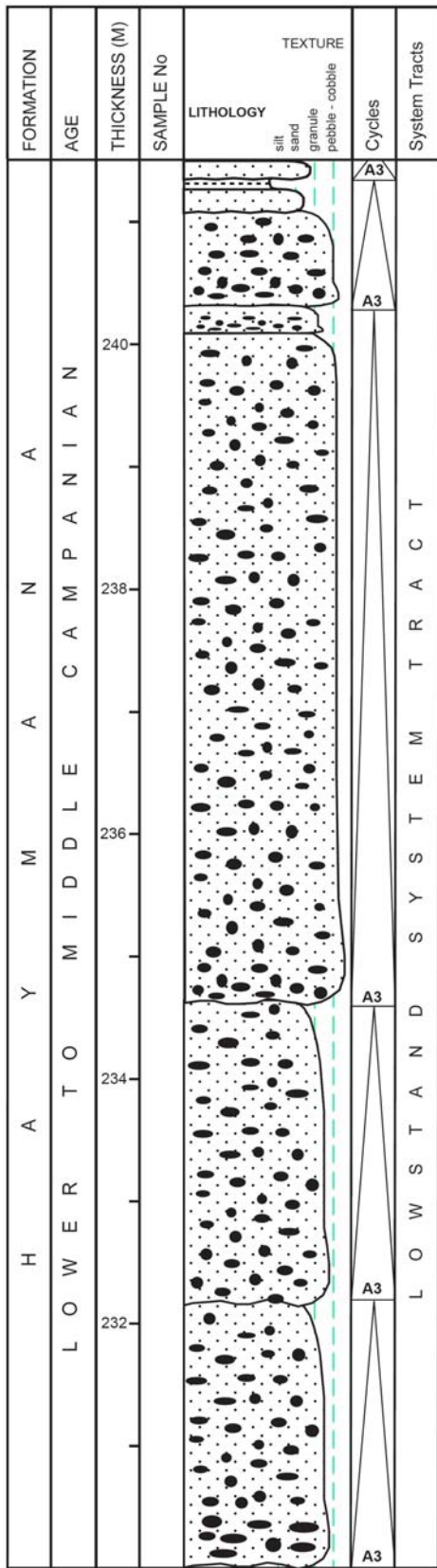
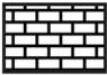
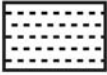
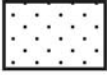
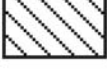
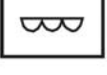
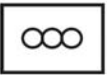


Figure A11. Detailed measured section (continued)

LEGEND

Lithology		Sedimentary structures	
	Limestone		normal graded bedding
	Shale		reverse graded bedding
	Sandstone		parallel lamination
	Conglomerate		flute cast
	Mudstone		load cast
	Coarsening and/or thickening-up unit		ball structures
	Fining and/or thinning-up unit		burrows
SB - Sequence Boundary			

APPENDIX B

LIMESTONES

Samples No	Quartz %	Rock Fragments %	Cement %	Plagioclase %	Matrix %	Muscovite %	Opaque %	Chlorite %	FF/Bioclust %	Biotite %	Facies	Classification
HAH1	-	-	-	-	72.1	-	-	-	27.9	-	Limestone	Wackestone
HAH2	2.3	-	-	-	91.6	0.6	0.7	-	4.8	-	Limestone	Mudstone
HAH3	0.9	-	-	-	79.3	-	-	-	19.8	-	Limestone	Wackestone
HAH4	1	-	-	-	91.4	-	-	-	7.6	-	Limestone	Mudstone
HAH5	0.8	-	-	-	86.6	0.4	-	-	12.2	-	Limestone	Wackestone
HAH6	0.4	-	-	-	96.3	-	-	-	3.3	-	Limestone	Mudstone

MUDSTONES AND SHALES

Samples No	Quartz %	Rock Fragments %	Cement %	Plagioclase %	Matrix %	Muscovite %	Opaque %	Chlorite %	FF/Bioclust %	Biotite %	Facies	Classification
HAH7	21.5	-	-	-	74.9	3.3	0.3	-	-	-	Mudstone	Mudstone
HAH8	13.7	0.2	-	-	85.6	0.5	-	-	-	-	Mudstone	Mudstone
HAH9	9.8	-	-	-	90	0.2	-	-	-	-	Shale	Shale
HAH12B	8	-	-	-	91.5	-	0.5	-	-	-	Shale	Shale
HAH16B	8.8	-	-	-	89.6	1	-	0	0.6	-	Shale	Shale
HAH18	12	-	-	-	87	0.6	0.4	-	-	-	Shale	Shale
HAH19	14	-	-	-	85.6	0.1	0.3	-	-	-	Shale	Shale
HAH21	2.5	0.7	-	-	96.2	0.3	0.2	-	0.1	-	Mudstone	Mudstone
HAH22	6.5	0.3	-	-	92.2	0.8	-	-	0.2	-	Mudstone	Mudstone

Figure B1. Point counting data derived from the samples of studied section limestones and mudstone/shales.

MUDSTONES AND SHALES

Samples No	Quartz %	Rock Fragments %	Cement %	Plagioclase %	Matrix %	Muscovite %	Opaque %	Chlorite %	FF/Bioclast %	Biotite %	Facies	Classification
HAH24	11	-	-	0.3	84.8	0.8	1.5	-	0.7	0.9	Shale	Shale
HAH25	15.8	21.9	-	0.2	60.5	0.8	-	-	-	0.8	Shale	Shale
HAH28	12.9	6.8	-	-	79.1	0.6	-	-	-	0.6	Shale	Shale
HAH30	15.3	9.3	-	-	72.4	1.5	0.6	-	-	0.9	Shale	Shale
HAH33	4	-	-	-	95.1	0.6	0.3	-	-	-	Shale	Shale
HAH38	19.9	11.8	-	-	65.8	1.8	-	-	-	0.7	Shale	Shale
HAH49	5.1	-	-	-	94.9	-	-	-	-	-	Shale	Shale
HAH51	9.6	0.8	-	-	89	0.6	-	-	-	-	Shale	Shale
HAH56	9.7	25.6	-	0.7	62.9	0.3	-	-	0.3	0.5	Shale	Shale
HAH62	9	-	-	-	91	-	-	-	-	-	Shale	Shale
HAH64	12.2	-	-	-	87.8	-	-	-	-	-	Shale	Shale
HAH66	7.2	-	-	-	92.8	-	-	-	-	-	Shale	Shale
HAH71	6.8	-	-	-	93.2	-	-	-	-	-	Shale	Shale
HAH72	7.8	-	-	-	90.9	0.8	-	-	0.5	-	Shale	Shale
HAH76	8.2	1.1	-	-	90.7	-	-	-	-	-	Shale	Shale

Figure B2. Point counting data derived from the samples of studied section mudstone/shales.

SANDSTONES

Samples No	Quartz	Rock Fragments	Cement	Plagioclase	Matrix	Muscovite	Opaque	Chlorite	FF/Bioclast	Biotite	Facies	Classification
	%	%	%	%	%	%	%	%	%	%		
HAH10	32.8	41.1	18.2	0.5	-	0.7	-	-	-	6.7	Sandstone	Litharenite
HAH11	53.5	16.1	25.9	-	-	-	0.3	-	-	4.2	Sandstone	Litharenite
HAH12	41.2	7.3	40.7	0.5	3.9	1.5	0.2	0.3	0.4	4	Sandstone	Litharenite
HAH13	42.9	11	40.3	0.7	-	1.3	0.7	0	1.2	1.9	Sandstone	Litharenite
HAH14	42.1	2.9	41	1.1	6.2	1.1	-	0.1	1.5	4	Sandstone	Litharenite
HAH15	36.6	21.8	33	1.5	-	0.9	-	0	0.5	5.7	Sandstone	Litharenite
HAH16	35.4	17	38.9	-	-	0.8	0.7	1.6	-	5.6	Sandstone	Litharenite
HAH17	29.5	34	27	0.5	1.7	1.4	0.8	-	-	5.1	Sandstone	Litharenite
HAH20	29.3	29	37.7	0.7	-	1.5	0.5	-	-	1.3	Sandstone	Litharenite
HAH23	20.5	24.2	51	0.2	-	1.1	0.3	-	0.7	2	Sandstone	Litharenite
HAH26	11	39.1	37.5	0.2	10.2	0.7	0.2	-	-	1.1	Sandstone	Litharenite
HAH27	27.5	16.7	48.7	1.7	-	1.9	-	-	-	3.5	Sandstone	Litharenite
HAH29	14.9	50.5	31.4	0.4	-	-	-	-	-	2.8	Sandstone	Litharenite
HAH31	19.5	20.5	4.2	-	53	0.9	-	-	-	1.9	Sandstone	Lithic greywacke
HAH32	16.1	45.1	34.6	-	2	0.4	-	-	-	1.8	Sandstone	Litharenite
HAH34	14.1	11.4	-	-	69.4	3.1	-	-	0.9	1.1	Sandstone	Lithic greywacke
HAH35	15.9	59.7	22.9	0.3	-	-	-	-	-	1.2	Sandstone	Litharenite
HAH36	19.1	17.9	-	-	60.9	0.8	-	-	0.9	0.4	Sandstone	Lithic greywacke
HAH37	17.1	74.2	6.3	-	-	-	-	-	1	1.4	Sandstone	Litharenite
HAH39	13.7	75.6	9	-	0.7	-	-	-	0.1	0.9	Sandstone	Litharenite
HAH42B	25.3	41	3.6	1	24.5	1.6	-	-	-	3	Sandstone	Lithic greywacke
HAH42	15.9	68.4	11.9	0.9	-	0.8	-	-	-	2.1	Sandstone	Litharenite
HAH43B	29.8	32	2.2	-	31.9	0.3	-	-	-	3.8	Sandstone	Lithic greywacke
HAH43	11.8	64.5	0.8	0.5	18.4	1	-	-	-	3	Sandstone	Lithic greywacke
HAHX1	27.3	34.3	32.9	-	2.2	2.6	-	-	-	0.7	Sandstone	Litharenite

Figure B3. Point counting data derived from the samples of studied section sandstones.

SANDSTONES

Samples No	Quartz %	Rock Fragments %	Cement %	Plagioclase %	Matrix %	Muscovite %	Opaque %	Chlorite %	FF/Bioclast %	Biotite %	Facies	Classification
HAH48	12.2	61.1	20.9	-	1.9	1.5	-	-	2.4	-	Sandstone	Litharenite
HAH54	9.6	70.1	16	0.6	-	2.6	-	-	-	1.1	Sandstone	Litharenite
HAH59	15.6	42.6	9.5	2.3	28.3	1.7	-	-	-	-	Sandstone	Lithic greywacke
HAH60	16.1	59.1	5.7	1.3	15.1	0.9	-	-	-	1.8	Sandstone	Litharenite
HAH61	12	61.6	9.2	-	16.1	-	-	-	-	1.1	Sandstone	Litharenite
HAH68	11.7	47.7	3.8	0.7	34.7	0.7	-	-	-	0.7	Sandstone	Lithic greywacke
HAH69	19.5	56.3	19	1.7	-	1.5	-	-	0.1	1.9	Sandstone	Litharenite
HAH70	15.5	52.3	28.5	0.9	-	1.4	-	-	-	1.4	Sandstone	Litharenite
HAH75	7.1	54.5	4.9	-	31.8	1.1	-	-	-	0.6	Sandstone	Lithic greywacke

Figure B3. Continued

CONGLOMERATES

Samples No	Quartz %	Rock Fragments %	Cement %	Plagioclase %	Matrix %	Muscovite %	Opaque %	Chlorite %	FF/Bioclast %	Biotite %	Facies	Classification
HAH40	21	60	16.9	1.5	-	-	-	-	-	0.6	Conglomerate	Paraconglomerate
HAH41	6.1	57.8	2.8	-	32	-	-	-	-	1.3	Conglomerate	Paraconglomerate
HAH44	5.7	75.8	14.6	-	1.5	0.9	-	-	-	1.5	Conglomerate	Orthoconglomerates
HAH45	8.4	60.6	23.2	0.6	4.7	0.8	-	-	-	1.7	Conglomerate	Paraconglomerate
HAH46	9.7	71.8	15.8	-	0.9	0.8	-	-	-	1	Conglomerate	Orthoconglomerates
HAH47	9.2	66.3	12.3	-	9.5	1	-	-	0.4	1.3	Conglomerate	Paraconglomerate
HAH50	8.4	68.5	21.4	0.8	0.3	-	-	-	-	0.6	Conglomerate	Paraconglomerate
HAH52	11.4	66.3	17.5	1.2	-	2.4	-	-	-	1.2	Conglomerate	Paraconglomerate
HAH53	7.3	67.6	21.2	1.1	-	1.5	-	-	-	1.3	Conglomerate	Paraconglomerate
HAH55	9.5	78.5	8	0.6	-	1.8	-	-	-	1.6	Conglomerate	Orthoconglomerates
HAH57	7	78.5	12.5	-	-	1	-	-	-	1	Conglomerate	Orthoconglomerates
HAH58	13	57	27	0.7	-	2.1	-	-	-	0.2	Conglomerate	Paraconglomerate
HAH63	6.4	73.9	18	-	0.7	0.7	-	-	-	0.3	Conglomerate	Paraconglomerate
HAH65	6	72.4	21.2	-	-	0.4	-	-	-	-	Conglomerate	Paraconglomerate
HAH67	14	57.4	26.3	0.9	-	0.5	-	-	-	0.9	Conglomerate	Paraconglomerate
HAH73	13.2	60.6	23.6	1	-	1	-	-	-	0.6	Conglomerate	Paraconglomerate
HAH74	7.5	70.7	19	0.5	-	1.1	-	-	-	1.2	Conglomerate	Paraconglomerate

Figure B4. Point counting data derived from the samples of studied section conglomerates.

APPENDIX C

SANDSTONES

Samples No	Magmatic RF	Sedimentary RF	Igneous RF	Facies	Classification
	%	%	%		
HAH10	13.5	64.4	22.1	Sandstone	Litharenite
HAH11	22.4	58.6	19.0	Sandstone	Litharenite
HAH12	36.6	43.9	19.5	Sandstone	Litharenite
HAH13	31.9	42.6	25.5	Sandstone	Litharenite
HAH14	32.6	30.2	37.2	Sandstone	Litharenite
HAH15	35.2	17.0	47.7	Sandstone	Litharenite
HAH16	27.5	33.3	39.1	Sandstone	Litharenite
HAH17	31.4	6.7	61.9	Sandstone	Litharenite
HAH20	37.6	12.9	49.5	Sandstone	Litharenite
HAH23	22.6	17.0	60.4	Sandstone	Litharenite
HAH26	24.8	5.4	69.8	Sandstone	Litharenite
HAH27	23.3	2.3	74.4	Sandstone	Litharenite
HAH29	15.2	2.1	82.8	Sandstone	Litharenite
HAH31	18.4	10.2	71.4	Sandstone	Lithic greywacke
HAH32	13.5	1.7	84.8	Sandstone	Litharenite
HAH34	37.2	2.3	60.5	Sandstone	Lithic greywacke
HAH35	8.0	4.2	87.8	Sandstone	Litharenite
HAH36	12.7	12.7	74.5	Sandstone	Lithic greywacke
HAH37	3.1	12.8	84.1	Sandstone	Litharenite
HAH39	3.8	8.3	87.8	Sandstone	Litharenite
HAH42B	14.8	5.9	79.3	Sandstone	Lithic greywacke
HAH42	6.7	7.4	85.9	Sandstone	Litharenite
HAH43B	11.1	5.6	83.3	Sandstone	Lithic greywacke
HAH43	5.2	8.6	86.2	Sandstone	Lithic greywacke
HAHX1	7.5	14.0	78.5	Sandstone	Litharenite
HAH48	9.1	5.5	85.3	Sandstone	Litharenite
HAH54	6.0	18.8	75.2	Sandstone	Litharenite
HAH59	10.3	17.2	72.4	Sandstone	Lithic greywacke
HAH60	4.8	8.8	86.4	Sandstone	Litharenite
HAH61	5.1	18.4	76.5	Sandstone	Litharenite
HAH68	6.9	16.1	77.0	Sandstone	Lithic greywacke
HAH69	6.4	12.9	80.7	Sandstone	Litharenite
HAH70	5.8	9.9	84.3	Sandstone	Litharenite
HAH75	7.6	14.0	78.4	Sandstone	Lithic greywacke

Figure C1. Point counting data derived from the samples of studied section (rock fragments) sandstones.

CONGLOMERATES

Samples No	Magmatic RF	Sedimentary RF	Igneous RF	Facies	Classification
	%	%	%		
HAH40	4.2	11.9	83.9	Conglomerate	Conglomerate
HAH41	2.9	16.3	80.8	Conglomerate	Conglomerate
HAH44	3.8	3.5	92.7	Conglomerate	Conglomerate
HAH45	4.3	5.1	90.6	Conglomerate	Conglomerate
HAH46	2.9	20.3	76.8	Conglomerate	Conglomerate
HAH47	2.8	15.4	81.8	Conglomerate	Conglomerate
HAH50	5.7	5.4	88.9	Conglomerate	Conglomerate
HAH52	4.6	11.1	84.4	Conglomerate	Conglomerate
HAH53	5.2	8.8	86.0	Conglomerate	Conglomerate
HAH55	7.3	19.5	73.2	Conglomerate	Conglomerate
HAH57	5.0	23.1	71.9	Conglomerate	Conglomerate
HAH58	7.0	24.1	69.0	Conglomerate	Conglomerate
HAH63	3.3	8.5	88.2	Conglomerate	Conglomerate
HAH65	5.0	20.0	75.0	Conglomerate	Conglomerate
HAH67	6.4	8.8	84.8	Conglomerate	Conglomerate
HAH73	6.5	11.9	81.6	Conglomerate	Conglomerate
HAH74	4.4	22.0	73.6	Conglomerate	Conglomerate

Figure C2. Point counting data derived from the samples of studied section (rock fragments) conglomerates.

APPENDIX D (Bed one)

Sample No	Pebble Orientation (degree)
1	33
2	50
3	15
4	24
5	80
6	12
7	28
8	350
9	40
10	33
11	50
12	340
13	25
14	75
15	5
16	10
17	305
18	3
19	40
20	55
21	20
22	120
23	65
24	40
25	70
26	40
27	345
28	150
29	25
30	10
31	95
32	25
33	5
34	235
35	30
36	240
37	5
38	105
39	35
40	10
41	6
42	40
43	70
44	60
45	75
46	30
47	50
48	5
49	0
50	20

Sample No	Pebble Orientation (degree)
51	90
52	70
53	110
54	115
55	0
56	120
57	100
58	140
59	50
60	0
61	240
62	200
63	25
64	80
65	190
66	185
67	170
68	195
69	210
70	180
71	200
72	50
73	45
74	110
75	60
76	65
77	90
78	240
79	320
80	60
81	105
82	315
83	50
84	185
85	30
86	125
87	20
88	110
89	138
90	140
91	185
92	240
93	24
94	286
95	70
96	328
97	100
98	54
99	67
100	59

Figure D1. Palaeocurrents analysis for bed one.

APPENDIX D (bed two)

Sample No	Pebble Orientation (degree)
1	332
2	321
3	180
4	184
5	190
6	236
7	271
8	178
9	154
10	142
11	180
12	86
13	174
14	176
15	134
16	170
17	156
18	142
19	145
20	200
21	152
22	13
23	145
24	346
25	358
26	336
27	328
28	324
29	2
30	2
31	142
32	322
33	347
34	340
35	320
36	316
37	0
38	310
39	318
40	340
41	150
42	156
43	148
44	182
45	155
46	168
47	142
48	155
49	143
50	183

Sample No	Pebble Orientation (degree)
51	158
52	158
53	136
54	180
55	188
56	164
57	173
58	175
59	159
60	164
61	178
62	180
63	156
64	173
65	179
66	180
67	191
68	154
69	153
70	154
71	174
72	156
73	150
74	145
75	168
76	152
77	122
78	167
79	140
80	152
81	175
82	157
83	12
84	164
85	143
86	125
87	320
88	316
89	154
90	158
91	190
92	320
93	182
94	180
95	165
96	153
97	152
98	130
99	158
100	181

Figure D2. Palaeocurrents analysis for bed two.

APPENDIX E (Bed one)

Sample No	Long (cm)	Intermediate (cm)	Short (cm)	Sphericity	OP index
1	1.35	1.12	0.74	0.71	-2.24
2	4.16	3.38	1.14	0.45	-8.82
3	5.62	4.24	2	0.55	-3.34
4	3.42	2.95	2.46	0.84	-0.14
5	3.95	1.96	1.36	0.62	7.79
6	2.24	1.98	0.82	0.53	-8.66
7	2.68	2.14	1.05	0.58	-4.31
8	2.25	1.29	1	0.70	6.03
9	2.69	1.55	1.09	0.66	5.24
10	4.4	2.16	1.2	0.53	7.33
11	3.12	2.39	1.42	0.65	-1.55
12	2.63	1.95	0.93	0.55	-2.83
13	2.24	1.88	1.3	0.74	-2.02
14	3.45	2.08	1.47	0.67	4.50
15	3.22	2.17	1.33	0.63	1.35
16	3.68	2.61	1.29	0.56	-1.49
17	7.07	6.12	3.35	0.64	-5.16
18	2.22	1.34	1.12	0.75	5.95
19	2	1.55	1.14	0.75	0.41
20	2.4	2.05	1.47	0.76	-2.02
21	2.39	2	1.24	0.69	-3.10
22	4.47	3.8	1.98	0.61	-5.21
23	2.7	2.35	1.48	0.70	-3.89
24	3.94	2.73	2.07	0.74	2.80
25	2.5	1.75	1.44	0.78	3.60
26	3.72	2.72	2.63	0.88	5.90
27	2.81	2.86	1.45	0.64	-10.40
28	2.45	1.95	1.25	0.69	-1.63
29	3.66	3.24	2.05	0.71	-4.27
30	3.41	2.5	1.15	0.54	-2.89
31	2.26	1.9	1.46	0.79	-0.77
32	3.23	2.46	2.09	0.82	2.71
33	3.48	2.45	1.68	0.69	1.50
34	3.25	2.78	1.69	0.68	-3.82
35	5.79	4.23	2.24	0.59	-1.57
36	3.17	2.55	1.55	0.67	-2.40
37	4.19	3.49	1.99	0.65	-3.83
38	2.41	1.94	1.7	0.85	2.30
39	2.34	1.72	1.23	0.72	1.11
40	3.63	3.24	2.05	0.71	-4.48
41	2.85	2.19	1.19	1.00	-2.45
42	3.12	2.27	1.45	0.67	0.19
43	3.35	1.93	0.95	0.52	3.23
44	3.35	2.3	1.17	0.56	-0.53
45	4	3.57	1.3	0.49	-10.48
46	2.86	1.78	1.15	0.64	3.27
47	3.91	3.55	1.63	0.58	-8.21
48	3.41	2.09	0.7	0.41	-0.63
49	5.8	3	1.5	0.51	5.84
50	2.55	1.33	1	0.67	7.32

Figure E1. Sphericity analysis and OP index for bed one.

Sample No	Long (cm)	Intermediate (cm)	Short (cm)	Sphericity	OP index
51	4.77	1.74	1.21	0.56	13.84
52	3.88	2.83	1.68	0.64	-0.52
53	3.25	2.26	1.24	0.59	-0.20
54	3.86	3.47	2.18	0.71	-4.74
55	6.15	4.85	3.1	0.69	-1.46
56	6.89	5.42	4.13	0.77	0.54
57	3.4	2.29	1.45	0.65	1.62
58	2.94	2.43	1.82	0.77	-0.72
59	2.46	1.54	1.25	0.74	5.12
60	3.72	2.11	1.55	0.67	5.81
61	3.03	2.24	1.05	0.55	-2.91
62	2.95	2.04	1.74	0.80	4.27
63	3	2.23	1.45	0.68	-0.07
64	3.34	2.85	1.35	0.58	-6.28
65	2.84	2.32	1.44	0.68	-2.54
66	2.74	2.5	1.34	0.64	-6.72
67	3.28	3.02	1.63	0.64	-6.89
68	3.43	3.08	1.66	0.64	-6.25
69	2.85	1.73	0.92	0.56	2.49
70	3.62	3.02	2.12	0.74	-1.71
71	3.98	3.01	1.77	0.64	-1.37
72	3.63	2.28	2.03	0.79	6.15
73	2.88	2.24	1.64	0.75	0.28
74	3.12	2.67	1.28	0.58	-6.23
75	2.69	2.26	1.6	0.75	-1.77
76	2.93	2.67	1.58	0.68	-5.70
77	2.41	1.72	1.4	0.78	3.15
78	7.85	5.6	2.67	0.55	-1.93
79	2.75	2.36	1.6	0.73	-2.76
80	3.21	2.84	1.8	0.71	-4.24
81	2.52	1.85	1.03	0.61	-1.23
82	4.1	3.63	1.72	0.58	-7.21
83	4.69	3.6	2.24	0.67	-1.15
84	3.33	2.5	1.81	0.73	0.85
85	3.69	2.48	1.4	0.60	0.75
86	3.17	1.93	1.5	0.72	5.13
87	3.62	2.92	1.31	0.55	-5.44
88	3.43	2.56	1.46	0.62	-1.37
89	4.26	3.27	1.28	0.49	-5.58
90	3.46	2.96	2.15	0.77	-1.90
91	4.3	3.12	1.83	0.63	-0.52
92	3.29	2.58	1.51	0.65	-2.20
93	2.71	2	1.31	0.68	0.15
94	3.82	2.13	1.43	0.63	5.53
95	3.21	2.14	1.55	0.70	2.99
96	3.49	3.15	1.51	0.59	-7.59
97	2.86	2.13	1.65	0.76	1.79
98	2.39	1.8	0.7	0.48	-5.15
99	2.38	1.69	0.94	0.60	-0.53
100	3.62	3.15	1.1	0.47	-10.32

Figure E1. Continued.

APPENDIX E (bed two)

Sample No	Long (cm)	Intermediate (cm)	Short (cm)	Sphericity	OP index
1	4.62	3.03	1.74	0.60	1.38
2	4.8	3.6	3.27	0.85	4.17
3	5.25	3.17	1.81	0.58	3.04
4	5.96	3.98	2.14	0.58	0.51
5	2.98	2.25	1.46	0.68	-0.40
6	5.24	4.02	1.56	0.49	-5.66
7	4.67	2.29	1.69	0.64	8.25
8	5.65	2.95	1.83	0.59	6.39
9	12	9	4.5	0.57	-2.67
10	6.7	5.9	2.88	0.59	-6.76
11	2.09	3.87	2.73	0.97	17.46
12	3.7	3.44	1.93	0.66	-6.77
13	2.12	1.9	0.96	0.61	-6.85
14	5.82	3.55	2.95	0.75	5.74
15	4.45	3.73	2.92	0.80	-0.45
16	2.8	1.58	1.27	0.71	6.56
17	2.4	1.89	0.9	0.56	-4.27
18	4.33	2.98	1.54	0.57	-0.45
19	3.34	2.4	1.8	0.74	2.05
20	2.35	2.22	1.3	0.69	-6.80
21	3.71	2.28	2.15	0.82	7.19
22	2.46	2	1.41	0.74	-1.08
23	3.55	3.15	2.15	0.74	-3.54
24	6.5	3.91	3.12	0.73	5.55
25	6.42	5.02	3.97	0.79	1.16
26	4.93	3.49	2.09	0.63	0.17
27	5.11	3.45	1.98	0.61	0.78
28	3.06	1.61	1.5	0.77	8.76
29	4.94	2.95	1.82	0.61	3.74
30	4.7	3.7	2.25	0.66	-1.92
31	3.77	3.32	1.69	0.61	-6.33
32	7.37	5.43	4.2	0.76	1.97
33	9.91	6.91	5.16	0.73	2.53
34	3.17	2.55	2.02	0.80	0.61
35	3.87	2.86	1.89	0.69	0.21
36	7.98	5	3.32	0.65	3.35
37	3.68	3.11	1.15	0.49	-8.79
38	3.02	1.61	0.89	0.55	5.50
39	6.32	4.11	2.85	0.68	3.04
40	4.81	2.81	2.04	0.68	5.23
41	2.49	2.05	1.36	0.71	-2.03
42	6.1	2.96	1.95	0.59	8.03
43	5.28	3.68	1.52	0.49	-2.59
44	5.93	3.72	3.22	0.78	5.81
45	8.2	4.28	2.9	0.62	6.78
46	7	6.53	3.41	0.63	-7.58
47	3.05	3	1.4	0.60	-10.23
48	3.74	2.49	1.74	0.69	2.69
49	4.35	2.93	2	0.68	2.27
50	4.02	2.66	1.48	0.59	0.96

Continued

Figure E2. Sphericity analysis and OP index for bed two.

Sample No	Long (cm)	Intermediate (cm)	Short (cm)	Sphericity	OP index
51	8.74	6.12	3.54	0.62	0.09
52	3.67	2.6	0.88	0.43	-4.86
53	19	14.2	9.8	0.71	0.42
54	7	5.31	1.9	0.46	-6.21
55	4.66	3.31	1.63	0.56	-1.56
56	9.34	7.18	5.15	0.73	0.28
57	3.2	2.4	1.55	0.68	-0.31
58	3.65	2.34	1.51	0.64	2.71
59	2.5	1.27	1.06	0.71	8.35
60	3.48	2.96	1.29	0.54	-7.08
61	3.49	1.74	1.07	0.57	7.28
62	4.76	3.74	2.1	0.63	-2.64
63	5.25	3.35	2.35	0.68	3.47
64	4.01	2.41	2.01	0.75	5.99
65	5.27	3.54	2.28	0.65	1.82
66	7.75	4.2	2.43	0.57	5.34
67	4.45	2.42	1.41	0.57	5.29
68	5.11	4.06	2.55	0.68	-1.80
69	6.15	3.61	2.11	0.59	3.75
70	3.95	2.95	1.55	0.59	-2.12
71	8.06	4.22	3.25	0.68	7.40
72	6.1	4.48	2.87	0.67	0.03
73	5.95	4.45	1.84	0.50	-4.37
74	5.68	5.44	2.23	0.54	-10.96
75	4.17	3.75	2.44	0.72	-4.40
76	4.12	3.2	2.2	0.72	-0.39
77	3.07	2.81	2.31	0.85	-2.10
78	6.21	5.68	2.91	0.62	-7.24
79	5.3	4.25	3.15	0.76	-0.20
80	8.52	6.35	4.52	0.72	0.80
81	12.5	8.9	5.4	0.64	0.16
82	35	25.4	16.9	0.68	0.63
83	13	9.5	8.5	0.84	4.25
84	17.5	11.4	8.5	0.71	3.66
85	13	9.7	7.6	0.77	1.90
86	23.9	12	10.9	0.75	9.11
87	4.66	4.18	2.74	0.73	-4.25
88	2.91	2.65	1.22	0.58	-8.26
89	1.68	1.55	1.17	0.81	-3.52
90	23	16.5	13.8	0.79	3.44
91	15.3	10.3	6.4	0.64	1.48
92	3.1	2.63	0.93	0.47	-9.45
93	4.12	1.93	0.76	0.42	8.23
94	4.53	3.93	2.57	0.72	-3.42
95	4.2	2.72	1.67	0.62	2.14
96	5.32	3.89	3.06	0.77	2.31
97	14.5	8.2	5.29	0.62	5.04
98	5.19	3.93	2.34	0.65	-1.28
99	5.27	3.54	2.28	0.65	1.82
100	3.74	2.49	1.74	0.69	2.69

Figure E2. Continued

APPENDIX F

THIN SECTION PHOTOMICROGRAPHS

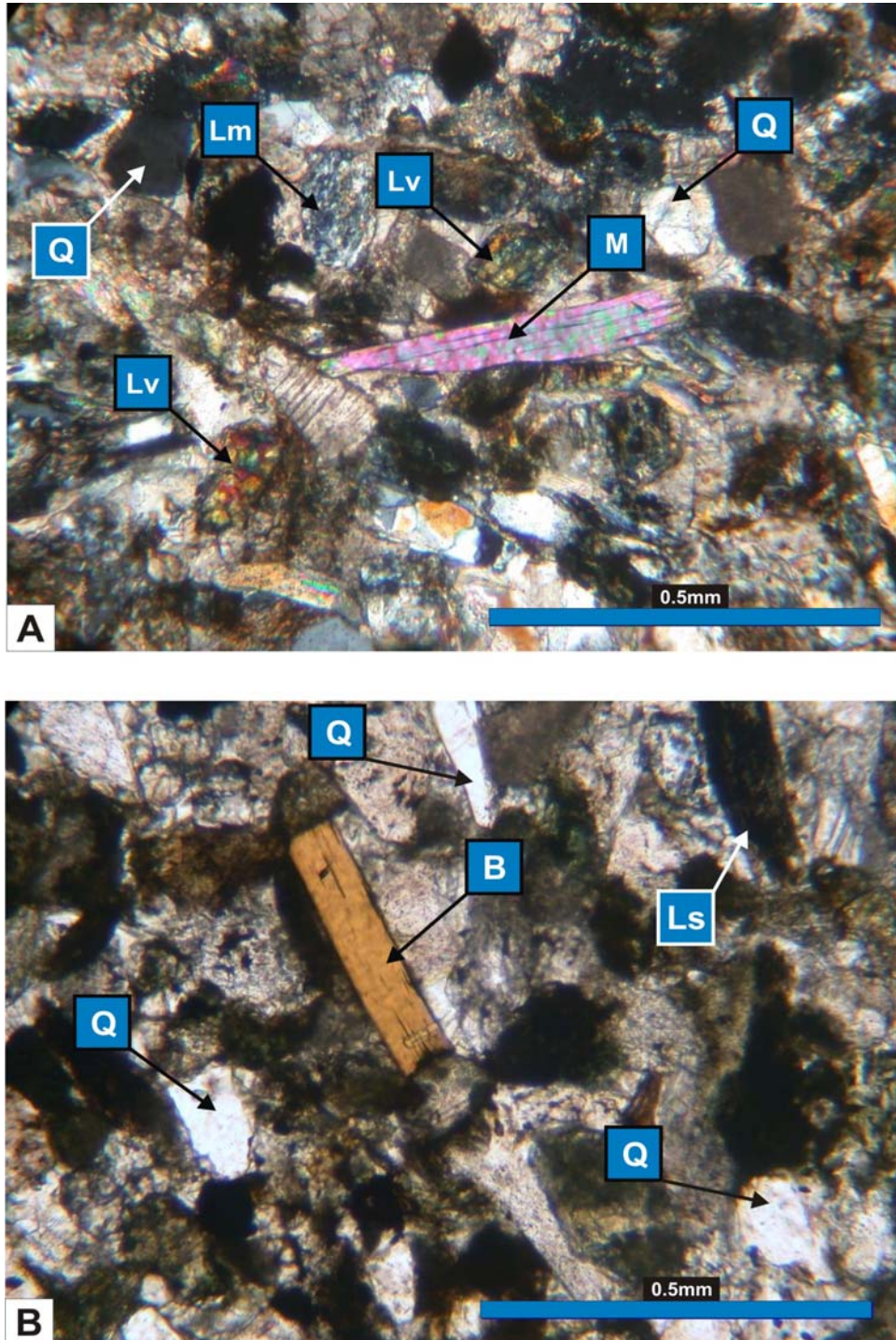


Figure F1. A and B lithic greywacke, (Q – quartz, M- muscovite, B-biotite, Lv – volcanic rock fragment, Lm – metamorphic rock fragment, Ls - sedimentary rock fragments), sample number: A and B HAH 23

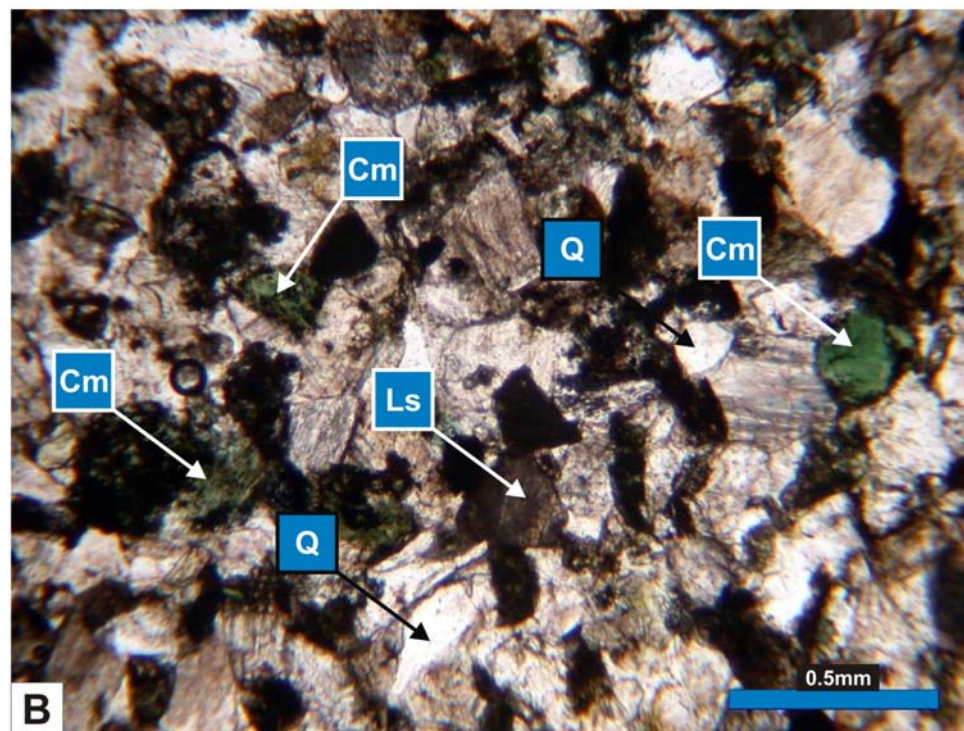
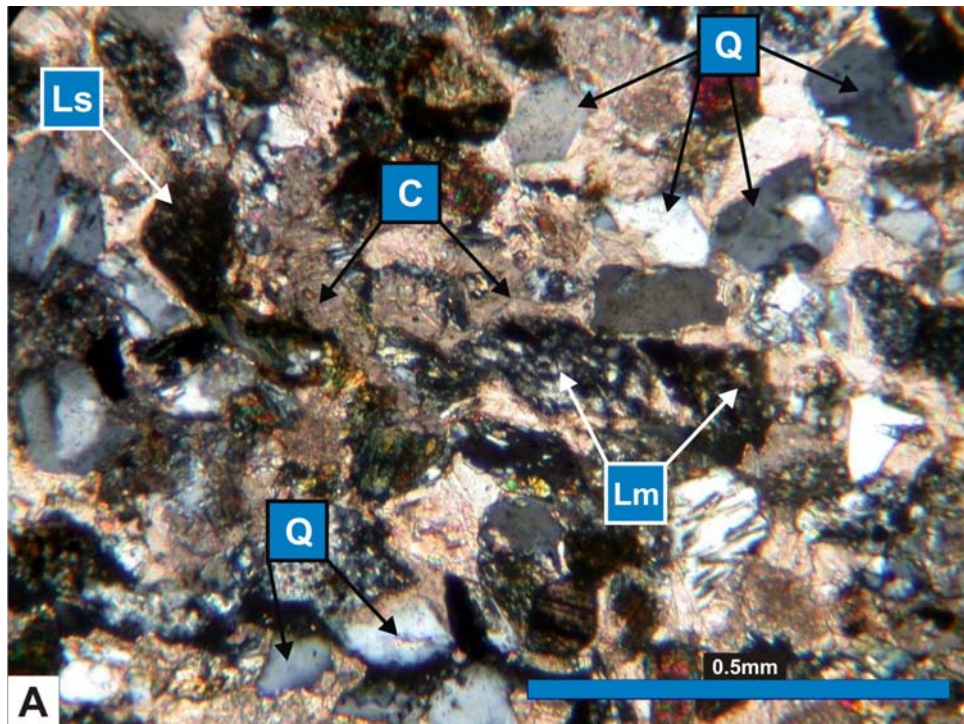


Figure F2. A and B lithic greywacke, (Q – quartz, C – calcite cement, Cm- clay minerals chlorite/glaucoune, Ls – sedimentary rock fragment, Lm – metamorphic rock fragment), sample number: A- HAH 23, B – HAH 26

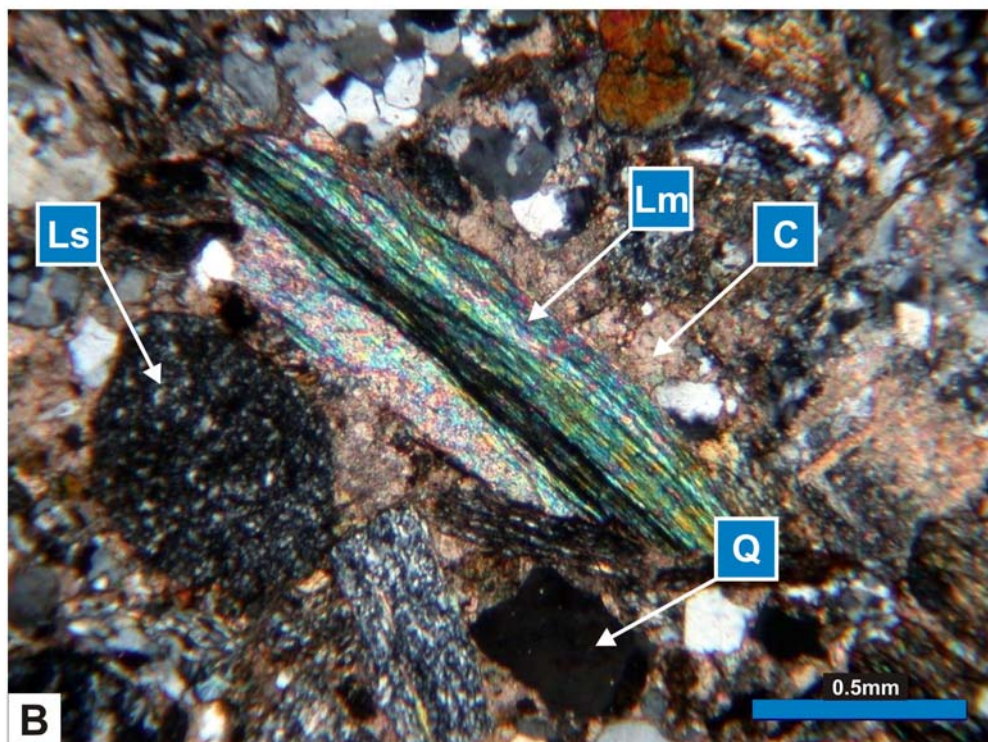
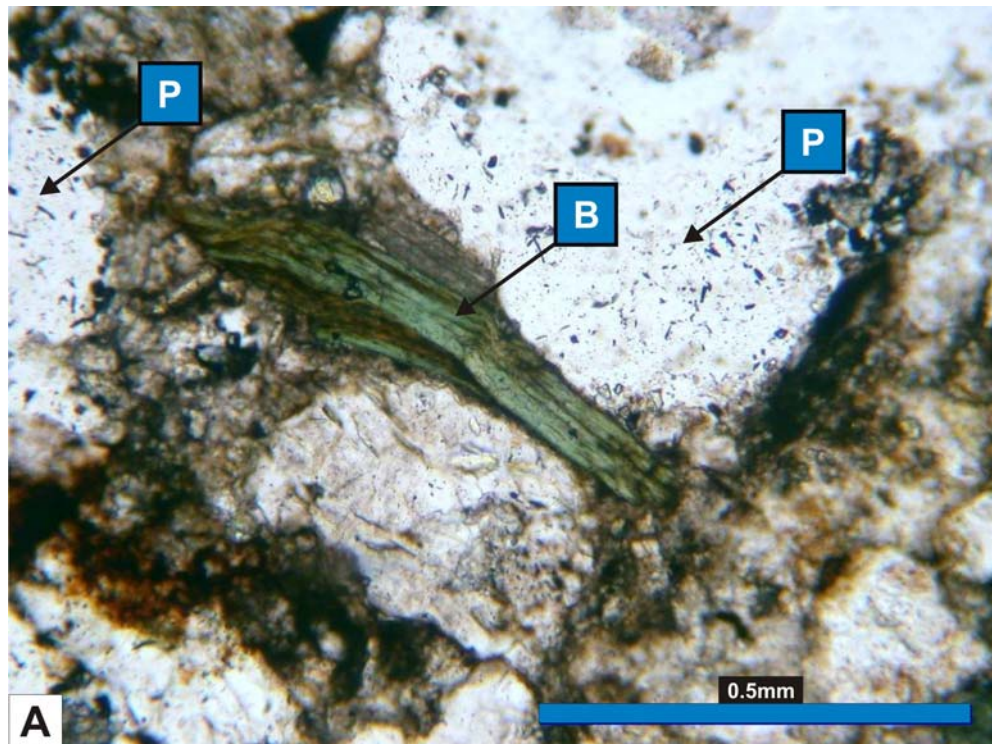


Figure F3. A and B litharenite, (Lm – metamorphic clast, slaty schist, B –green biotite, P – pore, Ls –sedimentary clast, Q-quartz, C-cement (calcite)), sample number: A and B HAH 42.

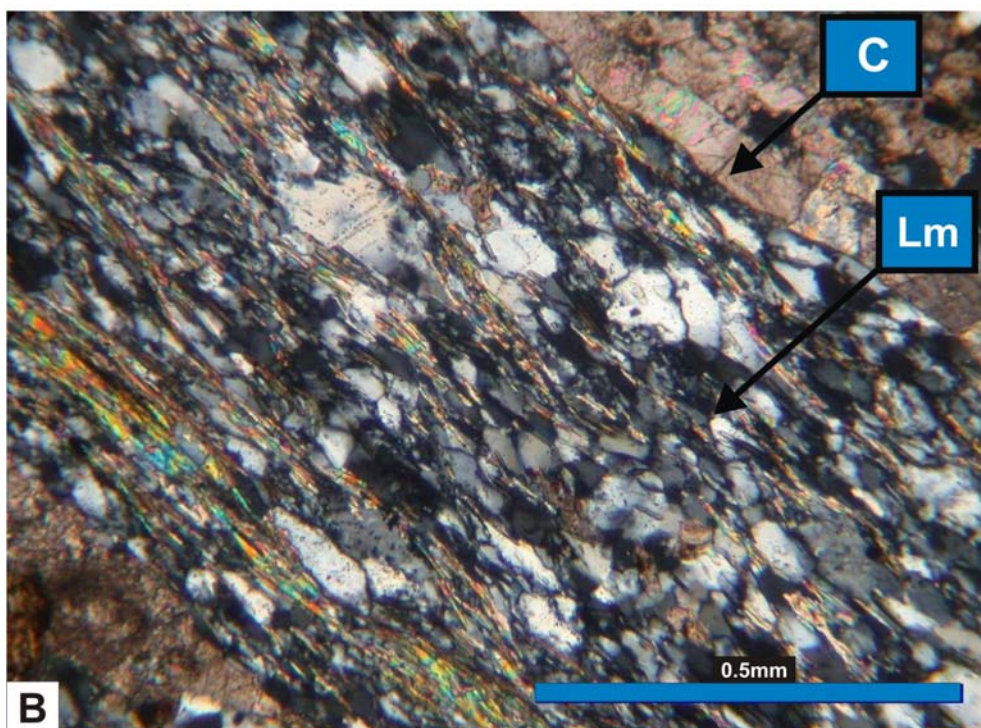
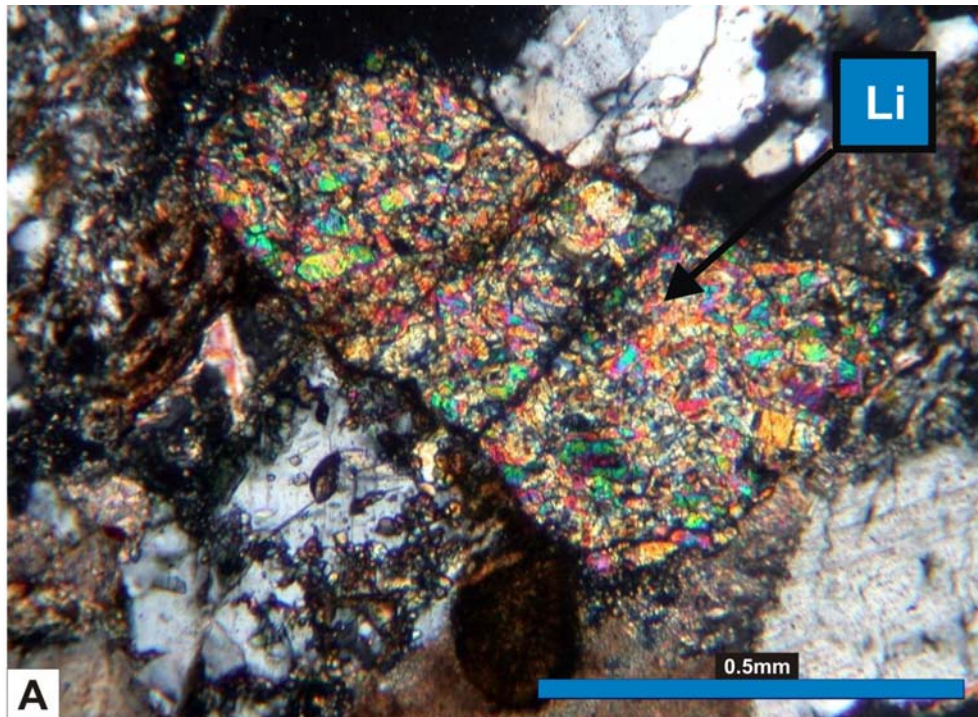


Figure F4. A – conglomerate, B - litharenite, (Lv – igneous rock fragment clinopyroxene, Lm – metamorphic rock fragment, C-cement (calcite)), sample number: A- HAH 41, B – HAH 42